Alma Mater Studiorum - Universitá di Bologna

DOTTORATO DI RICERCA IN

Ingegneria Civile, Ambientale e dei Materiali

Ciclo: **XXX**

Settore Concorsuale di afferenza: **08A1**

Settore Scientifico disciplinare: **ICAR/01**

Numerical analysis of floating structures for off-shore and harbour engineering

---

Presentato da: Agnese Paci

Cordinatore Dottorato:

Prof. Ing. Luca Vittuari

Supervisore:

Prof. Ing. Renata Archetti

Co-Supervisore:

Prof. Ing. Alberto Lamberti

Co-Supervisore:

Prof. Javier Lara Lopez

Esame finale anno 2018

Abstract

The aim of the research carried out during this Ph.D. was to create an open source numerical model able to simulate every kind of harbour and offshore structure, both fixed and floating. The code implemented was able to reproduce a physical wave tank and can be used during the design phase as an integration to physical tests.

The Computational Fluid Dynamic tool, OpenFOAM, was used as a starting point to develop the new code, furthermore the boundary condition IHFOAM tool was applied to generate and absorb waves. In order to reproduce deep water conditions, the code was improved with new boundary conditions and a new turbulent model. Furthermore an additional numerical restraint was implemented in the solver interDyMFOAM for representing a realistic mooring line when simulating floating structure with OpenFOAM. The new numerical tool was calibrated and validated thanks to a comparison with experimental tests. Different applications of the code are illustrated in the present work, as floating breakwater, horizontal and vertical floating cylinders, hit by waves and currents, with various mooring settings. Furthermore, the way to generate coupled waves and currents was explained and shown. Results of all the tests carried out were promising; showing good agreement with theoretical values and physical tests.

An application to a real study case was finally shown; a floating wind turbine was designed for an offshore area in Mazara del Vallo, (Sicily, Italy) and its response to wave loads was analysed with the new code. In this way, the feasibility of an offshore floating wind park in the Mediterranean Sea was studied.

The real case application demonstrated the model can be helpful in the design phase and it can be used for a wide range of applications, from harbour floating piers to offshore structures. Moreover, this methodology, with active absorption, lead to reduce the domain covered by the 3-D model and to simulate the interaction between sea states and structures in competitive times and computational costs.

To whom it may concern,

Acknowledgements

Contents

List of Figures

List of Tables

1

Introduction

1.1   Numerical Modeling of Floating Structures

Floating structures play an important role in the world today, they are used for many purposes such as: substructures for oil and gas rig (Fig. 1.1 and 1.2), harbour piers (FIg. 1.3), breakwater (Fig.1.4) . Each of them may have its own and different function and they can be installed in shallow water or in deep water. The floating structures installed in either shallow or deep water possess similar technical features and problems caused by sea loads and the corresponding mooring systems tensions, and the importance of the station keeping. Floating systems are particularly suited for deepwater: the Floating Production Storage and Offloading (FPSO), Semi-submersible, Tension Leg Platform (TLP) and Spar. Floater types might be distinguished by several characteristics such as functions, stability, motions, load or volume capacities, transportability, reusability. Each has a significant difference in terms of design drivers, performance, construction and installation. FPSOs have a relatively shallow draft, but a large waterplane area. They provide a large area for process facilities, and large storage volumes. Semi-submersibles have a small waterplane area and a moderate draft. Spars have a very deep draft and a moderate to small waterplane area. Since each platform requires significantly different design considerations, the design of each is covered in a separate subsection herein. Hull stability and structural design are relatively generic and are described under specific subsections (12).

Furthermore, climate change and the associated sea level rise has caused a change in the policies of governments around the globe, impulsing the move from fossil fuels to renewable energies. The European Union has been one of the leaders in this process by presenting in 2010 an ambitious plan within the framework of the Europe 2020 strategy

Figure 1.1: *Floating oil and gas rig.*

to limit the effects of climate change. By 2020, the greenhouse gas emissions should be a 20% lower than 1990 levels, a 20% of energy should come from renewable sources, and there should be an increase in the energy efficiency of 20%. To achieve these targets the blue energy field and, in particular, the research on renewable energy resources has been developing in recent years covering different types of wave and current energy converters and wind turbines, that are mainly floating structures.

On the other hand, floating structures are chosen more frequently because they are more environmentally friendly and because of the necessity to exploit resources from offshore and deep water areas. Resources nowadays are not anymore just oil and gas, we need to utilise more and more renewable energies, which are numerable. They can be classified in four major categories according to its nature: geothermal, hydroelectric, biomass and solar. Energy coming from the sun can be harvested directly and indirectly. Direct solar energy is divided into two main categories, photovoltaic: taking advantage of the semiconductor properties of silicon, and thermal, in which sun beams are focused onto a reduced area. This energy, concentrated in the form of heat, is then stored in a fluid, typically water.

Wind energy is an indirect form of solar energy. Energy coming from the sun is distributed irregularly throughout the planets surface, reaching its maximum at latitudes near the equator and decreasing gradually as moving away from it. This causes remarkable pressure differences in the atmosphere, which in turn creates winds, trying

Figure 1.2: *Transportation of Floating wind turbine foundation.*
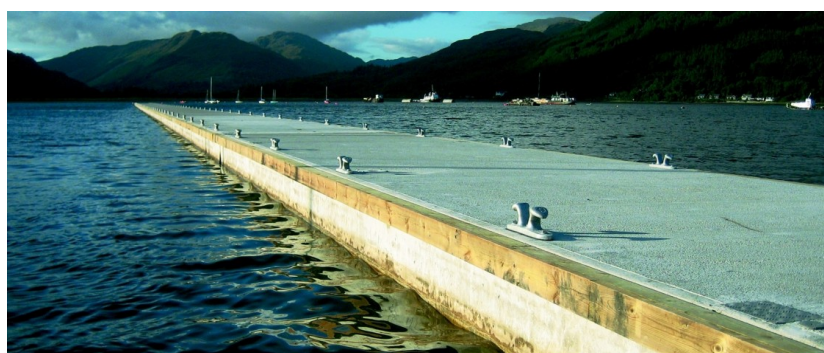
Figure 1.3: *Floating breakwater example.*
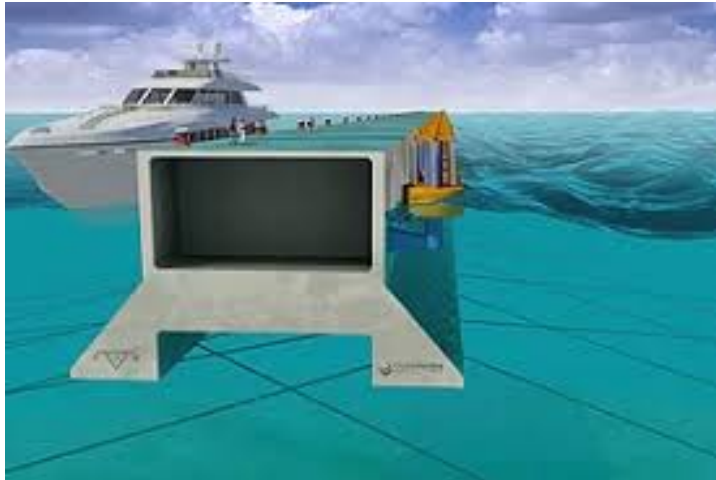
Figure 1.4: *Floating breakwater concept.*

to displace huge amounts of air from high pressure regions towards low pressure regions. When winds blow over the water surface, part of its energy is transferred to the water by friction thus, generating waves. Again, energy in waves ($2 - 3kW/m^2$) is denser than both, wind and solar. Even though most of solar irradiation energy is lost in this transmission chain, the gain in energy density is a factor that should attract expectation for future energy harvesting. Waves are generated far from the coasts, where wind and storms constantly blow over the fetch and then travel vast distances with practically no loss of energy. As a result, it becomes a very constant source of energy, there is no need of site-specific climatic events in order to ensure the presence of waves. As waves reach the shore may have been generated a few days ago and thousands of miles away. Furthermore, wave energy is a highly predictable resource, nowadays wave propagation computer models provide an accurate forecast of incoming waves up to a week in advance. Above 2/3's of the planet surface is covered by oceans and approximately 1/2 of the world's population lives within a $100km$ from the coast. Furthermore, electricity demand and wave seasonal variability match quite well, specifically in northern countries where peaks occur during late autumn and winter. The great availability of the resource is another factor to take into account when estimating its potential. In addition, very low environmental impact has been proved to occur when installing. Due to its reduced size and its typical deployment location (offshore) visual impact is naught as well as other impacts for the majority of other human activities, the only exception could be with ship routing (FIgures 1.5, 1.6 and 1.7).

Similar considerations, concerning the same advantages when moving offshore, can
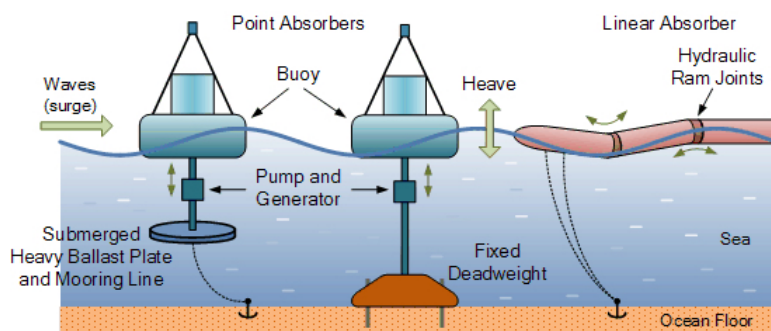
Figure 1.5: *Different wave energy converter concepts.*

Figure 1.6: *Pelamis wave energy converter.*

Figure 1.7: *Ocean Power Technology wave energy converter.*

Figure 1.8: *Floating wind turbine, with TLP substructure.*

be done for wind resources. Wind turbines were initially designed for installing on land and they had a rapid increase in term of number of wind turbines installed and maximum wind power capacity (25). However, this rapid increase encountered several obstacles such as a substantial environmental impact, the limitation of being high-capacity and making large wind farms. So, the attention moved to offshore sites, a less restrictive installation area. Offshore wind turbines are classified largely into two categories, fixed or floating according to how the turbine tower is supported. Differing from the fixed-type, the floating wind turbine is under the concept design stage because several core technologies have not fully settled down (41), particularly the maintenance of dynamic stability against irregular wind, wave and current loads (20). In order to secure the dynamic stability of floating off-shore wind turbines, the station keeping becomes critical (77). Because of this essential requirement, these offshore wind turbines require additional equipments like substructure, mooring lines or tension legs and anchors, if compared to the fixed ones. Many different types of floating structures can be adopted, they are classified according to how the draft control is generated, such as submerged, TLP (tension-leg platform) (Fig. 1.8), spar-types (46) (37) (Fig. 1.9 and 1.10), and barge-type. However, all have some features in common such as the station keeping and the vertical and rotational oscillation control of them are secured by a combined use of the buoyancy force and the tension of mooring lines or tension legs.

The dynamic response of a floating wind turbine to wind and wave excitations is usually evaluated in terms of rigid body degrees of freedom of the structure, where horizontal movements are related to the station keeping, surge and sway are largely

Figure 1.9: *Hywind floating wind turbine, Statoil desing.*
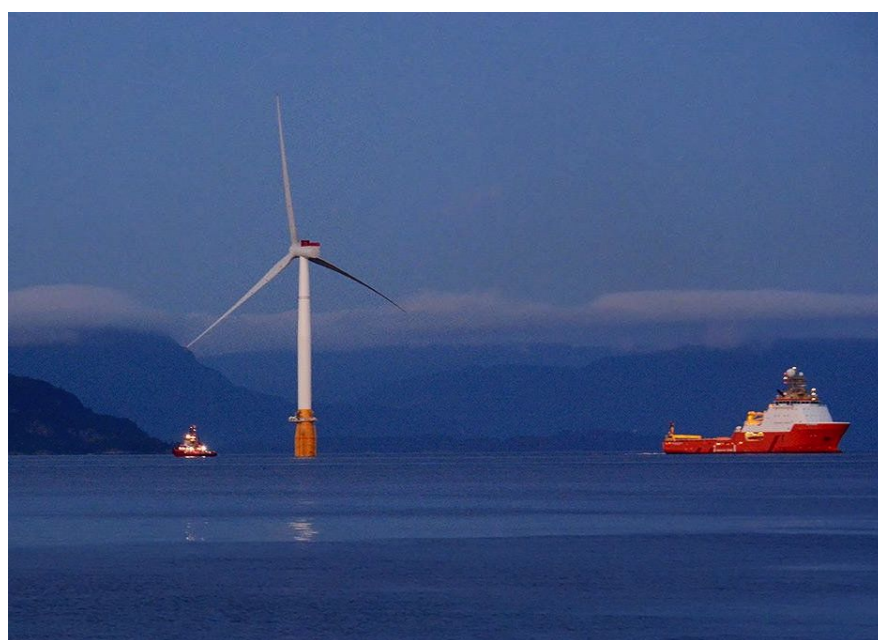
Figure 1.10: *Hywind floating wind turbine, Statoil desing.*

Figure 1.11: *Physical test of a wind turbine in IH Cantabria wave basin.*

influenced by the mooring system, and the other degrees of freedom are mainly affected by the floating platform characteristics. This dynamic response and the best substructures design and the best mooring systems set up have to be evaluated for each site and wind turbine so the design process becomes more and more challenging. Building a structure in deep waters requires high standards and the analysis needs experiments. Scaled physical modelling in a laboratory (Fig. 1.11) is still the key method in the design of ocean structures. Usually small-scale prototypes have been tested in a wave basin (56) (80) (23). This approach can reduce the uncertainty of the structural response of a structure and it is especially necessary when the structures are non-conventional or present three-dimensional effects. Nevertheless, this approach presents certain limitations: intrusive measuring devices, scale effects and high costs (in time and money) of the experiments.

These studies can also be carried out in an analytically/numerically way with the simplified wind turbine geometry and the analytically derived wind/wave loads (79)(45)(39)(17), or by the combined use of CFD, hydro, FSI (fluid-structure interaction) or/and MBD (multibody dynamics) codes (88)(37)(36). In case of numerical simulation, 3D full Navier-Stokes equations were rarely used because extremely long slender mooring lines not only require a large simulation domain but cause high turbu-

lence flow around them (34).

Besides, in order to obtain accurate numerical results, the model must be validated to prove that it is capable of reproducing the processes of interest. Moreover, if the model depends on calibration parameters, they need to be adjusted. In either case this is to be performed by comparing the model results with experimental results. In conclusion, numerical modelling must be regarded as a tool complementary to the physical modelling. The combined use of both techniques can help to identify the pros and cons of each method as there are processes that can only be replicated experimentally or numerically because of their time or space requirements. Within this symbiotic framework, numerical modelling unveils its full potential with two main roles: assisting with the pre-design of the physical experiments, and extending the experimental database with detailed results after validation (26). Furthermore; numerical modelling is significantly cheaper than physical experiments and it can be applied as a tool to characterise the hydrodynamics around the structure beforehand to highlight the zones of interest, to find the most suitable places where the measuring devices can be placed, to anticipate problems or even to select the most relevant cases to be tested physically. Once numerical models have been validated, they can be applied to extend the database, simulating different wave conditions and structural alternatives at the same time. Moreover, the new cases can be run at prototype scale, avoiding scale effects, hence, reducing the uncertainty linked to this kind of calculations.

In conclusion, it is possible to say that advanced numerical modelling of sea loads and floating structures interaction still offers a wealth of challenges and research opportunities. This thesis is devoted to overcome some of the most pressing challenges to make three-dimensional numerical modelling available for the offshore and harbour engineering community.

1.2 Structure of the Thesis

The present document is structured as follows: This introductory chapter serves to highlight the topics studied in this thesis, stressing the advantages that three-dimensional numerical modelling could offer to the design of floating offshore and coastal structures.

In Chapter 2; a review of the state of knowledge in numerical modelling of waves interacting with structures is presented. First, the literary review focuses on the different types of models, comparing the pros, cons and limitations of each approach. Then it

1. INTRODUCTION

defines the objectives of the present work according to the gaps found in state of the art.

In Chapter 3; OpenFOAM, the computational fluid dynamics (CFD) code used in this study is illustrated. Full details are given on the equations solved and how the model operates. Next comes the description of the boundary conditions that have already been developed for wave generation and absorption in IHFOAM tool.

Chapter 4 is devoted to the new features developed and added to the code to achieve the proposed goals. I.e. a new turbulence model and new boundary conditions for generating and absorbing waves in deep water and a new mooring system equation added to the code.

In Chapter 5; all the tests carried out to calibrate and validate the new code are illustrated, and the capabilities of it are demonstrated. First, the interaction between a floating caisson and waves is tested. Next, simultaneous wave and current generation is showed and different floating structures are tested.

Chapters 6 is where the previous methodology is incorporated into a global methodology that enables the simulation of wave interaction with real floating structures. The new methodology is applied to a floating offshore wind pilot park situated in Mazara del Vallo, Sicily, Italy.

Finally, the conclusions of all the work are discussed in Chapter 7, analysing the results obtained for the initial objectives.

2

Objectives of the Thesis and State of Art

2.1 Objectives of the Thesis

As listed in the previous chapter, numerical modelling plays a very important role when designing floating structures, both at harbours and offshore. Open source Computational Fluid Dynamics codes are not yet in a ready to use state, there is not at the moment a unique code able to analyse the entire floating system, from the structure response to the mooring systems tensions. So the aim of my Ph.D. research was to implement and validate a tool able to simulate the entire floating system and to assist offshore and harbour engineers during the design phase. In other words, the objectives of this work was to fill the gaps that have been found in previous studies and to enhance features that currently the code used, i.e. OpenFOAM, has, in order to make it a fully validated and ready to be applied tool in the design process of real coastal structures tool.

The objectives of this work and the methodology to achieve them are listed below.

The first objective was to prepare a numerical wave basin to test every kind of coastal, harbour and offshore structure. To do that, OpenFOAM has been chosen, because it is an open source and suitable to be implemented and improved. Then in order to create and absorb waves IHFOAM tool was selected because it had already the active wave absorption included, that is very useful to reduce domain sizes. This tool however, has been validated just for shallow and intermediate water conditions.

So, for this work the first thing to do was to check the feasibility of it in deep water

and to adjust it, because at the end, the model has to be universal, able to simulate any kind of sea state conditions, all over the relative water depth regimes.

To achieve this goal new boundary conditions were implemented in IHFOAM in order to generate and absorb wave in deep water conditions too. After several validation tests, wave decay phenomena was observed, so a new turbulence model was studied and added to OpenFOAM and IHFOAM in order to avoid this problem.

These new numerical features were validated with analytical and experimental tests, as it demonstrated their efficiency.

At the end of this part the numerical wave basin was ready to use for every kind of sea state and water depth simulation.

The second objective of the thesis was to create an OpenFOAM based tool able to represent a floating system, both the structure and the mooring lines hit by waves.

At present, all CFD simulations concerning these type of structures have been carried out by other specific and licensed codes.

The already implemented features in OpenFOAM were tested and checked in order to know which parts needed improvements. Floating bodies simulations were considered in the code, but not yet ready for ocean engineering purposes. So the first step to achieve this objective was to couple floating bodies setting with wave generation and absorption.

After that the way to represent mooring systems in the code was evaluated. As it was implemented, it didn't work properly, so a new mooring equation was added to the solver and validated with experimental tests.

The results showed very good agreements, so the second goal was reached. The new code was able to represent real floating anchored structures in both shallow and deep water.

Finally, the code was ready to work as a physical wave basin, the last thing was to apply it the simulations to real structures at prototype scale and demonstrate the forcefulness and potentiality of it. For this last objective, a floating wind turbine was analysed and simulated for an offshore site in the Mediterranean Sea.

In this way, it was demonstrated that the model would be suitable for a wide range of applications, from harbour floating piers to offshore spar buoys. Furthermore, the possibility of simulating real structures opens new perspectives for design purposes.

The new methodology, with active absorption, lead to reduce the domain covered by the 3D model and to simulate the detailed interaction between sea states and the

structure in competitive times. Generally three-dimensional models present long run-times and they require intensive computational resources. Therefore in order to obtain the most suitable conditions to integrate the model in real designs is by reducing both, so the numerical model can be integrated in the design process of floating structures.

By achieving this objective the engineers benefit from an advanced tool to assist in making decisions and to obtain more optimal designs.

2.2   State of art

The numerical simulation of free surface flow problems is a challenging topic, let alone with the presence of a moving structure, however, it has been of considerable importance to the development of offshore structures. Several types of models are commonly seen in numerical simulation of the non-linear waves and wave-structure interaction. These models can be categorised as, either, Boussinesq, potential flow, or Navier-Stokes-type models, referring to the governing equations driving the model. Boussinesq-type models have been widely used to solve free surface flows since the computational costs are reasonable and the accuracy of the approximation of water waves is valid for linear and weakly nonlinear waves, given that the wavelength is large compared to the water depth. A review of the developments of these types of models, as well as the description of a state-of-the-art model, is given by Madsen et al. (48). Potential flow theory has been very successful in modelling the wave loading on offshore structures and has become a standard tool in ocean engineering. The potential solver WAMIT is based on linear and second-order potential theory and is considered one of the best of its class. This is just one of the industries many state-of-the-art numerical models which are based on the potential flow theory, two other good examples are AQUAPLUS and AEGIR. These potential flow models in general well equipped to calculate first and second order wave loads and fluid-structure interaction at acceptable computational costs. They are very useful for demonstrating the initial feasibility of a floating structure. For instance by identifying the natural frequencies of the system, which, in order to minimise the dynamic response, need to be placed away from the wave spectrum. However, for the investigation of the strongly nonlinear hydrodynamics phenomena involved with wave-structure interaction during extreme wave events, the potential flow theory is inadequate and fully non-linear numerical methods are required. The advancements in computational power in the last years have paved the way for fully nonlinear CFD models. These solve the Navier-Stokes equations in combination with the continuity

equations to compute strongly nonlinear wave loads, fluid-structure and in some models it is even possible to simulate surface effect such as wave breaking. The Navier-Stokes-type models can either be meshless or grid-based, each of these types has its own advantages and disadvantages. A major distinction between the two is the need for an additional equation to describe the free surface. In a grid-based model the Navier-Stokes equations by themselves are unable to fully describe the interface of a two-phase flow. Therefore, an additional equation needs to be introduced. Methods for describing the free surface in multiphase flows can be categorized as Lagrangian-type surface methods and Eulerian-type volume methods, also referred to as surface tracking and surface capturing methods. The surface tracking methods are based on a representation of the free surface by special marker points, this allows for explicit tracking of the interface. Interpolation is used to approximate the points between marker points. The advantage of this approach is that the position of the interface is known and that the interface remains sharp as it is advected across the domain. However, these models experience problems when simulating coalescence and breakup of the interface, so, for instance when a droplet of water is dropped into a bucket filled with water, or more apt, when wave spray is caused by a large wave colliding with an offshore structure.The most widely used surface tracking method is the level-set method developed by Osher et al. (60). Here, the interface is defined as a zero level of a signed distance function from the interface. To distinguish between the fluids on either side of the interface a negative sign is attached to the distance function for one of the fluids. The level-set methods are conceptually simple, relatively easy to implement and yielding accurate results. However, the method is known to experience loss of mass when the interface is significantly deformed or when there is considerable vorticity. In contrast to surface tracking methods, the surface capturing methods support an implicit tracking of the free surface of a two-phase flow. These approaches mark the fluid on either side of the interface, either by massless particles or by an indicator function. One of the drawbacks of these techniques is that the exact position of the interface is not known explicitly and special techniques are needed to reconstruct the interface. The most widely used surface capturing method is the Volume of Fluid (VoF) method (29). Here, a scalar indicator function between zero and one, known as volume fraction is used to distinguish between two different fluids. The free surface is treated as the transitional layer between the two fluids. Due to the diffusive nature of this method, special interface compression techniques are developed to maintain the sharpness of the interface. A major advantage of this method is that, in contrary to the level-set method, it is mass conserving and a

far more robust approach to when it comes to the simulation of coalescence and breakup of the interface. Navier-Stokes-type models coupled with a VOF method for capturing the free surface are a commonly seen combination in the field of fluid mechanics. They form one of the more robust methods for simulating the highly nonlinear phenomena caused by fluid-structure interaction during extreme wave events. A couple of state-of-the-art commercial software CFD packages are based on the combination of these two models. Note that these software packages are generally not single purpose, but instead designed for a broader spectra of fluid mechanics problems. There are many researches in which commercial software was utilised for the analysis of floating offshore structures, as STAR-CCM+, a commercial CFD package, developed by CD-Adapco and ComFLOWis another commercial state-of-the-art, Navier-Stokes/VOF solver. In addition to commercial software packages, some open-source models are available which can be of great scientific value if they have a progressive community. Open Field Operation And Manipulation (OpenFOAM), is an excellent example of such an open source CFD package. The standard OpenFOAM software package is distributed with a large number of solvers and utilities to cover a wide range of problems. Due to the open-source nature of OpenFOAM, it is possible for users to write their own codes and solvers for their specific problems or to modify the existing solvers.

3

OpenFOAM

3.1 Introduction

Floating structures are widely adopted in offshore engineering, because the necessity to exploit resources from offshore is increasing. For example, floating wind turbine technology would open up a large majority of the continental shelf as a wind power resource. Floating oil-platform technology can provide a basis for design; however further study is required as the floating systems need to be stable, structurally sound, and economical (76). Understanding the behaviour of a floating structure in a real sea state is as difficult as important to determine its performance and resistance (40) (62). Designing new floating structures engineering requires detailed knowledge of forces, flow directions and velocities, rotations and displacements. Traditionally, this was done in towing tank, but in the last years computational fluid dynamic (CFD) methods developed to a stage, where they become interesting, not only from a financial but also from a performance point of view, as an extra input or a full alternative to the experiments. Several dodes have been implemented, one of the opensource is OpenFOAM: it offers a possibility to include a modern CFD method without expensive investments into the design process.

3.2 Computational Fluid Dynamics

Since for most complex flow situations an analytic solution is not available, ruleof-thumbs are not detailed enough and experiments are expensive, computer generated solutions become more and more popular with increasing computational power and better mathematical models. Computational fluid dynamic (CFD) is a branch of fluid mechanics that uses numerical analysis and algorithms to solve and analyze problems

that involves fluid flows. The fundamental bases of almost all CFD problems are the NavierStokes equations. The finite volume method (FVM) is a common approach used in CFD codes, as it has an advantage in memory usage and solution speed, especially for large problems, high Reynolds number turbulent flows, and source term dominated flows (like combustion).

3.2.1 Governing Equations

In the finite volume method, the governing partial differential equations are recast in a conservative form, and then solved over discrete control volumes. This discretization guarantees the conservation of fluxes through a particular control volume. The RANS equations, which include continuity and mass conservation equations, are the governing mathematical expressions which link pressure and velocity. The assumption of incompressible fluids has been used, which is applicable for most coastal engineering practical problems.

$$\bigtriangledown U = 0 \tag{3.1}$$

$$\frac{\partial \rho U}{\partial t} + \bigtriangledown(\rho UU) - \bigtriangledown(\mu_{\text{eff}} \bigtriangledown U) = -\bigtriangledown p^* - gX \bigtriangledown \rho + \bigtriangledown U \bigtriangledown \mu_{\text{eff}} + \sigma k \bigtriangledown \alpha \tag{3.2}$$

where ρ is the density, which is calculated as presented in Eq. 3.4, U is the velocity vector; p* is the pseudo-dynamic pressure; g is the acceleration of gravity; X is the position vector. The last term on the right is the effect of surface tension: σ is the surface tension coefficient; k is the curvature of the interface and it is calculated as follows:

$$k = \bigtriangledown \frac{\bigtriangledown \alpha}{|\bigtriangledown \alpha|} \tag{3.3}$$

and α is the indicator function, which will be commented later. Finally μ_{eff} is the efficient dynamic viscosity, which takes into account the molecular dynamic viscosity plus the turbulent effects: $\mu_{\text{eff}} = \mu + \rho \nu_{\text{turb}}$. The newly introduced ν_{turb} is the turbulent kinetic viscosity, and it is given by the chosen turbulence model (as described in the next section). The different fluids are identified by the indicator function α which is bounded between 0 and 1. $\alpha = 0$ means air phase, and $\alpha = 1$ water phase. A value of 0.5 would thus mean the cell is filled with equal volume parts of both fluids. Intensive

properties of the flow like the density ρ are evaluated depending on the species variable α and the value of each species ρ_b and ρ_f:

$$\rho = \alpha\rho_f + (1 - \alpha)\rho_b \tag{3.4}$$

The transport equation for α is:

$$\frac{\partial \alpha}{\partial t} + \bigtriangledown(U\alpha) = 0 \tag{3.5}$$

The interface between the two fluids requires special treatment to maintain a sharp interface, numerical diffusion would otherwise mix the two fluids over the whole domain (27). More information on general CFD methods can be found in (83). OpenFOAM makes use of an artificial compression term ($\bigtriangledown U_c\alpha$ (1 -α)), instead of using a compressing differencing scheme. This approach is conservative and takes non-zero values only at the interface. Furthermore the flow is not compressed if Uc is normal to the interface $\bigtriangledown \alpha$, which points towards greater values of α, and therefore from the air to the water phase. This yields the final expression:

$$\frac{\partial \alpha}{\partial t} + \bigtriangledown U\alpha + \bigtriangledown U_c\alpha(1 - \alpha) = 0 \tag{3.6}$$

in which |Uc| = min[cα |U|, max(|U|)], where the user can specify factor cα. By default it takes value 1, but it can be greater to enhance the compression of the interface. The boundedness of such equation is achieved by means of a especially designed solver called MULES (multidimensional universal limiter for explicit solution). It makes use of a limiter factor on the fluxes of the discretised divergence term to ensure a final value between 0 and 1 (27).

3.2.2 Turbulence modeling

The Reynolds stresses have to be modeled, when a RANS method is used. Most turbulence models are based on the eddy viscosity concept where the effect of the turbulence on the flow processes is described by an increased viscosity. The Reynolds stresses are then defined by the so called Boussinesq Hypothesis which is represented by Equations below, where k is the turbulent kinetic energy.

$$\tau_i j = -\rho\overline{u_i'u_j'} = \mu_i(\frac{\partial U_i}{\partial x_j} + \frac{\partial U_j}{\partial x_i}) - \frac{2}{3}k\rho\delta_i j \tag{3.7}$$

$$k = -\frac{1}{2}\overline{u_i' u_j'} \tag{3.8}$$

$$\mu_t = -\rho C_\mu L\sqrt{2k} = C_\mu LV \tag{3.9}$$

μ_t is the turbulent viscosity and can be written as above including the constant C_μ, the turbulent velocity V and the length scale for large-scale turbulent motion L. To calculate V and L it is necessary to express k and μ_t. The different approaches to do this divide the models into algebraic, zero-equation, one-equation and two-equation models, which are all linear eddy viscosity models. Industry standard and the most widely used models are the two-equation models, because it is quite simple to implement these kinds of RANS equations into a CFD program. It is basically the same code as for laminar flow, but has two differences:

- $\mu_{\text{eff}} = \mu + \mu_t$
- Solving of two transport equations extra.

In this work, both the k-ϵ model and the k-ω model have been used, maybe the most used and known method in CFD simulations. Talking about the first one, based on the fact that kinetic energy is dissipated into internal energy at high Re another way of computing the turbulent length is using the turbulent dissipation $\epsilon(= 3k/2L)$. This turbulent model is based on the equation:

$$\mu_t = -\rho C_\mu \frac{k^2}{\epsilon} \tag{3.10}$$

Instead, in the k-ω model, the eddy viscosity, ν_t, is given by:

$$\nu_t = \frac{k}{\omega} \tag{3.11}$$

3.2.3 OpenFOAM

OpenFOAM (Open Field Operation And Manipulation) is a free and open source finite volume CFD toolbox originally developed at the Imperial College by (31) and (72). It is a cell-centred finite volume framework for computational fluid dynamics supporting unstructured polyhedral meshes. OpenFOAM consists in a bundle of libraries and codes to solve complex problems such as turbulence, fluid flows, electromagnetics, chemical reactions, combustion... It also features applications to pre- and post- process, including

mesh generation tools (e.g. blockMesh, snappyHexMesh), setting and modifying field values, mesh decomposition and sampling data . It is prepared to run cases in parallel, allowing an easy set up and a straightforward calculation method (59).

The code is written in C++ and is object oriented. Unlike commercial codes Open-FOAM is not a black box, the user can control and modify each of the steps of the solving process by changing the source code. This is a great advantage, since several modules include data conversion from and to commercial CFD codes (Ansys, Fluent, CFX) or formats (VTK), allowing cross validations. Other extended capabilities are added by third party programmes. The most representative case is undoubtedly Kit-ware's ParaView, which is the main programme used for postprocessing purposes since it has two specific readers for native OpenFOAM data. As mentioned above, meshing tools are included in OpenFOAM: blockMesh and SnappyHexMesh. Starting with a block structured mesh that defines the extensions of the domain, created by the means of the first tool, SnappyHexMesh then can include automatically any .stl file (stereo lithography), which describe the geometry of modelled objects. The solver then starts to split all cells close to the .stl surface. When the refinement is finished, all cells inside the .stl are removed. The user defines the outside with a Cartesian coordinate before-hand. Specific refinement regions (boxes, cylinders or spheres) can be assigned. It is useful to emphasize specific parts of the domain, like the area around the floating structure. Furthermore, SnappyHexMesh incorporates many parameters to ensure a good quality mesh. To adapt the changing computational domain when simulating moving bodies, different algorithms are available. OpenFOAM supports mesh morphing six degree of freedom (6-DoF) body motion. A 6-DoF solid body can be specified through a boundary condition on a patch prescribing the boundary of the solid body. With the dynamic mesh method the mesh quality around the body is preserved without per-forming expensive remeshing even when simulating arbitrary angles of rotation. Mesh deformation can mathematically be considered as a map between the domain D, which represents the configuration at a certain time t with a boundary B, and D' at times later (33) (32). The idea is to move the points on the body and the cells neighbouring it, as it is not possible to move only a few points in the mesh without destroying the shape of the cells, the neighbouring points needs to be moved as well, this is done by the motionFvSolvers by a diffusion algorithm. The mesh update that follows right after the implementation of the movements resets the mesh and it is therefore crucial to assign the accumulated displacement at each step. In version 2.3.0, the one adopted in this study, the rigid body motion framework uses a specialized motion solver, which works

with an interpolation of displacement and rotation based on the distance to the object to move. The interpolation method is spherical linear interpolation, or Slerp, which enforces smoothness and the distance function has a cosine profile to preserve shape of cells close to the moving surface.

3.2.3.1 Dynamic Mesh Approach

The fluid structure interaction (FSI), in OpenFOAM, is managed through the dynamic-MotionSolverFvMesh. This solver morphs the mesh around a specified set of boundaries. The meshing motion is calculated based on the pressures on those boundaries. In turn, the dynamicMotionSolverFvMesh provides feedback to the fluid simulation. It alters the velocity boundary conditions (U field) on the included boundaries to specify the local velocity of the defined body. This mesh control is almost exclusively used to solve problems involving rigid body motion.

Moreover, when simulating moving bodies, to adapt the changing computational domain , different algorithms are available in CFD models. OpenFOAM supports mesh morphing six degree of freedom (6-DoF) body motion. A 6-DoF solid body can be specified through a boundary condition on a patch prescribing the boundary of the solid body. With the dynamic mesh method, the mesh quality around the body is preserved without performing expensive remeshing even when simulating arbitrary angles of rotation. The mesh deformation problem can be stated as follows. Let D represent a domain configuration at a given time t with its bounding surface B and a valid computational mesh. During a time interval Δt, D changes shape into a new configuration D'. A mapping between D and D' is sought such that the mesh on D forms a valid mesh on D' with minimal distortion of control volumes (32). As it is not possible to move only a few points in the mesh without destroying the shape of the cells, the neighbouring points needs to be moved as well, and this is done by the motionFvSolvers by a diffusion algorithm.

Polyhedral FVM discretises the space by splitting it into convex polyhedra bounded by convex polygons. Temporal dimension is split into time-steps and equations are solved in a time-marching manner. Having resolved the issues of discretisation support and data mapping, it remains to determine the motion of mesh points in response to prescribed boundary motion, ideally in an automated manner. The overriding criterion for the success of automatic mesh motion is mesh validity: an initially valid mesh must remain valid after deformation. In terms of FVM metrics, this condition reduces to positivity of cell volumes and face areas, preservation of cell and face convexness and
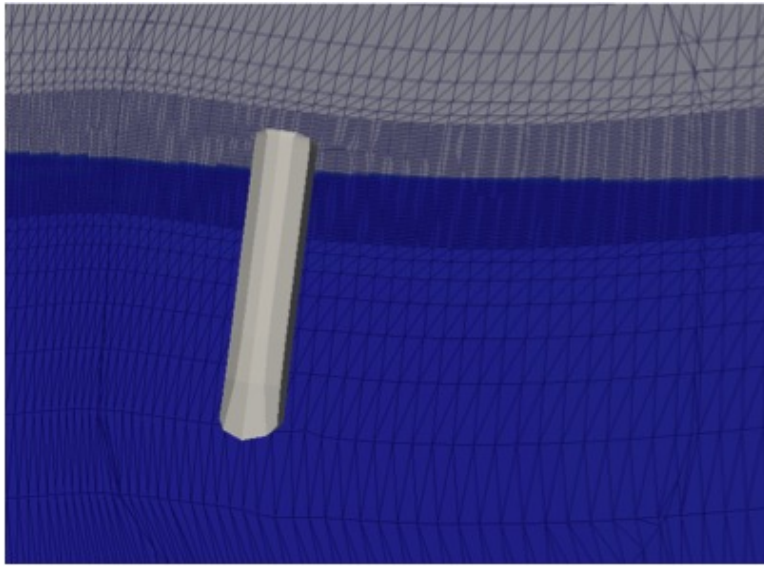
Figure 3.1: *Dynamic Mesh Approach in OpenFOAM.*

mesh non-orthogonality bounds. Also while the mesh is deforming, the quality mesh parameters have to be kept in the correct range, as Face and cell aspect ratios, the cell volumes, the mesh non-orthogonality and the skewness.

Furthermore, dynamic mesh refinement allows to refine the cells in a coarse mesh at specific regions, the moving ones, that requires smaller cells (Fig. 3.1). It is a good way to get accurate results with reduced computational time in comparison to a total refined static mesh. The coarse mesh should be refined enough to give an accurate result outside the region that requires small cells. In two-phase flow, the refinement should be on the interface between the fluids because of the steep gradients in the volume fraction function and potentially the material properties of the fluid system, and if a floating structure is simulated, the refinement has to be around it too.

The solver employed in this study is the interDyMFoam. It solves the three dimensional Reynolds Averaged Navier Stokes (RANS) equations for two incompressible phases using a finite volume discretisation and the volume of fluid (VOF) method and it handles dynamic meshes (DyM stands for it). Hence it can simulate floating body movements or dynamic mesh refinement along the free surface. On the fluid-structure interface a moving wall boundary condition is applied for the fluid velocity field in order to ensure the no-slip condition. The spatial discretisation is based on arbitrarily unstructured meshes which consist of arbitrary convex polyhedral cells. These cells have to be continuous, which means they do not overlap with each other. The main control

over time step is the Courant number, which represents the portion of a cell that the flow will transverse due to advection effect in one time step. The Courant number has the following form for the one dimensional case (15):

$$C_o = \frac{\partial t U}{\partial x} \tag{3.12}$$

where, ∂t is the maximum time step, ∂x is the cell size in the direction of the velocity and U is the magnitude of the velocity at that location. To ensure stability of the model and improve accuracy, the maximum value of the Courant number should be 1 throughout the whole domain; in this work, the Courant number was set below 0.3 for all the tests.. Based on the computational mesh, the Navier Stokes equations are subsequently discretized into a set of algebraic equations, which are pressure and velocity equations in the PIMPLE algorithm (59). The PIMPLE algorithm is composed of an implicit momentum predictor and several pressure velocity correctors. In the PIMPLE loop, the velocity equations are firstly solved by using the velocity and pressure fields of the previous time step, known as momentum predictor. The velocity and pressure are corrected several times afterwards to satisfy mass conservation. Many methods are offered by OpenFOAM to solve the set of linear equations, such as the geometric algebraic multi grid (GAMG) and faster diagonal incompletecholesky (FDIC) methods. Additionally, there are several built-in numerical schemes in OpenFOAM to discretize terms that may be found in a PDE, such as derivative terms. The Standard Gaussian finite volume integration method, which based on summing values on cell faces, is usually used to get higher accuracy of the integrations for derivative terms. The values on cell faces are interpolated from cell centres. There are several interpolation schemes, such as central differencing, upwind differencing and blended differencing methods, are provided for users to choose on a case-by-case basis. The time integration of the 6 DOF body motion ordinary differential equations (ODE) is performed using a special symplectic integrator, which is characterized as a leapfrog time integration method. This ensures the correct two-way coupling between the body motion and the transient solution of the flow equations.

This solver adopts an adaptive time step depending on the Courant number. To choose the new time step, a maximum Courant number is calculated from the flow conditions, using U and ∂t from the previous time step.

To work with interDyMFoam, many parameters have to be defined. The mass properties of the entire body, the centreOfMass is the centroid of the Body, in the world

coordinate system at initial position. The momentOfInertia defines the moment of the inertia of the body in the three principal axes (x, y, z).

Three solver types can be selected: Newmark and CrankNicolson, that are second order implicit solvers, and symplectic that is a second order explicit solver. More information is available on the OpenFOAM source documents. Here, the Newmark solver was adopted.

The boundary conditions must be set with specific keywords to use the information from the 6DoF solver. This provides the feedback. The surface velocities from the 6DoF Body are supplied as boundary conditions to the fluid solver. The velocity condition is specified as a movingWallVelocity. The uniform value of zero only applies to the initialization. The boundary will be overwritten with calculated velocity values from the 6DoF solver on the next timestep and going forward. The pointDisplacement is necessary for the mesh morphing. This must be set to type of "calculated". This will tell the mesh morpher to look at the 6DoF solver results to perform the morphing. Specifically, the library writes a field file called pointDisplacement and another field called pointMotionU. These are used to perform the mesh morphing. They can also be viewed as an output. The pressure field is specified as a zeroGradient. This is typical for normal wall boundaries.

The motions of floating bodies are computed by the native rigid body solver that uses a nested explicit leap-frog time step within each PIMPLE loop. Resulting forces and moments are collected from integration of the pressure force, p_n, and shear force vector s over the body surface S.

Here FM is the mooring force and position vectors r_{CM} and r_{CS} denote the vector from the centre of mass to the mooring attachment point and the centre of each surface panel respectively.

InnerDistance and outerDistance parameters have to be specified too. These control how the sixDof solver morphs the mesh. Anything within the innerDistance directly moves the mesh nodes as a rigid body. Between the innerDistance and outerDistance, the mesh nodes are morphed. Outside the outerDistance, no morphing occurs.

3.2.4 IHFOAM

To generate waves and currents in the numerical wave tank, IHFOAM boundary condition tool based on OpenFOAM, developed by the Environmental Hydraulics Institute, IH Cantabria, Santander, Spain was applied. IHFOAM (27) is an open source numerical model to simulate waves and wave interaction with coastal structures. IHFOAM

solves the three-dimensional Reynolds Averaged Navier - Stokes (RANS) equations, for two incompressible phases (water and air) using the Volume of Fluid (VOF) technique to track the water surface. It incorporates a set of algorithms to generate and absorb waves at the boundaries without the use of relaxation zones, speeding-up the simulations and ensuring a correct representation of the wave-induced hydrodynamics in the numerical domain. Moreover, it supports a large number of turbulence models (e.g. k-ϵ, k-ϵ SST and LES). The features that make this model unique include wave generation and active wave absorption (27) working at static and moving boundaries. Therefore, the computational cost does not noticeably increase, unlike for internal methods.

Based on the experience achieved with Navier-Stokes models simulating waves only, it is concluded that accounting for wave reflection is relevant not only at the generation boundary but also at the inner boundary where there is a need to cancel out reflected waves generated as a consequence of the interaction of waves with solid or porous bodies. Both features need to be treated simultaneously not only at the waves- current generation boundary but also at every boundary of the numerical domain. There are mainly two techniques to simulate waves in numerical Navier-Stokes models. The first makes use of a Dirichlet-type boundary condition for the velocity field at the inflow boundary to create a wave-current flow field. Free surface is also defined at that boundary. The second makes use of an internal flow generator, which induces an increase of mass or momentum in the domain to generate the target combined waves and current flow.

Active wave absorption is needed to absorb the waves incident to the wave paddles, which will reflect back into the domain, otherwise. This system prevents an unbounded increase in the agitation, that will contaminate the results. In order to perform the absorption, the position of the paddles is corrected every time step according to a given feedback. There are different techniques available in literature depending on the feedback used, for example, the measured free surface elevation at each paddle (74) or in front of them (14), or even the force acting on the wavemaker (73). The absorption procedure developed in IHFOAM is based on a two-dimensional approach that appears in (74), the same applied in (27). The underlying assumption is linear theory in shallow water (i.e. nondispersive waves), although more sophisticate approaches are available in literature (85) to account for wave dispersion. The starting point is a simple digital filter, as follows:

$$U_c = -\sqrt{\frac{g}{h}}\eta_\mathrm{f} n \qquad (3.13)$$

where U_c is the correction velocity that will absorb the incident wave, positive when pointing towards the inside of the domain; g is the acceleration due to gravity; h is the water depth; η_f is the free surface elevation incident to the boundary, calculated by subtracting the measured (actual) elevation at the wavemaker from the target (expected) one; and n is a unit vector normal to the boundary and pointing inwards to the domain. As it can be noted, the bold variables indicate vectors. Therefore, the correction velocity will yield the following correction in paddle displacement (ΔX_c):

$$\Delta X_c = U_c \Delta t \tag{3.14}$$

The negative sign in Eq. 3.13 indicates that to absorb a wave crest ($\eta_f > 0$) the velocity must be negative, causing a paddle movement that stretches the domain towards the outside.

The Dirichlet-type boundary conditions can indistinctly work with both static or dynamic meshes. The model uses a modified version of the OpenFOAM standard interFoam solver. In this work, IHDYMFOAM was used, it is the version of IHFOAM which handles dynamic meshes (DYM stands for Dynamic Mesh). The wave generation tool was already validated by (27) so here the validation was not needed.

4

First Approach to Floating Bodies Simulations with OpenFOAM

4.1 Model Set Up

In offshore deep waters, many floating concepts have been proposed to capture the abundant wind potential available. Out of the many solutions suggested, the major ones are the spar buoy, TLP, semisubmersible and barge type floaters. In the present study, the modeled system is a simplification of the systems mentioned before, also the water depth is limited, in order to lighten computational domain and make easier to test several configurations. The total system is modeled using one mass connected through a mooring line, to represent the concept of a TLP. In 3D space, the platform has six DOFs, surge, sway, and heave translations and the corresponding rotations of roll, pitch, and yaw. All the DOFs are coupled to each other. As the tendon mass is small compared to the mass of the floater, the inertia and hydrodynamic forces from the tendons are neglected in the equations of motion. The 6DOF model of OpenFOAM is used to simulate the motion of a rigid body in response to pressure and shear force exerted by the fluid, as well as to additional forces defined by the user, e.g. mooring line force. The model calculates the resultant force and moment acting on the body due to all influences, and solves the governing equations of rigid body motion to find the new position of the rigid body. The impact of this motion is transferred to the computational mesh. Hence at each time step of the solution algorithm, the fluid-structure boundary surface is displaced and reoriented in accordance with the total hydrodynamic plus external forces and torques on the structure. The solver of OpenFOAM adopted is interDyMFoam.

4. FIRST APPROACH TO FLOATING BODIES SIMULATIONS WITH OPENFOAM
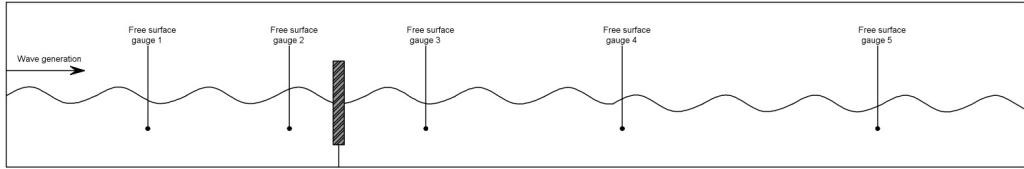
Figure 4.1: *Geometry of the numerical wave tank.*

4.1.1 Geometry and Mass Properties

In order to validate numerical results with McCormick experiments (52), the modelled structure is a vertical floating cylinder with a diameter of 0.2 m, a 1.5 m height, with a draft of 1 m and a mass of 31.42 kg. The centre of mass is located at the bottom of the cylinder and the radius of gyration are: $I_x=I_y=0.87$ m and $I_z=0.07$ m. Two kinds of tests were performed: i) free decay tests, in order to assess and validate the code with literature results (52), ii) simulation of the cylinder floating body forced by regular waves. In the first free decay test, the cylinder was unmoored in order to replicate McCormick data, then the moored one was simulate, and the same setting was adopted in wave-structure interaction simulations. In these last tests, the body was anchored to the bottom with a vertical mooring line, modeled as linear spring, with negligible bending stiffness. The numerical wave tank was 1.5 m deep and 2.5 m x 26 m wide.

4.1.2 Computational domain and settings

The computational mesh of the fluid domain was an unstructured hexahedral mesh. In the z direction, in order to better capture the free surface, the cell size was 0.0125 m, in x and y direction was 0.05 m. Around the body the mesh size was refined in all directions, by the means of snappyHexMesh tool, in order to better capture the motion of the body. The total number of cells in the mesh was roughly 877500 cells. The structure of the domain and the global mesh can be seen in the Figures 4.2, 4.3 and 4.4. The time step was set as 0.01 sec, but adjustable time step with a Courant number limit of 1 was used.

4.2 Free decay tests in heave

To evaluate the capabilities of OpenFOAM in simulate floating structures, hydrostatic validation were performed through free decay tests in heave. The linear motion for a
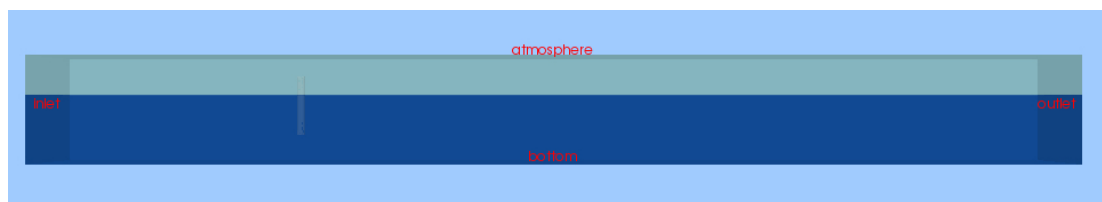
Figure 4.2: *Computational domain.*
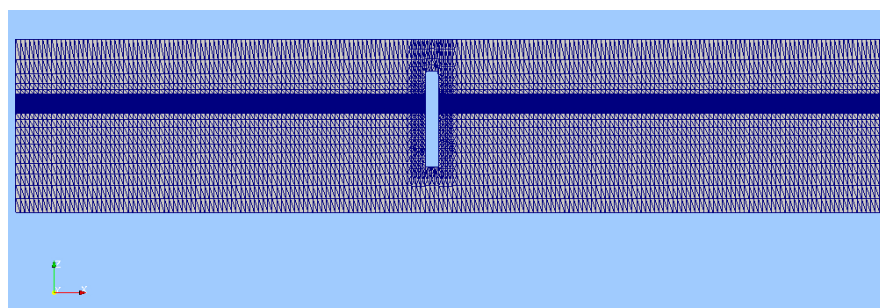

Figure 4.3: *Mesh refinements around free surface level and cylinder.*
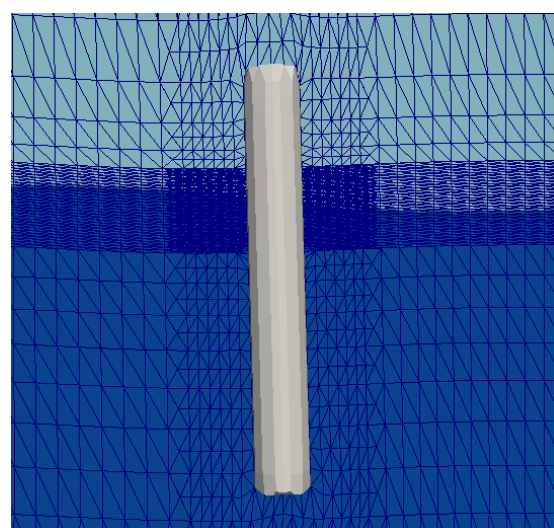
Figure 4.4: *Zoom on the Mesh refinements around free surface level and cylinder.*

purely heaving floating cylinder, in calm water, can be analytically predicted by the solution of the following homogeneous equation, where the time rate of change of linear momentum of a body must equal the sum of the external forces on the body:

$$(m + a_{wz})\frac{d^2z}{dz^2} + (b_{rz} + b_{vz})\frac{dz}{dt} + (\rho g A_{wp} + Nk_s)z = 0 \tag{4.1}$$

As calm water conditions are considered, external forces are 0. a_{wz} is the added mass, b_{rz} is the radiation damping coefficient, b_{vz} is the viscous damping coefficient, A_{wp} is the waterplane area when the body is at rest, k_s is the effective mooring spring constant of each line and N is the number of lines (52).

The most relevant hydrodynamic parameters are natural period, T_{nz}, and damping ratio, Δz, (1)(2). Their equations are listed below. The natural heaving frequency is mathematically represented by

$$\omega_n = \frac{2\pi}{T_{nz}} = \sqrt{\frac{\rho g A_{wp} + Nk_s}{m + a_{wz}}} \tag{4.2}$$

T_{nz} is the natural heaving period. A_{wp} for a vertical cylinder can be approximately calculated as πa^2. The critical damping coefficient is:

$$b_{cz} = 2\sqrt{(\rho g A_{wp} + Nk_s)(m + a_{wz})} \tag{4.3}$$

The logarithmic decrement is:

$$\ln(\frac{Z_j}{Z_{(j+1)}}) = \pi \frac{\Delta z}{\sqrt{1 - \Delta z^2}} \tag{4.4}$$

The resonant damping ratio is:

$$\Delta z = \frac{b_z}{b_{cz}} = \frac{b_{rz} + b_{vz}}{2(\rho g A_{wp} + Nk_s(m + a_{wz}))} = \frac{\ln(\frac{Z_j}{Z_{(j+1)}})}{\sqrt{\pi^2 + [\ln(\frac{Z_j}{Z_{(j+1)}})]^2}} \tag{4.5}$$

The viscous damping coefficient can be considered as:

$$b_{vz} = \frac{1}{2}\rho C_d A_d \tag{4.6}$$

The added mass can be found as

$$a_{wz} = \frac{\rho g A_{wz} + Nk_s}{\omega_{nz}^2} - m \tag{4.7}$$
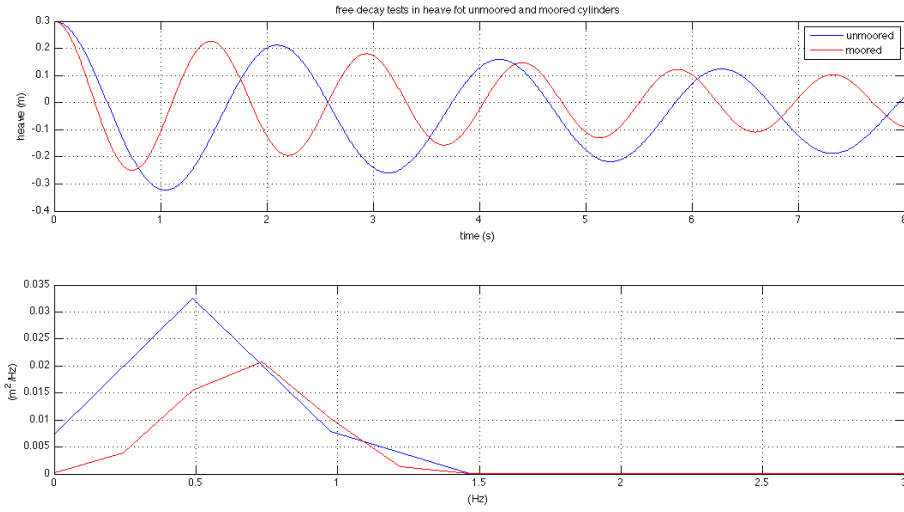
Figure 4.5: *OpenFOAM simulation results of free decay test for the unmoored and moored cylinder.*

4.2.1   Numerical Results

As written before, for this test, firstly the unmoored cylinder was implemented, in order to reproduce exactly the experimental data reported in (52). As it is possible to see in Table 4.1, OpenFOAM hydrodynamic parameters from the simulation agreed well with the experimental data. Second and third oscillation amplitudes were considered as Z_1 and Z_2 respectively, and then the hydrodynamic parameters were calculated and compared to the experimental ones. The imposed initial displacement, Z_0 , was 0.3 m. Then, the moored cylinder was simulated. The line stiffness, k_s, was set to 308 N/m. That value was calculated considering a line force equal to the difference between the weight and the buoyancy of the object. As shown in the Figure 4.5 and from hydrodynamic parameters, the natural damped period, Td, decreased and the critical damping coefficient, b_{cz}, increased, as predictable from analytical expressions. In fact, the natural damped period is inversely proportional to the mooring restoring force $(N*k_s)$, instead the damping coefficient is directly proportional to that force (Eqs. 4.13 and 4.14).

33

Hydrodynamic parameters	Experimental Data (McCormick, 2009)	OpenFOAM data unmoored cylinder	OpenFOAM data moored cylinder
Z_1 (m)	0.22	0.211	0.226
Z_2 (m)	0.17	0.16	0.18
T_d (s)	2.12	2.08	1.47
$\omega_{dz}(rad/sec)$	2.96	3.02	4.28
$\ln(Z_j/Z_{j+1})$	0.258	0.277	0.23
Δz	0.082	0.088	0.072
$\omega_{nz}(rad/sec)$	2.97	3.03	4.29
$a_{wz}(kg)$	3.43	2.09	2.13
$b_{cz}(Nsec/m)$	207.28	203.26	287.57
$b_z(Nsec/m)$	16.95	17.83	20.78
$b_{rz}(Nsec/m)$	1.08	1.14	1.32

Table 4.1: *Results from experimental and numerical data for the heaving vertical cylinder.*

4.3 Wave-Structure Interaction

After the validation of the code in calm water, wavefloating body interaction was simulated. The wave generation boundary condition, IHFOAM, a specific tool able to replicate laboratory wave maker, developed by IH Cantabria (27) (28), was included in OpenFOAM. In this way, the behaviour of the floating cylinder, hit by waves, was analyzed. Here, the body was moored to the bottom, with the same settings explained previously.

4.3.1 Numerical Results

For this study, two different regular wave conditions were generated:

-Wave1: wave height, H=0.25 m and wave period, T=1.5 sec;

-Wave2: wave height, H=0.3 m and wave period, T=2 sec.

These wave parameters were chosen to see the different responses of the cylinder when it is moved i) by a wave with a period equal to its natural damped period (Wave1) and ii) by a wave with a greater period (Wave2), Fig. 4.6. In order to keep unchanged the wave steepness, wave heights, associated with those periods, were calculated. As example of wave gauges signals, in Fig. 4.7, Wave1 simulation results are reported.

Results of both simulations can be seen in the Figures 4.6, 4.7 and 4.8: wave heights and cylinder heave displacements are plotted. To analyze the interaction between the floating cylinder and waves, the Response Amplitude Operator (R.A.O.) and phase
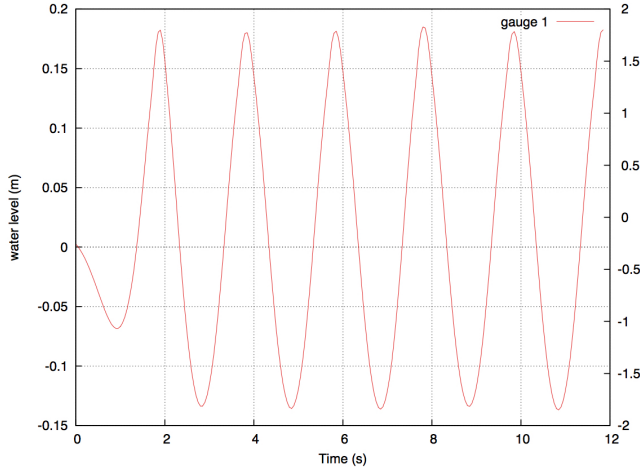
Figure 4.6: *Wave gauge 1 signals in Wave2.*

difference between the two series were calculated. These parameters are reported in Table 4.2 for each wave condition. It is possible to see that the Wave1 conditions induced larger movements, as the R.A.O. is 0.584. Instead, Wave2, with the period bigger than the floater's natural damped one, created smaller movements.
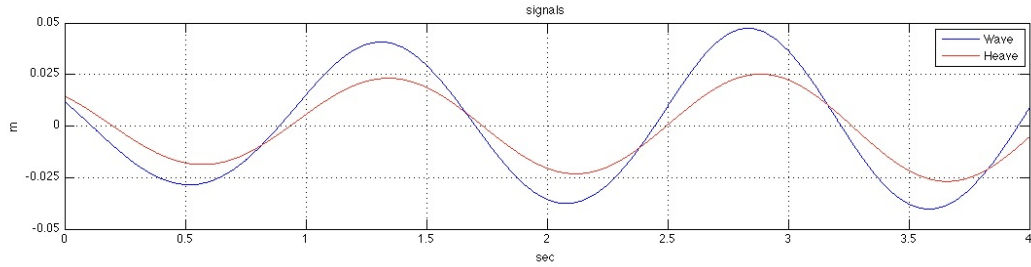
Figure 4.7: *Heave displacements and wave signals in Wave1.*
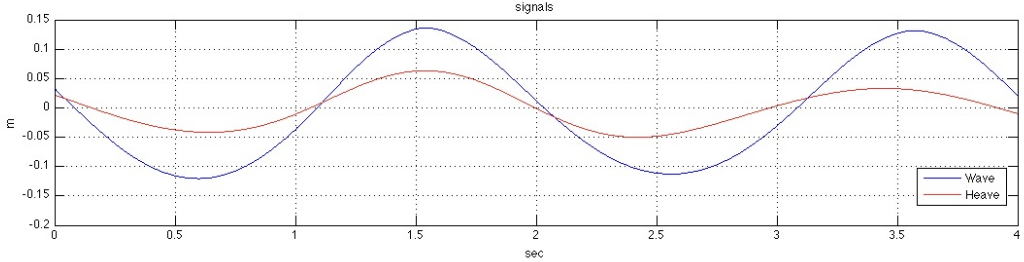
Figure 4.8: *Heave displacements and wave signals in Wave2.*

Case	H (m)	T (s)	R.A.O.	Phase difference
Wave1	0.25	1.5	0.584	-0.05
Wave2	0.3	2	0.375	0.02

Table 4.2: *Results from numerical data for wave-cylinder interactions.*

Another output of CFD model is video animation, in Figure 4.9 it is reported a snapshot series from Wave1 simulation.

4.4   Conclusions

The aim of this work was to validate OpenFOAM capability in simulating floating structureswave interaction, a topic for which this code was not implemented yet. We did it by the means of comparison between numerical results and experimental data, and we found out good agreements. So it is possible to conclude that OpenFOAM, with the wave generation tool IHFOAM, it is a valid and realible instrument to model not only coastal processes (28) or fixed offshore structures (13), but also floating bodies-wave interactions. One of the problem could be the dynamic mesh approach to moving parts of the domain, but thank to that simulations, it was possible to understand that for moored structures that have limited displacements this approach can manage perfectly that kind of tests. This innovative application with OpenFOAM represents the first step to develop a numerical wave tank where it is possible to study wave- floating structure interaction, as an extra input or a full alternative to the experiments in design process.
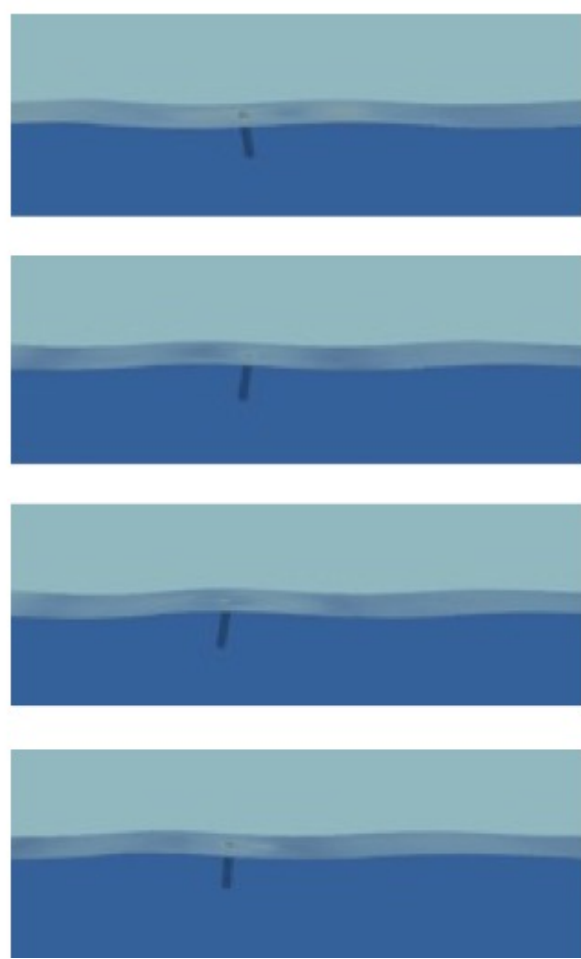
Figure 4.9: *Chronological series of snapshots from the Wave1.*

5

New Developments of the Numerical Code

5.1 Introduction

The numerical code used in this work was OpenFOAM with IHFOAM tool, as already explained in the previous chapter. This code was not applied yet to offshore studies, and it had not been set up and validated for deep water conditions. So, when this work started, some problems in terms of wave generation and absorption came out. As the aim of this Ph.D. was to implement a numerical wave tank able to simulate every kind of sea conditions, I initially dealt with these issues. New boundary conditions were developed and added to IHFOAM tool, then a different turbulent model was implement in OpenFOAM. Furthermore, a new numerical restraint was added to the solver interDyMFOAM, in order to be able to represent a real mooring line effect on floating strucures.

All that numerical implementations and respective tests done to validate the new code are illustrated in the following section.

5.2 New Boundary Conditions for Deep Water

IHFOAM solves the three-dimensional, two-phase Reynolds Averaged Navier-Stokes equations, namely, continuity of mass and linear momentum, as described in chapter 3. Two-phase flow is treated by means of the VOF method following equation, which allows the tracking of the free surface.

5. NEW DEVELOPMENTS OF THE NUMERICAL CODE

IHFOAM has been widely validated and used for coastal processes, but never for offshore applications. For the aim of this research, deep water conditions had to be simulated with IHFOAM, and some problems were pointed out, as the generation and absorption were not working well and wave height had a decay along the numerical channel. So, in order to achieve the proposed goals, some improvements needed concerning the boundary conditions of IHFOAM.

In order to discern exactly what was going wrong in deep water simualtions, many different tests in a simple wave flume were carried out. The first thing that was figured out was that generation in deep-water needed always a ramping time of at least 3 times the wave period, as it was not necessary for shallow and intermediate water conditions.

The tests were performed for shallow, intermediate and deep water conditions, both in laminar and turbulent ways, below all the features are listed, H stands for the wave height, T for the wave period and L for the wave length:

-Shallow water:
shallow1: H=0.12 m, T=1.6 sec, h=0.5 m, L=10.86 m
shallow2: H=0.24 m, T=1.6 sec, h=0.5 m, L=10.86 m
12 free surface gauges were inserted along the channel, the position from the begging of the flume are here listed: G1=0.5m, G2=1m, G3=2.5m, G4=5m, G5=8m, G6=10m, G7=14m, G8=16m, G9=20m, G10=22m, G11=25m, G12=29.5m.

-Intermediate water:
intermediate1: H=0.083 m, T=1 sec, h=0.3 m, L=1.37 m
intermediate2: H=0.04 m, T=1 sec, h=0.3 m, L=1.37 m
9 free surface gauges were inserted along the channel, the position from the begging of the flume are here listed: G1=0.2m, G2=0.5m, G3=0.8m, G4=1m, G5=1.5m, G6=2m, G7=2.5m, G8=3m, G9=3.5m.

-Deep water:
deep1: H=0.025 m, T=0.75 sec, h=0.547 m, L=0.87 m
deep2: H=0.05 m, T=0.75 sec, h=0.547 m, L=0.87 m
16 free surface gauges were inserted along the channel, the position from the begging of the flume are here listed: G1=0.2m, G2=0.5m, G3=0.3m, G4=1m, G5=1.5m, G6=2m, G7=2.5m, G8=3m, G9=3.5m, G10=4.3m, G11=4.9m, G12=5.5m, G13=6m,
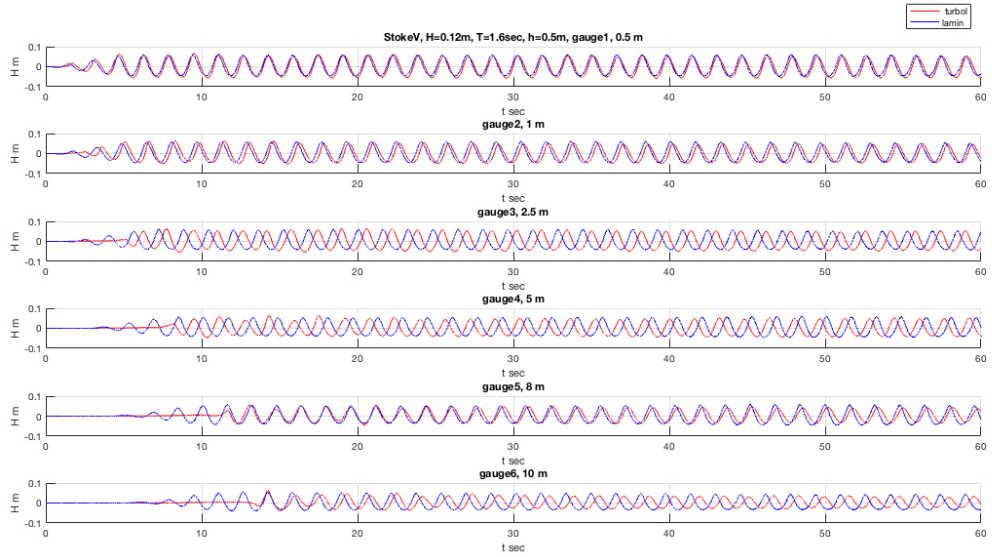
Figure 5.1: *Shallow1, free surface signals from gauges 1, 2, 3, 4, 5, 6. Blue line corresponds to the laminar simulation, red line to the turbulent one.*

G14=6.8m, G15=7m, G16=7.5m.

Free surface signals are plotted from Figures 5.1 to 5.14.

Looking at that tests, we had the confirmation that the generation and absorption for deep water was not working well. So we decided to go on also with the development of a new boundary condition. The implementation of a new boundary condition to actively absorb in deep water conditions was done by the changing the formula of the correction of the velocity in both inlet and outlet patches. That velocity equation contains the celerity expression:

$$\Delta u = -\frac{c}{\eta}\Delta y \tag{5.1}$$

As for shallow water, it was calculated with shallow water approximation, now, for deep water, it is with the corresponding approximation:

$$c = \frac{gT}{2\pi} \tag{5.2}$$

$$\Delta u = (h - \eta)\frac{gT}{2\pi\eta} \tag{5.3}$$
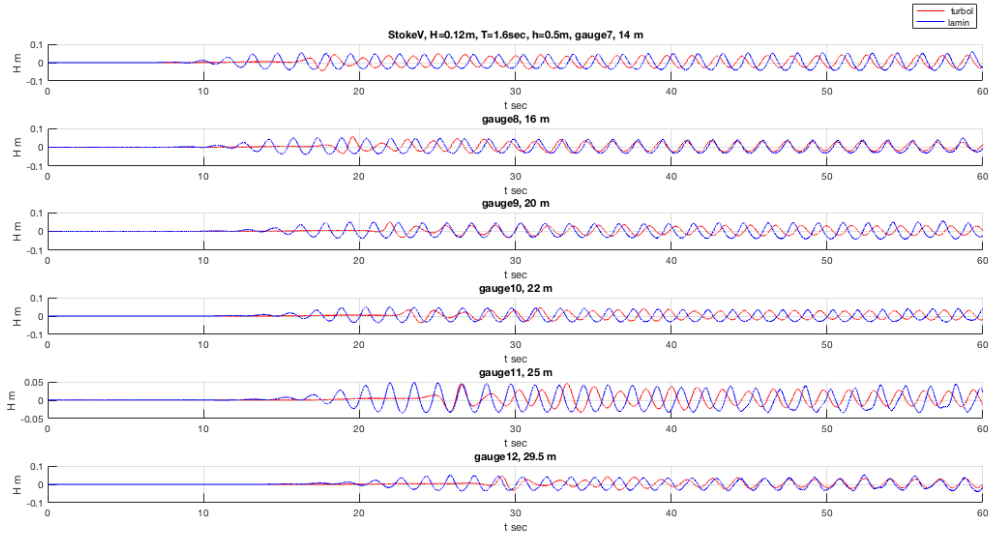
Figure 5.2: *Shallow1, gauges 7, 8, 9, 10, 11, 12. Blue line corresponds to the laminar simulation, red line to the turbulent one.*
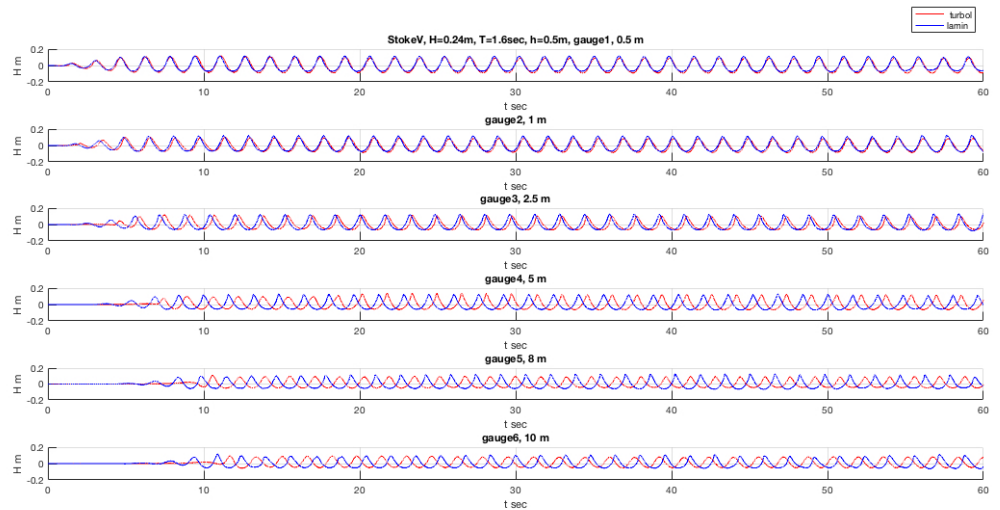
Figure 5.3: *Shallow2, gauges1, 2, 3, 4, 5, 6. Blue line corresponds to the laminar simulation, red line to the turbulent one.*
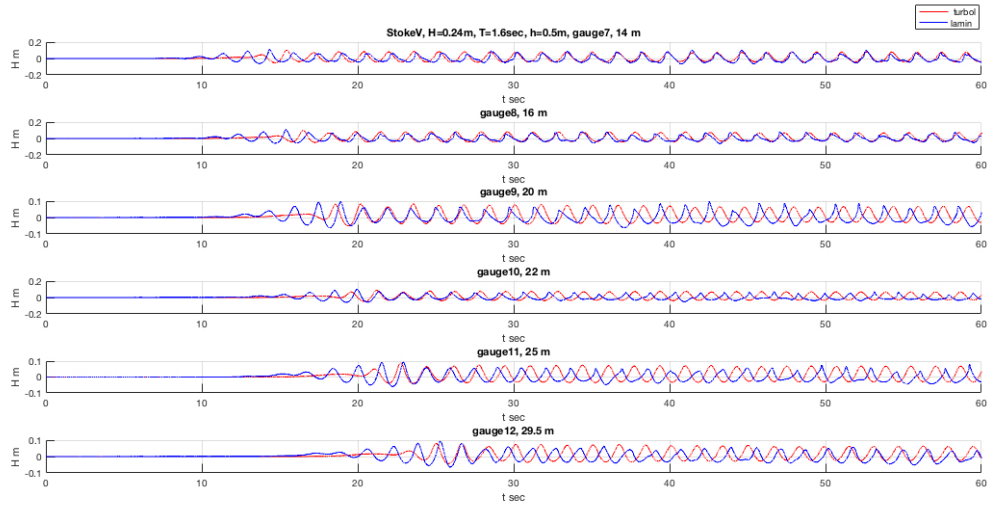
Figure 5.4: *Shallow2, gauges 7, 8, 9, 10, 11, 12. Blue line corresponds to the laminar simulation, red line to the turbulent one.*
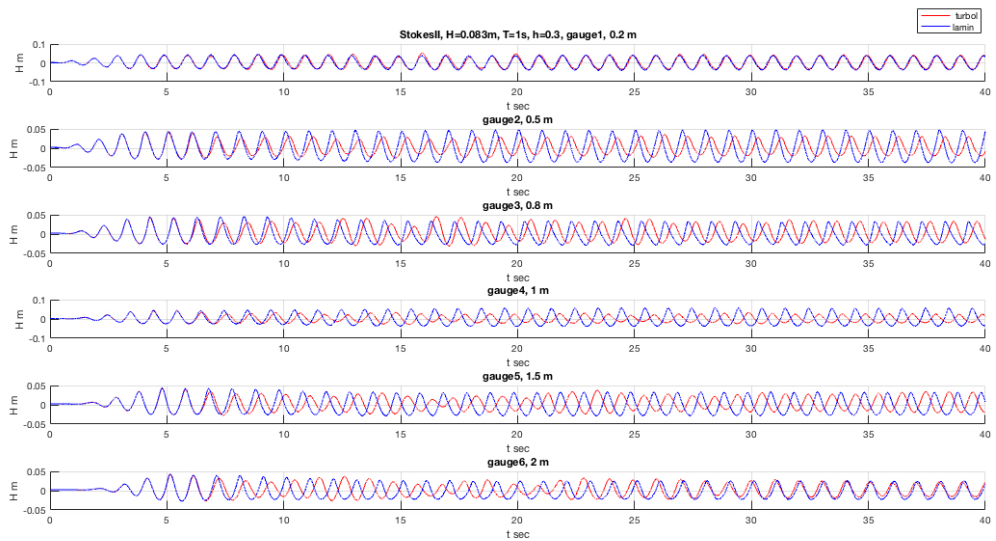
Figure 5.5: *Intermediate1, gauges 1, 2, 3, 4, 5, 6. Blue line corresponds to the laminar simulation, red line to the turbulent one.*
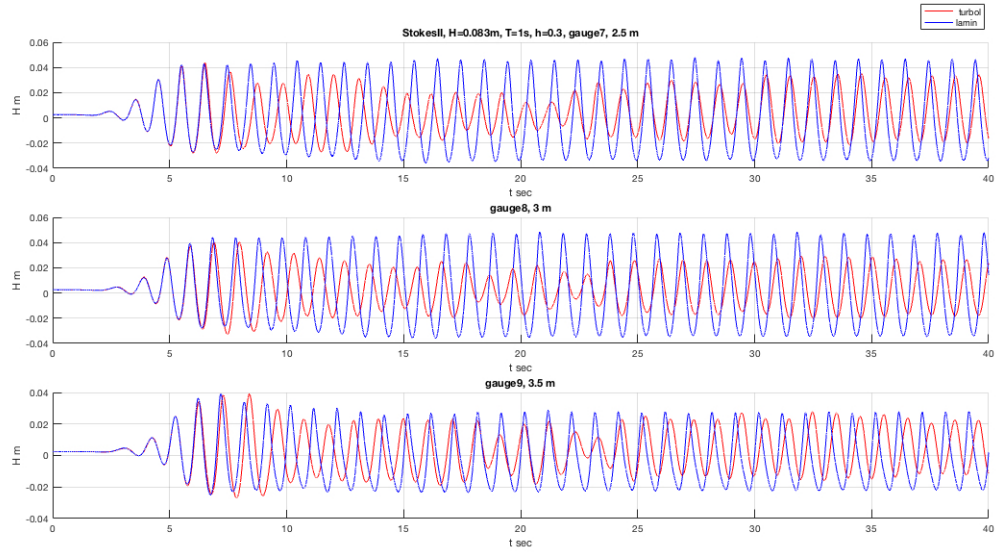
Figure 5.6: *Intermediate1, gauges 7, 8, 9. Blue line corresponds to the laminar simulation, red line to the turbulent one.*
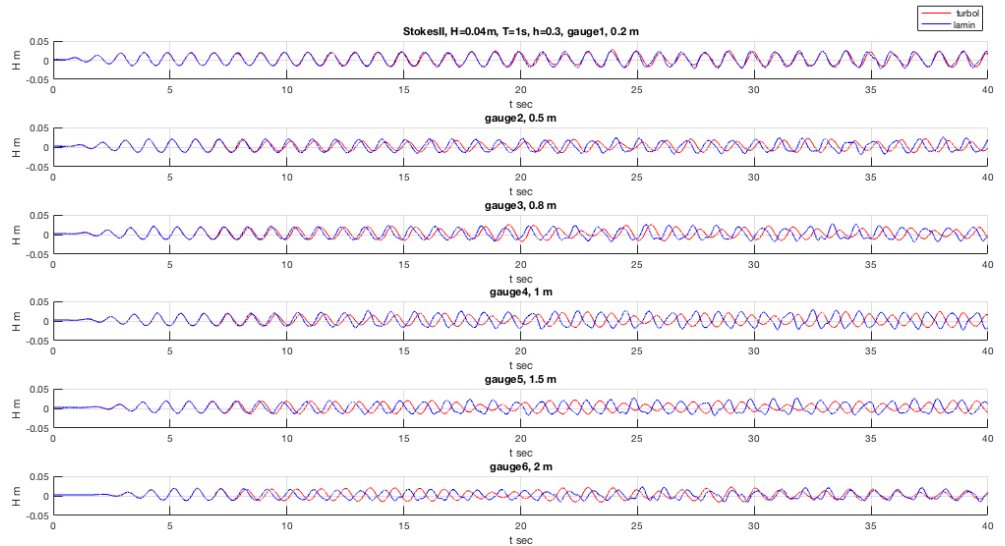
Figure 5.7: *Intermediate2, gauges1, 2, 3, 4, 5, 6.Blue line corresponds to the laminar simulation, red line to the turbulent one.*
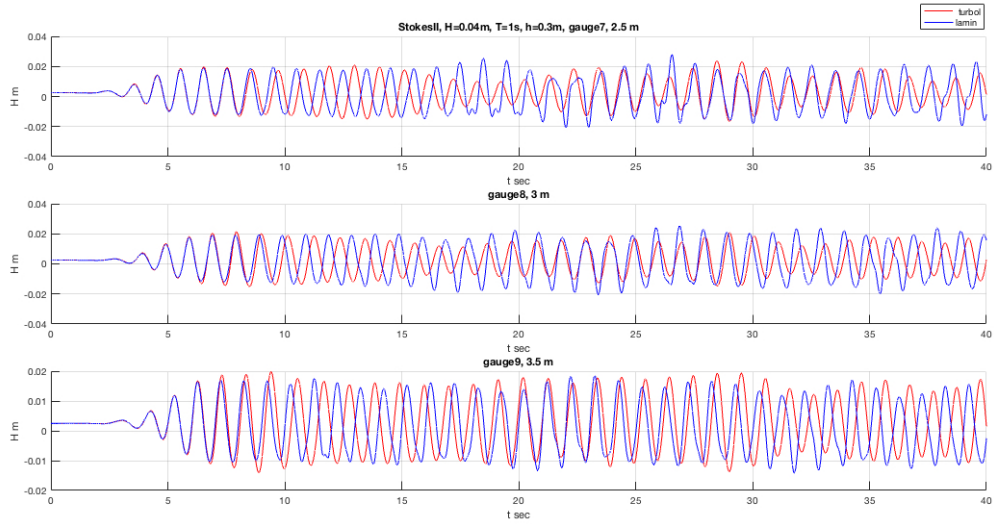
Figure 5.8: *Intermediate2, gauges 7, 8, 9. Blue line corresponds to the laminar simulation, red line to the turbulent one.*
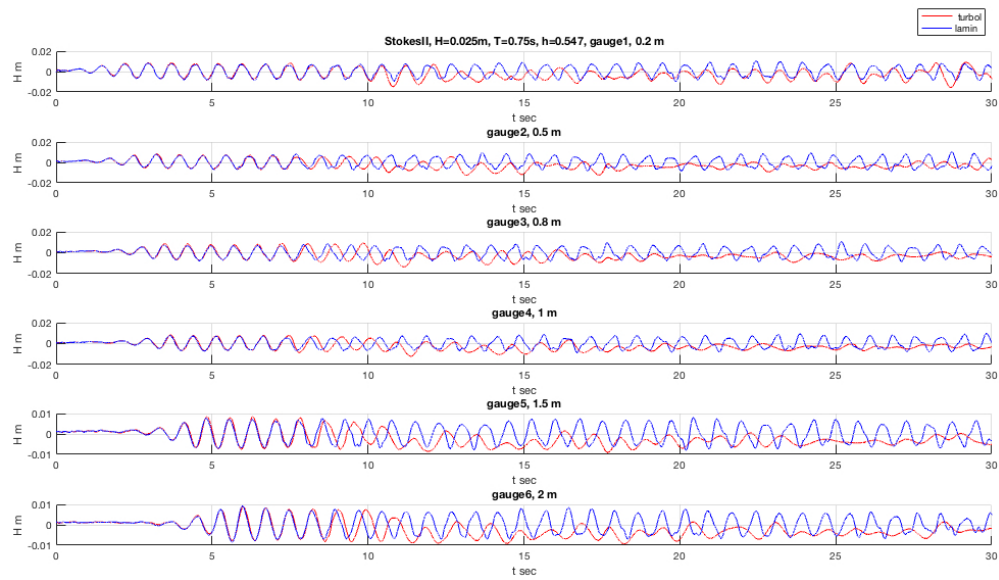
Figure 5.9: *Deep1, gauges 1, 2, 3, 4, 5, 6. Blue line corresponds to the laminar simulation, red line to the turbulent one.*

45
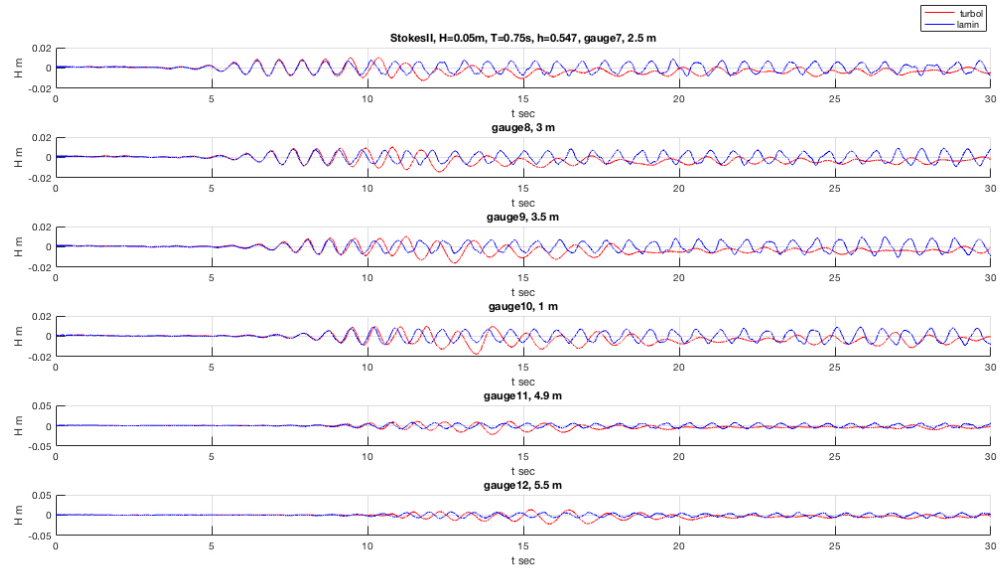
Figure 5.10: *Deep1, gauges 7, 8, 9, 10, 11, 12. Blue line corresponds to the laminar simulation, red line to the turbulent one.*
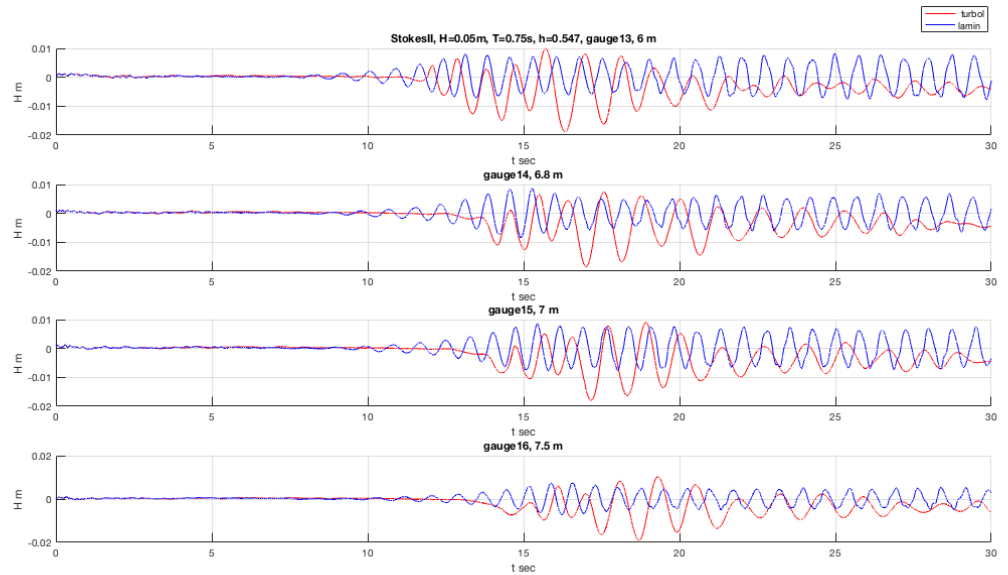
Figure 5.11: *Deep1, gauges13, 14, 15, 16. Blue line corresponds to the laminar simulation, red line to the turbulent one.*
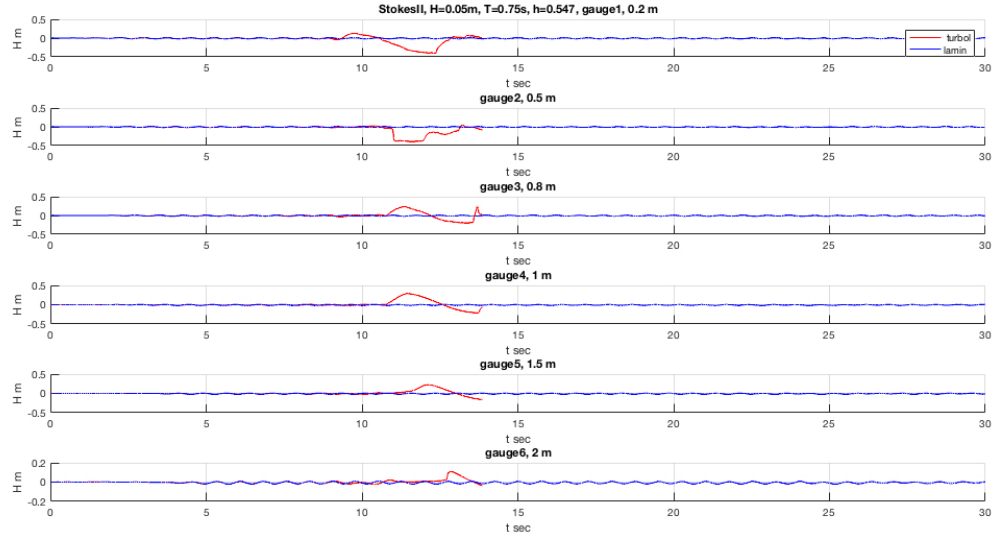
Figure 5.12: *Deep2, gauges1, 2, 3, 4, 5, 6. Blue line corresponds to the laminar simulation, red line to the turbulent one.*
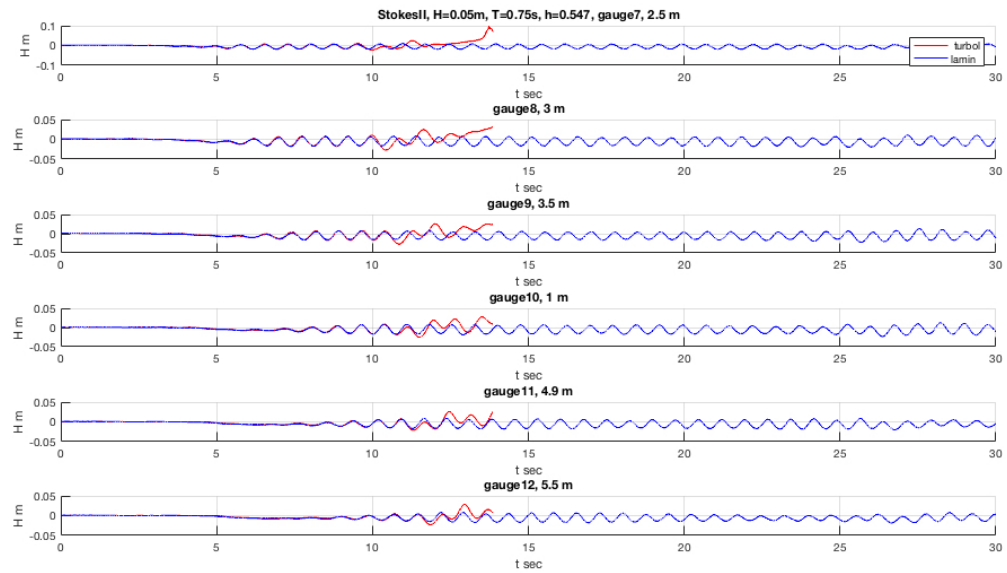

Figure 5.13: *Deep2, gauges 7, 8, 9, 10, 11, 12. Blue line corresponds to the laminar simulation, red line to the turbulent one.*
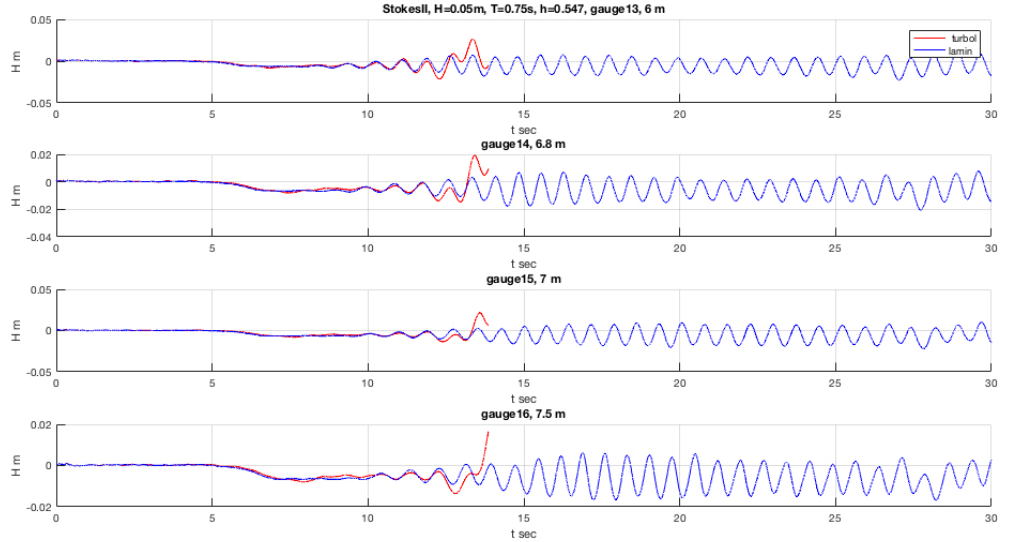
Figure 5.14: *Deep2, gauges 13, 14, 15, 16. Blue line corresponds to the laminar simulation, red line to the turbulent one.*

Then, all the tests were carried out again with this new implementation, and it resulted that the generation and absorption worked properly for the deep water conditions too. The wave shape was improved and the damping was quite neglected. Hereby comparisons between simulation with the old and new deep water absorption are reported below from Figures 5.15 to 5.20.

Thanks to all those tests, and the new implemented boundary conditions, IHFOAM tool can now generate and absorb all the water depth regimes. It is, nevertheless, useful to remind that, when simulating in deep-water conditions, the ramping time has to be larger and the choice of turbulence model has a great influence on the results, because as shown in the figures, turbulence terms can change both period and shape of waves.

5.3   New Turbulence Model

Numerous numerical modelling of wave-induced force on offshore structures and wave run-up are reported in literature. Many of these compared numerical results with analytical and experimental results. Lara et al. (44) presented a numerical simulation of a pile group subjected to waves using the IHFOAM toolbox. Only numerical results were presented which indicated that IHFOAM is a capable toolbox for analysing wave run-up
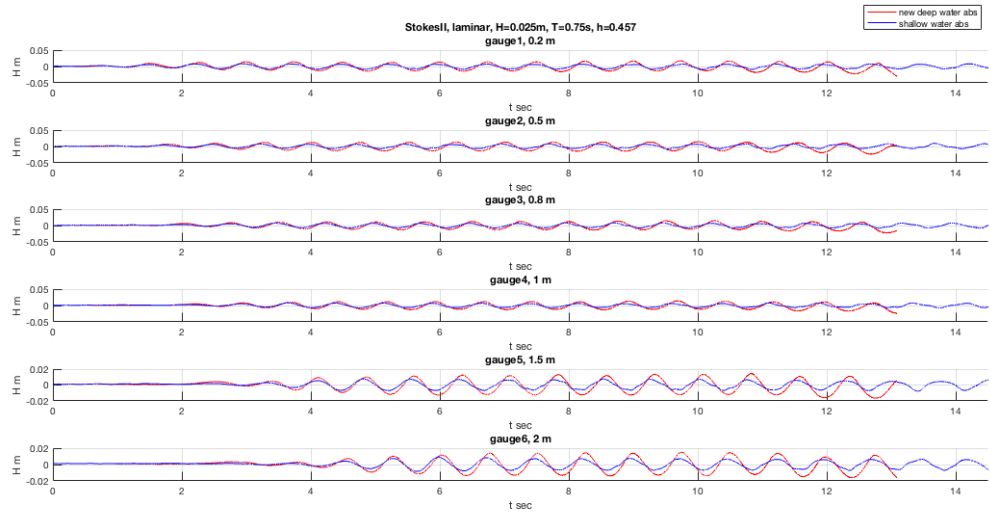
Figure 5.15: *Deep1 new condition, gauges1, 2, 3, 4, 5, 6. Blue line corresponds to the shallow water absorption simulation, red line to the deep water one.*
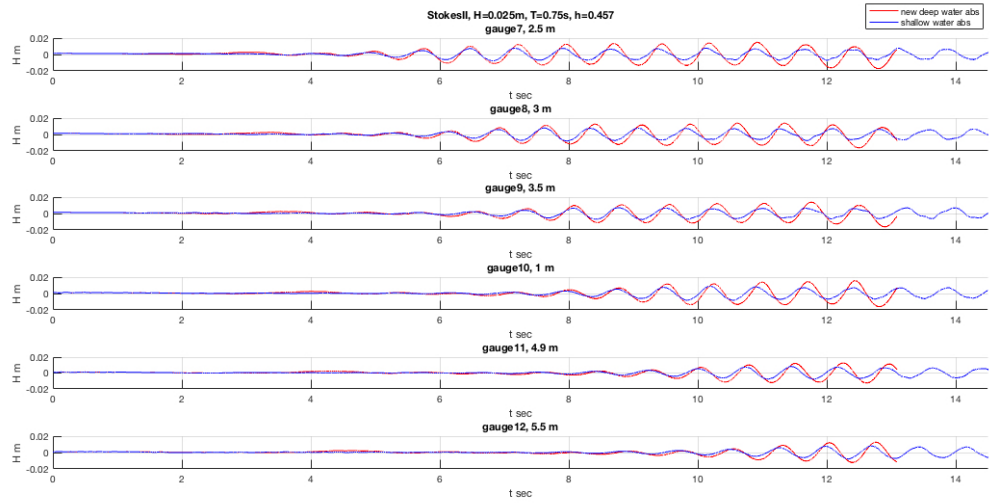
Figure 5.16: *Deep1 new condition, gauges 7, 8, 9, 10, 11, 12. Blue line corresponds to the shallow water absorption simulation, red line to the deep water one.*
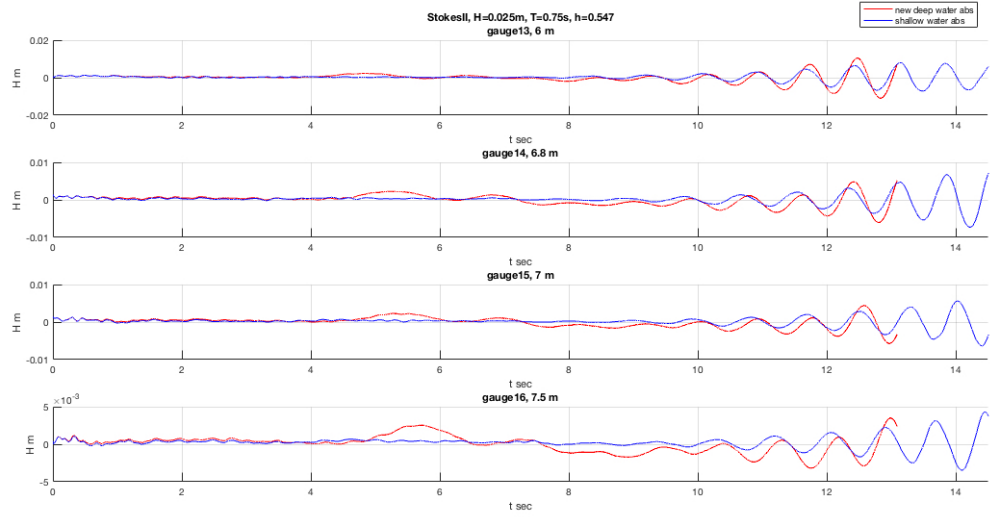
Figure 5.17: *Deep1 new condition, gauges 13, 14, 15, 16. Blue line corresponds to the shallow water absorption simulation, red line to the deep water one.*
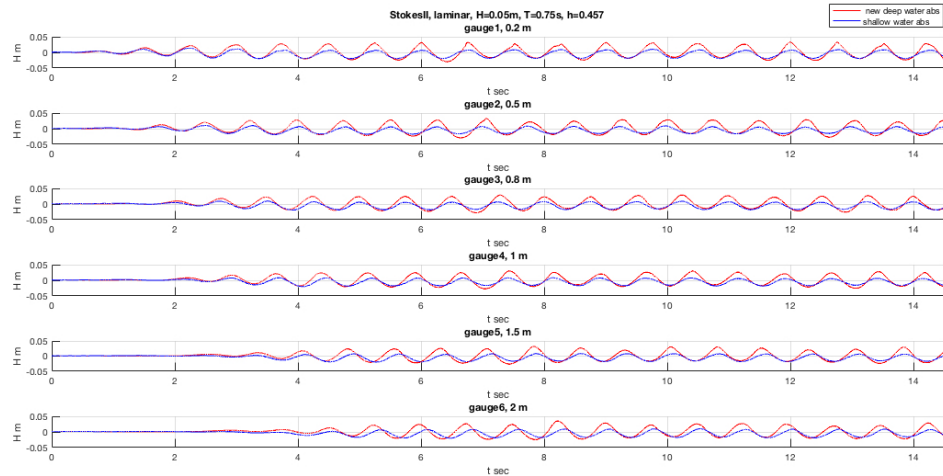
Figure 5.18: *Deep2 new condition, gauges1, 2, 3, 4, 5, 6. Blue line corresponds to the shallow water absorption simulation, red line to the deep water one.*
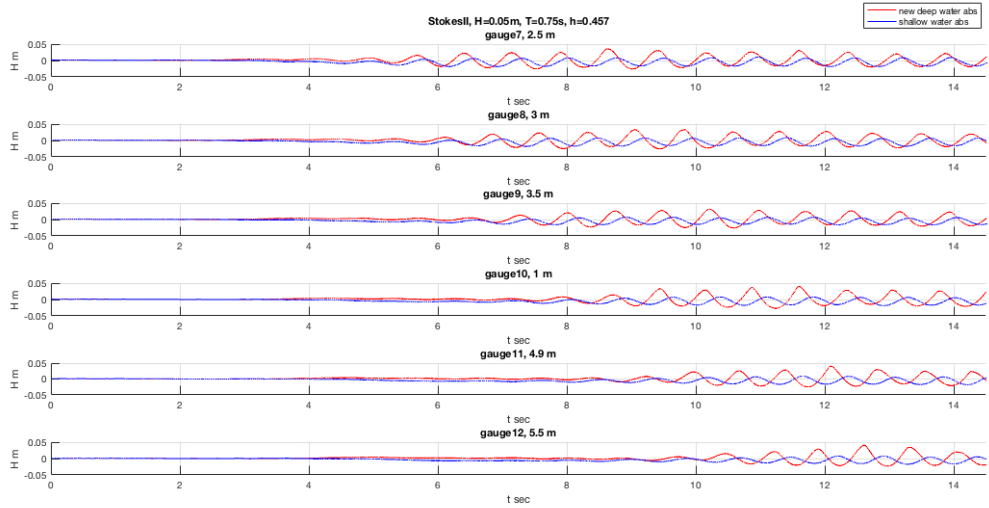
Figure 5.19: *Deep2 new condition, gauges 7, 8, 9, 10, 11, 12. Blue line corresponds to the shallow water absorption simulation, red line to the deep water one.*
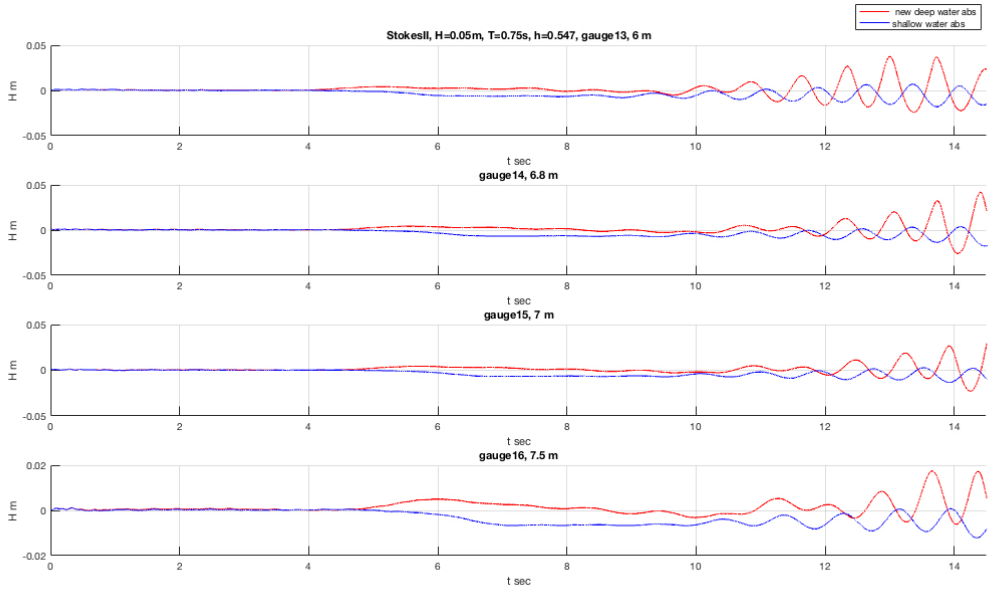
Figure 5.20: *Deep2 new condition, gauges 13, 14, 15, 16. Blue line corresponds to the shallow water absorption simulation, red line to the deep water one.*

around and wave-induced forces on offshore piles. On the other hand, Ransley et al. (67) compared numerical results with experimental data for extreme wave impacts on a fixed truncated circular cylinder. In that case, the numerical solution was obtained without turbulence modelling but the authors expect that it plays an important role in wave-structure interaction. El Safti et al. (18) presented a hybrid 2D-3D CFD model to investigate wave forces on piled structures. In this study, turbulent effects were incorporated by using a one-equation eddy-viscosity Sub-Grid Scale (SGS) Large Eddy Simulation (LES) model. Paulsen et al. (64) analysed strong nonlinear forces caused by steep or breaking waves and ringing loads due to steep nonlinear waves. Turbulence modelling was excluded because the forces acting on the monopile were mainly inertia dominated. A fair agreement was found between numerical and experimental data. Chen et al. (13) investigated nonlinear wave interactions with offshore structures for different wave conditions. More recently, Kamath et al. (38) reported CFD results of wave interaction with multiple vertical cylinders. They performed simulations using a k-ω turbulence model and observed unphysical wave damping based on RANS turbulence modelling. Therefore, both eddy viscosity limiters and free surface turbulence damping at the interface were applied. This unphysical wave damping caused by RANS turbulence modelling is not only observed during CFD simulations of monopiles. Several other authors also reported wave damping when using CFD for wave modelling (50) (30) (82) (19). Therefore, turbulence modelling was omitted and no indication of the influence of turbulence on wave run-up was given. However, some authors reported the necessity of using a turbulence model. For example Higuera et al. (27) applied both k-ϵ and k-ω SST turbulence models since they are widely used. Furthermore, turbulence modelling is needed in the case of significant vortex shedding or when wave breaking occurs. This can happen when irregular waves are generated, then energy is transferred between the different frequencies increasing the wave height at a particular time instant and at a certain location.

As found in literature and with all the tests carried out and showed previously, we understood that turbulence had a relevant influence on wave shape along the numerical simulation, so new turbulence model was implemented in OpenFOAM in order to try to avoid wave shape deformations and height decay.

Reynolds-Averaged Navier-Stokes (RANS) turbulence modelling is performed by applying the k-ω SST model. Sometimes, this RANS approach causes excessive wave damping (i.e. a significant decrease in wave height over the length of the numerical

wave flume). Therefore, a buoyancy term is implemented in the turbulent kinetic energy (TKE) equation of the k-ω SST model. The idea of adding a buoyancy term is taken from (81) who modify the k-ϵ model to simulate buoyant plumes. For water waves, the density is discontinuous at the free water surface resulting in an infinite density gradient. However, when a Volume of Fluid (VoF) method is applied for wave modelling, the density gradient is smeared out over several cells leading to a continuous change in density around the air-water interface. Consequently, the change in density around the interface between water and air is similar to the change in density observed in fire flows. As a result of implementing a buoyancy term, an overall stable wave propagation model without significant wave damping over the length of the flume is obtained, as can be observed in figures 5.21 - 5.26.

The numerical domain and mesh setting are the same used in the new boundary conditions test (section 5.2).

Turbulent effects are incorporated in the RANS Eqs. 5.1 and 5.2 by solving one or more additional transport equations to yield a value for the turbulent kinematic viscosity ν_t. The k-ω SST turbulence model is applied in all the simulations presented. k-ω SST has shown good results in literature to simulate the flow around circular cylinders and two-phase flows. For example, Rahman et al. (66) mentioned that the k-ω SST turbulence model is much more recommendable for high Reynolds numbers in a uniform free stream flow passing a 2D cylinder. Moreover, it has an adequate boundary layer treatment. The incompressible k-ω SST model for a single fluid is a two- equation model (53) and is formulated in OpenFOAM as:

$$\frac{\partial k}{\partial t} + \frac{\partial u_j k}{\partial x_j} - \frac{\partial [(\nu + \sigma_k \nu_t)\frac{\partial k}{\partial x_j}]}{\partial x_j} = P_k - \rho \beta^* \omega k \tag{5.4}$$

$$\frac{\partial \omega}{\partial t} + \frac{\partial u_j \omega}{\partial x_j} - \frac{\partial [(\nu + \sigma_\omega \nu_t)\frac{\partial \omega}{\partial x_j}]}{\partial x_j} = \frac{\gamma}{\nu_t} G - \beta \omega^2 + 2(1 - F_1)\frac{\sigma_{\omega 2}}{\partial \omega}\frac{\partial k}{\partial x_j}\frac{\partial \omega}{\partial x_j} \tag{5.5}$$

where k is the turbulent kinetic energy, P_k is the production term of k, ν is the kinematic viscosity, ν_t is the turbulent kinematic viscosity, ω is the specific dissipation rate, S is the mean rate of strain of the flow, $\beta^*= 0.09$, $a_1 = 0.31$, F_1 and F_2 are blending functions.

Alternative turbulence models, such as k-ϵ and k-ω, were also tested in this study but they caused more wave damping over the length of the wave flume compared to k-ω SST.

5. NEW DEVELOPMENTS OF THE NUMERICAL CODE

Furthermore, application of LES obliges very fine grids in order to resolve 80 % of the turbulence resulting in longer simulation times. Therefore, RANS modelling with the k-ω SST model is selected. However, even the original k-ω SST model causes significant wave damping. This damping is triggered by an increase in turbulent viscosity around the interface between water and air. This increase is induced by the large production of turbulent kinetic energy, k, in that zone. The production of k is linked to the velocity gradient which is large around the interface between water and air due to the large density ratio (1000/1). Two important insights are made according to the original k-ω SST model implemented in OpenFOAM (Eqs. 5.4 and 5.5).

The first one is already reported by Brown et al. (9). None of the incompressible solvers implemented in OpenFOAM, including two-phase flow, explicitly comprise the density. Only the turbulent kinematic viscosity ν_t is modelled rather than the dynamic viscosity $\mu_t = \rho \nu_t$. In a two-phase flow, the density varies around the interface between water and air which should therefore be included in the turbulence equations.

As mentioned in (81), a buoyancy term is needed in order to take the varying density around the air-water interface into account. The buoyancy term is only included in the turbulent kinetic energy (TKE) equation based on the Standard Gradient Diffusion Hypothesis (SGDH) where the density ratio is neglected. This density ratio is 1000/1 for water and air and could lead to instabilities in the solution method of this study. Moreover, Van Maele et al.(81) reported that the influence of buoyancy on the TKE-equation is negligible if the SGDH is used. However, neglecting buoyancy in the TKE-equation is influencing the results significantly. The more advanced Generalized Gradient Diffusion Hypothesis (GGDH) leads to failing simulations during this research due to an instability in the TKE-equation. Based on those two insights, a modified kω SST model (16) is implemented in OpenFOAM to prevent significant wave damping over the length of the wave flume. Firstly, the density ρ is explicitly implemented in both Eqs. 5.4 and 5.5 of the kω SST turbulence model to take its variability around the air-water interface into account. Secondly, a buoyancy term G_b described by the SGDH (Eq. 5.8), is added to the TKE-equation 5.4. The final equations for this buoyancy-modified kω SST turbulence model are formulated as follow:

$$\frac{\partial \rho k}{\partial t} + \frac{\partial \rho u_j k}{\partial x_j} - \frac{\partial [\rho(\nu + \sigma_k \nu_t) \frac{\partial k}{\partial x_j}]}{\partial x_j} = \rho P_k + G_b - \rho \beta^* \omega k \qquad (5.6)$$

$$\frac{\partial \rho \omega}{\partial t} + \frac{\partial \rho u_j \omega}{\partial x_j} - \frac{\partial [\rho(\nu + \sigma_\omega \, \nu_t)\frac{\partial \omega}{\partial x_j}]}{\partial x_j} = \frac{\gamma}{\nu_t}\rho G - \rho \beta \omega^2 + 2(1 - F_1)\rho \frac{\sigma_\omega 2}{\partial \omega}\frac{\partial k}{\partial x_j}\frac{\partial \omega}{\partial x_j} \quad (5.7)$$

with

$$G_b = -\frac{\nu_t}{\sigma_t}\frac{\partial \rho}{\partial x_j}g_j \quad (5.8)$$

in which the buoyancy term G_b is treated implicitly, the scalar $\sigma_t = 0.85$ and vector g = [0; 0; -9.81] m/s². The value of σ_t decides how much buoyancy is modelled and is kept constant during all the simulations presented. The purpose of including a buoyancy term in this study is to suppress the turbulence level at the free water surface, i.e. in the zone where a vertical density gradient exists. Because of the implicit treatment of the buoyancy term G_b in the TKE-equation, the very large vertical density gradient near the free water surface drives the turbulent viscosity ν_t to zero.

In order to validate the new turbulent model, the same tests carried out before were re-run and analysed.

So called Deep1 had the following settings:

H=0.025 m

T=0.75 s

h=0.457 m

The numerical wave channel was 8.1 m long, and 13 gauges were positioned along it.

The comparisons between the new implemented model and the standard one are shown from Figures 5.21 to 5.23. In Figures 5.24, 5.25 and 5.26, the influence of the buoyancy term G_b is highlighted.

It was possible to pointed out that for deep water conditions, that new turbulent model, is very important and influent on the wave shape and it is able to reduce the wave damping along the numerical channel.

Finally, thank to new boundary conditions and new turbulent model, IHFOAM is totally able to generate and absorb every kind of waves and it can be used for all coastal and offshore applications.
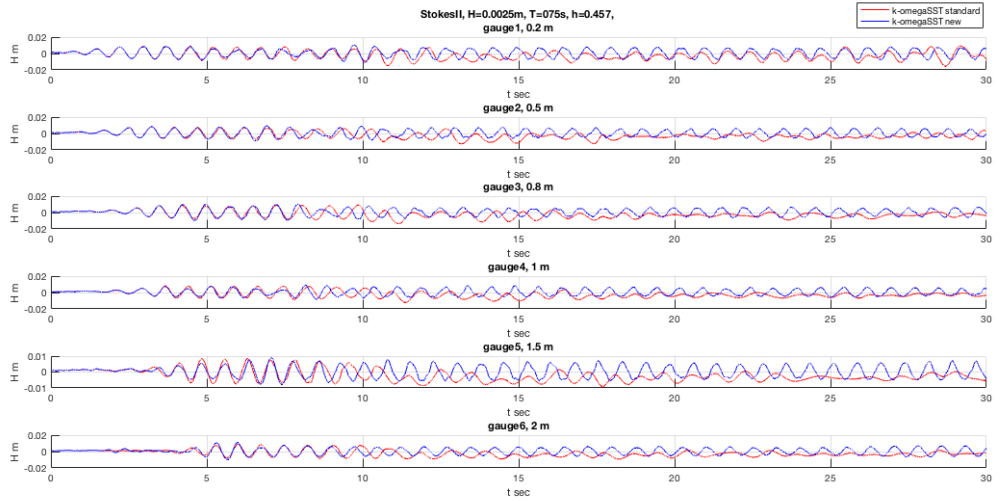
Figure 5.21: *Deep1, comparison between standard k-ω SST turbulent model (red line) and the new one (blue line), gauges 1, 2, 3, 4, 5, 6.*
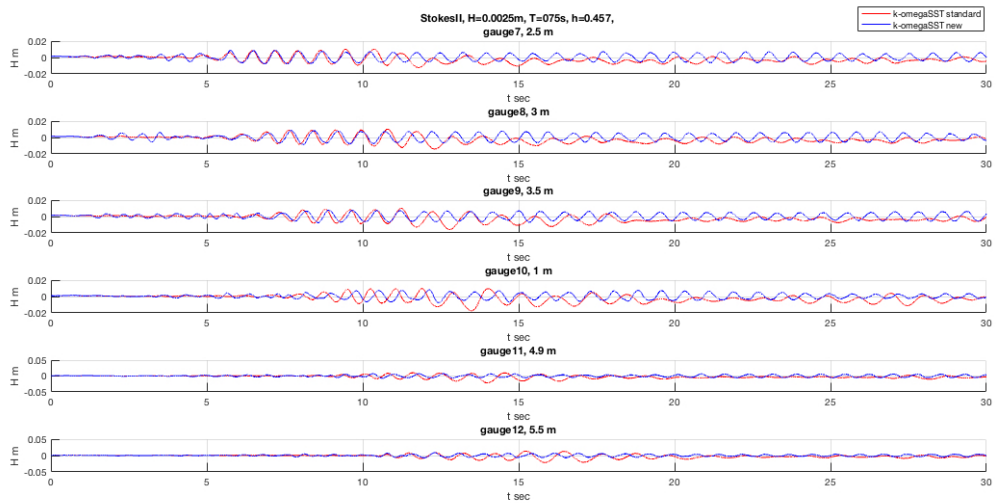
Figure 5.22: *Deep1, comparison between standard k-ω SST turbulent model (red line) and the new one (blue line), gauges 7, 8, 9, 10, 11, 12.*
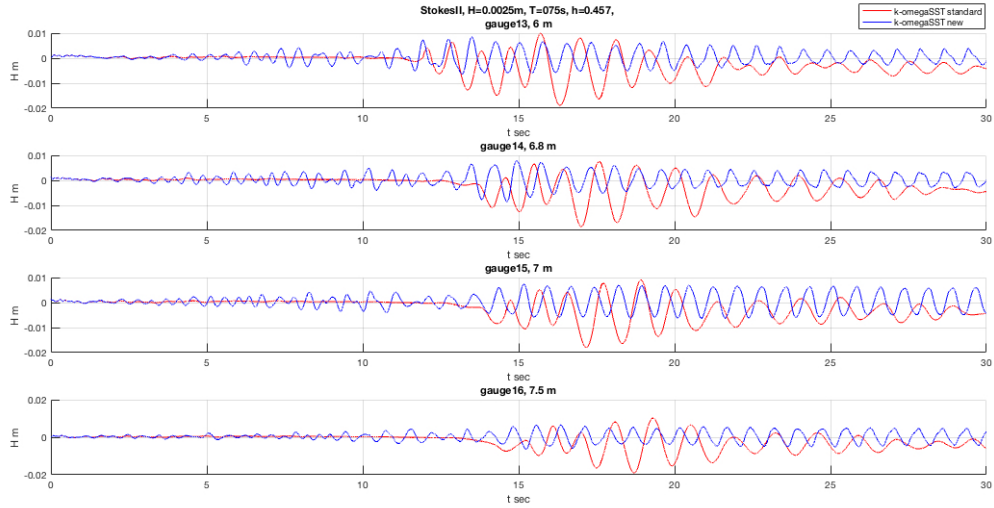
Figure 5.23: *Deep1, comparison between standard k-ω SST turbulent model (red line) and the new one (blue line), gauges 13, 14, 15, 16.*
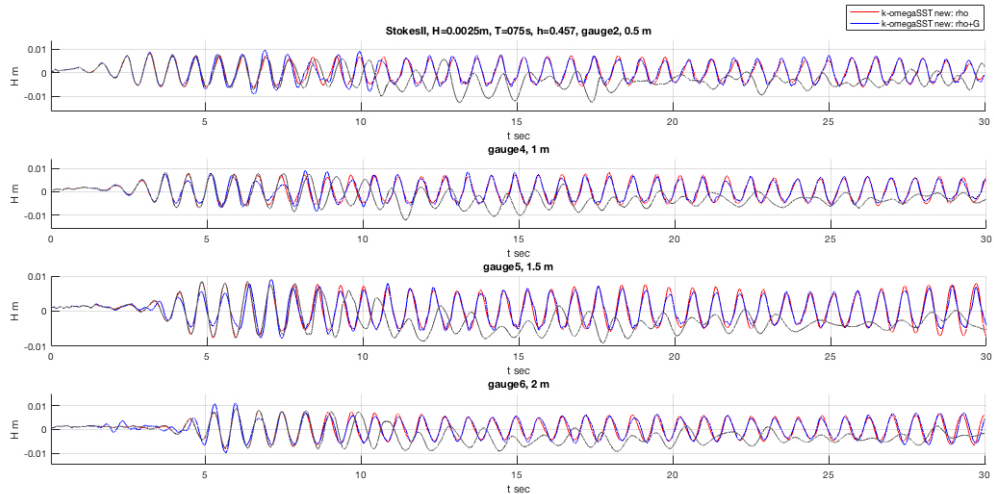
Figure 5.24: *Deep1, influence of the different new terms in the new k-ω SST turbulent model, gauges 1, 2, 3, 4, 5, 6. Grey line corresponds to the standard model, blue line to the new one, red line to the new one just with ρ term.*
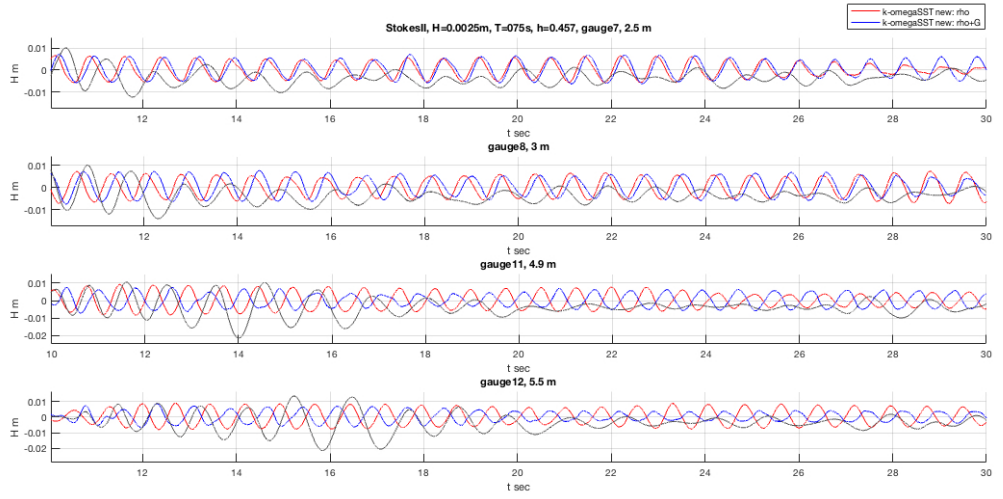
Figure 5.25: *Deep1, influence of the different new terms in the new k-ω SST turbulent model, gauges 7, 8, 9, 10, 11, 12. Grey line corresponds to the standard model, blue line to the new one, red line to the new one just with ρ term.*
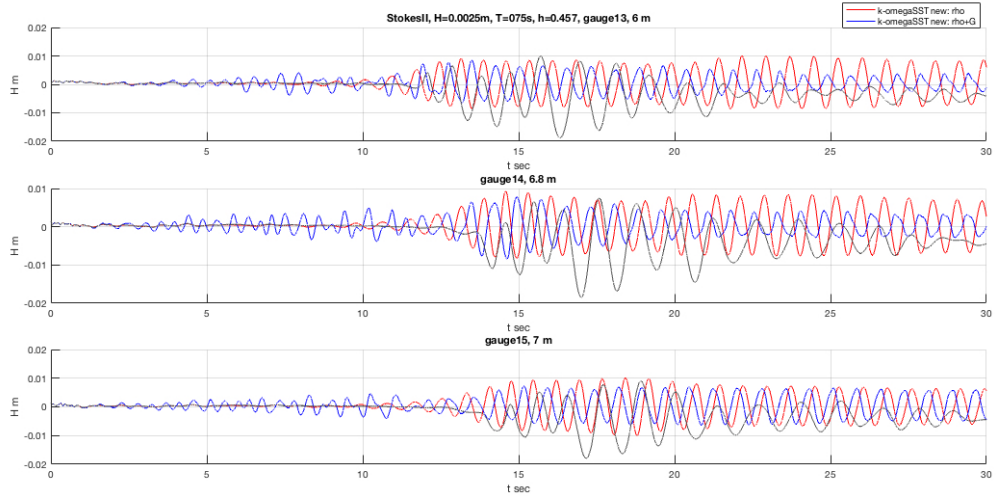
Figure 5.26: *Deep1, influence of the different new terms in the new k-ω SST turbulent model gauges 13, 14, 15, 16. Grey line corresponds to the standard model, blue line to the new one, red line to the new one just with ρ term.*

5.4 Wave and Current Generation

Non-linear wave-current interaction is analysed in this work by means of the use of Reynolds Averaged Navier-Stokes equations. The numerical analysis has been carried out using IHFOAM, a two-phase flow solver built on OpenFOAM platform, tracking the free surface evolution by means of a VOF technique. A new set of boundary conditions to generate and absorb combined waves and currents has been derived and implemented. The method presents important advantages compared to alternative existing techniques, since it does not increase the computational domain reducing the computational costs. The new implementation has been first validated with laboratory experiments for both rough and smooth beds found in the literature. Collinear waves following and opposing a current are simulated with a high degree of accuracy when compared to experimental results.

The method used to generate waves and current is an update of the boundary conditions presented by Torres et al.(78) and Higuera et al.(28). The new development presents a procedure to generate and absorb waves directly at the numerical domain boundaries. It has a number of advantages over alternative techniques, such as the introduction of artificial damping regions, as it does not increase the size of computational domain subsequently reducing the computational cost.

Two main modifications have been introduced in order to adapt the existing methodology to the combined generation of wave and current. They are related to the definition of the inflow/outflow boundary conditions and the active wave absorption to cancel out reflected waves in the domain.

Regarding the first, in this work the method proposed by Higuera et al.(28) for wave generation only has been improved and simplified. Besides the combined action of waves and currents is numerically simulated by adding flow velocities linearly. Waves can be represented by linear or nonlinear wave theories and current is considered to be uniformly distributed in the vertical. While forcing the model with a velocity distribution using a non-linear wave and current interaction theory may be more generic, several papers have not shown relevant improvements in flow prediction. Moreover, considering a depth-uniform current profile in the vertical requires the introduction of a regularisation zone in which non-linear wave and current interaction is developed and additionally the vertical velocity profile can accommodate to the bottom characteristics, either smooth or rough. One of the important issues to take is the definition of the flow velocity profile at the boundary. Because most of the existing wave theories are

based on small amplitude waves and potential flow theory, the flow field is only defined from the seabed to the still water level (SWL). Fluid particle velocities above the SWL need to be inferred. Although existing theories can provide wave kinematics above the trough by means of a modification of linear theory to account for the non-linearity of the waves due to their high amplitude, they are not considered in the current work. Linear superposition of flow velocity from waves and currents with these theories could yield an excessive particle velocity inducing wave breaking and modifying target wave-current conditions at the inflow boundary. The method proposed here presents a modification of the Dirichlet-type boundary condition for wave generation-only proposed by Higuera et al.(28). The new method simplifies and makes the approach more consistent by eliminating the dependency of the boundary conditions on the zones established in (28). Velocity, for both wave and current is defined from the bottom to the crest location. Since the wave theory is not specified above the SWL, velocity defined at z=0 is kept constant to the wave crest avoiding wave breaking when waves and current are generated simultaneously. This procedure is applied if the free surface is above the SWL (h>0). If the free surface is below the SWL (h<0), velocity is defined according to the wave theory used. This approach is in agreement with the boundary conditions used for the VOF method.

For collinear waves and currents propagating in the same direction, the angular wave frequency can be written as follows:

$$\sigma_{\mathrm{wc}} = \sigma_{\mathrm{w}} + U_{\mathrm{c}}\lambda \tag{5.9}$$

where λ is the wave number (2π/L, with L standing for wave length), σ_{w} is the wave angular frequency in absence of current ($\sqrt{g\lambda tanhk\lambda}$) and σ_{wc} is the modified angular wave frequency due to the presence of a current. It is defined as:

$$\sigma_{\mathrm{w}} = 2\pi/T_{\mathrm{r}} \tag{5.10}$$

where T_{r} is the wave period of a wave propagating on a current. U_{c} stands for a uniform in depth current velocity flowing in the same direction as the waves. In the following tests, that method is applied and the wave period is re-calculated for each case.

The new method presented here introduces flow condition as a linear superposition of waves and current. Then, inflow mass flow rate m_{inflow} of a wave propagating over a

current can be written as follows:

$$m_{\text{inflow}} = \alpha \rho_{\text{w}} U_{\text{wc}} h = \alpha \rho_{\text{w}} (U_{\text{c}} + U_{\text{w}}) h \tag{5.11}$$

where U_{wc} stands for combined wave-current velocity and U_{w} for wave velocity. The single-phase function (α) is included in equation (5.11) to account for the mass flow rate corresponding to water phase only. Since wave is defined to travel on a current, wave period in absence of current needs to be modified using equation (5.10) and T_{r} is used. This is a particular aspect of the new implementation presented in this work, which is needed when using Direchlet boundary conditions for wave-current generation. It has not been reported in previous works in literature which would need to apply the wave period correction. Other generation methods do not need to modify wave period since they use a different generation procedure for waves and current, an internal wave maker and a Direchlet type boundary condition for wave and current respectively.

A new active absorption boundary condition is implemented here to deal simultaneously with waves and current. It can be applied at both the inflow and the outflow boundaries to allow waves leaving the domain. The method introduces a modification of the inflow boundary condition according to the adjustment of the inflow mass flux. It is obtained by analyzing the existing mismatch along the simulation between the target flow conditions at the boundary and the actual flow in the numerical flume due to reflection. It is a dynamic method which allows to cancel out reflected wave-current flow along the simulation. Consequently, it can be applied for both regular and random wave conditions without restrictions to wave theory. At the inflow boundary, inflow mass flux is superimposed with the flux corresponding to the reflected waves from the inner domain. At the outflow boundaries, velocity for waves and current are matched to cancel out flow leaving the domain.

5.5 New Numerical Mooring Implementation for Floating Structures

The station keeping system is one of the most significant part of an offshore structure. Basically, two classes of mooring systems can be adopted: slack or tension cables. Tension lines are designed to minimize the wave-induced motions of the structure, whereas slack moorings are designed to reduce the loads on the structure. In slack mooring, the orientation of the mooring line depends on the cable weight and any current that might

exist, the line tension is due to the net weight and the length of the line. In tension mooring system, the geometry of the deployed mooring line is essentially rectilinear. The force on the line depends on both the buoyancy of the moored body and the mass density of the cable (20) (12). In this paper, all the experiments and simulations were carried out for tension mooring lines, so always no slack conditions were considered. The effect of the mooring system has great influence on resultant forces and movements of floating structures, but the response of mooring cable is nonlinear. So that part of the design is as critical as difficult to predict, analyze and simulate.

To numerically simulate mooring sytems dedicated commercial softwares are available, as, for example, Orcaflex and MooDy, that can be coupled to CFD code, like OpenFOAM. Otherwise, the aim of this work is to show a standalone OpenFOAM code able to simulate both the floating structures and the mooring systems.

Mooring systems within OpenFOAM can be modelled by means of numerical restraints. A simple linear numerical restraint is already included in the main code released by OpenFOAM, but the approach cannot consider a total real response of taut lines. A previous work by Paci et al.(61) applied this approach, called linearSpring, to simulate a simple moored freely heaving floating cylinder. The results have been further elaborated and used as starting point for the present work, where a new tension mooring system implementation, in OpenFOAM, is illustrated and validated. As explained in the previous paragraphs, in this code, to simulate moored floating bodies, it is possible to use the numerical restraint linearSpring, that depends on stiffness and damping coefficients, and on the restLength, the length of the cable when the body is at rest position. It takes into account the real response of a tension line, that is not a classical spring (as the linear spring implemented in standard OpenFOAM). The restraint equation has been changed to reproduce the effect of a mooring cable, it always pulls in order to keep the structure at the initial position. So, the restraint force has to be nullified whenever the spring is going to react in the opposite way, pushing. To obtain that, numerically, the restrain force is set equal to zero when the difference, Δx, between the effective length at each time step and the rest length is negative.

The new mooring equation reads:

$$F = -k\Delta x - d\Delta x \qquad (5.12)$$

$$F = -d\Delta x (if\,\Delta x < 0) \tag{5.13}$$

F is the mooring force acting on each line at each time step, Δx is the difference between the length at rest position and the real length at each time step, d is the damping coefficient, k is the stiffness coefficient. F is calculated in three directions, x, y and z. To pretension the mooringline, the restLength can be defined shorter than the effective distance from the anchor point and refAttachment point on the body at rest position, as it generates a force from the first time step of simulation. Then, for each time and corresponded movement of the floating, the distance Δx is re-calculated and just if it positive, the restraint force is applied to the structure at the attachment point along the direction of the cable.

In this way, the results of the simulations are improved and the approach can be adopted to predict dynamics of a floating structure and tensions on mooring systems.

6

Validation of the Model for Floating Structures

6.1 Introduction

Semi-submersible and floating structures are nowadays more and more adopted in coastal and offshore applications as breakwaters, docks, substructures for oil exploration and production, semi-submersible platform for wind turbine systems, wave energy devices, supporting structure for tidal energy devices, devices aimed to mitigate the problem of oxygen depletion in coastal and off-shore areas, and also for aquaculture farming (2) (3). Floating structures offer some important advantages compared with the traditional solutions: they can be installed in deeper water, they are cheap, they can be disassembled easily and they are more friendly to the ocean environment because of the reduced environmental impact (35). Furthermore, the transportation simplicity, potential relocation, flexibility for future extensions, relatively short duration of installation phase, existence of reduced requirements for foundation increase the benefit of floating structures employment (24) (84). Mainly floating structures have found their first field of application offshore but also in coastal areas they might have important impact. The utilization of floating breakwaters is enhanced by the existence of specific environmental design parameters such as large tidal excursion, poor geotechnical characteristic of the ground and/or deep water conditions, water circulation and/or aesthetic considerations (51), of course, on the other hand, it is necessary to consider that floating structures can resist to a more restricted range of environment conditions. With the ever growing industry interest in the blue growth, and in particular in wave and off-shore wind energy production, accurate tools for designing and modelling floating bodies are essen-

6. VALIDATION OF THE MODEL FOR FLOATING STRUCTURES

tial. There is a large variety of concepts for wave energy extraction and wind turbine substructures, each with their own set of challenges, and they all struggling towards cost reduction for commercial viability. The offshore wind production market is moving in deeper water too, where floating support platforms will be the most economical type. Numerous floating support platform configurations are possible for offshore wind turbines, particularly considering the variety of mooring systems, tanks and ballast options that are used in the offshore oil and gas industries (37). Recent concepts like: WindFloat (5) (11) (68), SWAY (7) and HYWIND system (55) have been progressing into full scale testing with HYWIND fully operating since 2009 (70). Spar structures were proven to be the best solutions in deep water areas, tension leg platform concepts were mentioned as the most viable alternative for intermediate water depths (57). For all that type of structures, the knowledge of the forces and the mooring line tensions are required for the structural design and mooring system design needs a carefully analysis, also in the numerical modelling phase. Due to the time varying nature of the environmental loading, such as wind, waves and currents, a dynamic analysis is necessary. Dynamic analysis also includes the evaluation of the motion responses of the floating body, (i.e. sway, heave, roll, etc...) and of the forces exerted by mooring lines. Such type of analysis is unlikely achievable through analytical approaches, thus physical or numerical tests have to be carried out. Design rules and modelling tools from the offshore industry are used when applicable, but wave and wind power companies heavily rely on experimental tests in model scale, as well as on large scale sea trials. Due to the increasing in accuracy and reliability of computational models the use of numerical codes is becoming popular, because of there are more and more fast and economical (63). Nowadays, quite well accurate commercial numerical tools are available to model the dynamics of floating structures as proposed in (3), but the open-source codes are getting more more reliability also for practical offshore and coastal design approach as presented by Morgan et al.(54) and Cao et al.(10) through the use of OpenFoam. Many works were carried out on the numerical simulation of mooring systems: Yang et al.(86) presented numerical results including motions and tensions at the top of mooring-lines for a truss Spar motion response simulation. The mooring-line dynamics were based on the rod theory and the finite element method (FEM), with the governing equations described in a global coordinate system. In the coupled dynamic analysis, the motion equation for the hull and dynamic equations for mooring-lines were solved simultaneously using the Newmark method. Kim et al.(42) compared the dynamic coupled behavior of floating structure and mooring system in time domain using two numerical

methods for the mooring lines such as the linear spring method and the nonlinear Finite Element Method, (FEM). Numerical simulation of the mooring systems is not simple, due to its non-linear response. Some dedicated commercial softwares are available, as Orcaflex and MooDy. OrcaFlex, firstly introduced by Masciola et al.(49), is the world's leading package for the dynamic analysis of offshore marine systems. MooDy, on the other hand, solves the mooring cable dynamic problem using a modal high-order finite element model (21) (21).

Many other researches were carried out in last years on that topic by means of different numerical codes and using different way for representing mooring lines in numerical models. Rahman et al.(66) used a VOF-based RANS model method to predict the wave deformation and dynamics of tension-leg floating breakwaters. Instead, Peng et al.(65) adopted the immersed boundary (IB) method to analyse submerged breakwater and the related mooring system under the action of regular waves. Bachynski et al.(6) and Ruiz et al.(71) highlighted the importance of mooring lines tension for different floating offshore bodies, both under the action of currents and waves, in order to properly design the lines. Recently, (21) proposed a study of floating wave energy device through full coupling between CFD and a licensed mooring lines tool: OpenFOAM and Moody.

Also Smoothed Particle Hydrodynamics (SPH), a relatively new but very promising instrument, can be used to simulate the movement of floating bodies in water. As Rogers et al.(69) did for a caisson breakwater in the surf zone under the forcing of periodic waves. He used the open-source code SPHysics with a Riemann solver-based formulation and obtained good agreement with experimental data for the displacement and the horizontal forces on the caisson. Another similar work was presented by Omidvar et al.(58); they developed SPH in three dimensions to include variable particle mass distribution using an arbitrary Lagrange - Eulerian formulation with an embedded Riemann solver. This model was applied to a single heaving -float wave energy converter, the "Manchester Bobber", in extreme waves and compared with experiments in a wave tank. A weakly compressible SPH solver was presented by Bouscasse et al.(8), too, for applications involving nonlinear interaction between water waves and floating bodies. A dedicated algorithm was developed to manage the intersection between the free surface and the solid profile. Stability, convergence and conservation properties were tested on several freely floating test cases and a final validation of the full algorithm was performed for the interaction between a 2-D box and a wave packet.

Furthermore, Lind et al.(47) shown as SPH can be a fast alternative to fully 3-D simulations which are computationally demanding. Variation of mooring line properties

and buoy position was efficiently analyzed using the same wave field and they concluded stating that the approach can be a useful design tool with further validation.

The main purpose of this study is to analyse and validate a new numerical tool developed on the basis of OpenFOAM solver for modelling submerged and floating structures moored by means of vertical and inclined elastic tension legs hit by waves and currents.

6.2 Numerical Model

The numerical model where the new features were implemented is OpenFOAM with IHFOAM wave and current generation tool, as illustrated in chapter 5.

6.3 Sensitivity Analysis

Many tests are carried out in order to calibrate the influence of all the parameters listed before. A simple lay out of floating horizontal cylindrical moored with four lines hit by waves is selected for the validation and calibration of the model. All these tests are carried out in a water depth of 0.6 m and the same wave condition is generated with Stokes V order theory: H=0.046 m and T=1 sec. The numerical wave tank is made of 1470000 cells.The refinement zone is done by SnappyHexMesh tool around the floating cylinder. The computational domain characteristics are listed in table 6.1, while the floating cylinder features are in table 6.2 and shown in fig 6.1.

	Tot. Dimension (m)	Number of cells	Cell size (m)
X	3.5	175	0.02
Y	0.7	70	0.01
Z	1.2	120	0.01

Table 6.1: *Computational domain characteristics.*

Centre of mass (m)	$(1, 0.35, 0.423)$
Radius of gyraton (m)	(1.156, 0.435, 1.483)
Mass (kg)	28.6

Table 6.2: *Floating cylinder characteristics.*
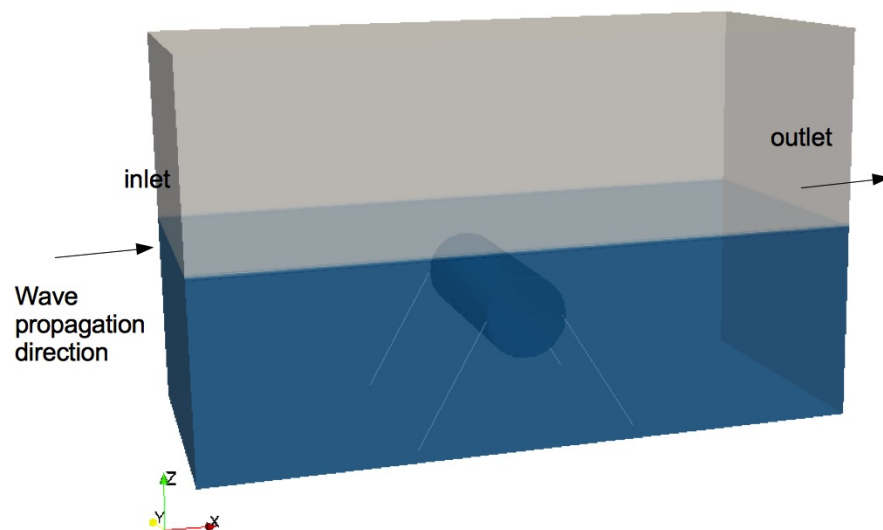
Figure 6.1: *Computational domain.*
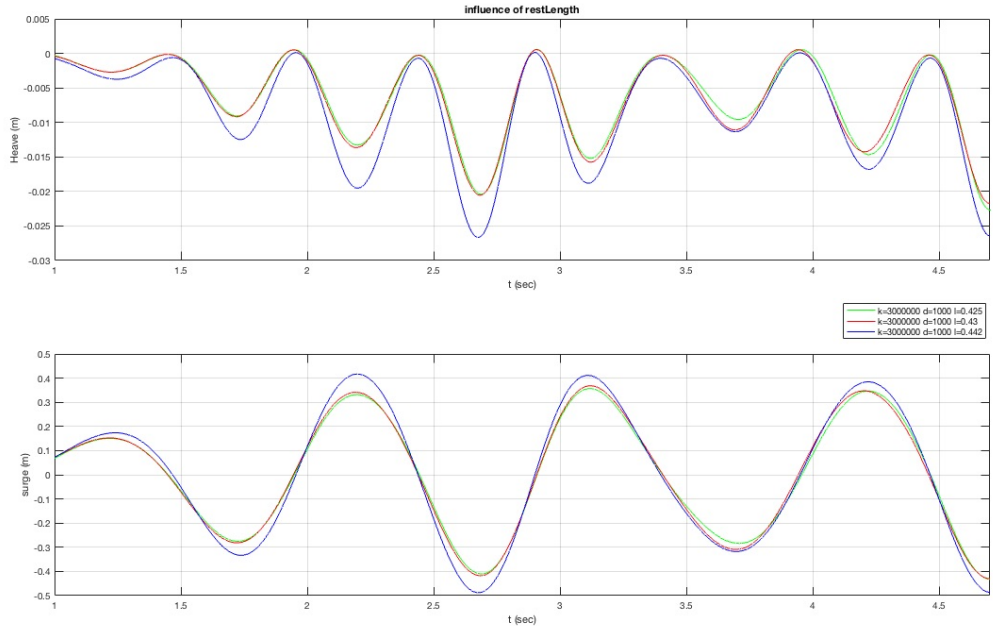
Figure 6.2: *Influence of spring parameters: restLength. The green line is for rest length equal to 0.425 m, red line is for rest length equal to 0.43m and blue line is for rest length equal to 0.442 m*

During each calibration test, only one parameter is changed in order to highlight how everyone can influence on the resulting dynamics and mooring forces. As first parameter the rest length is investigated, then the stiffness and lastly the damping coefficient. The rest length is a geometry initial data, so it cannot be change a lot, but we can see that little variations of its value, as 4% of the length, can induce different results.

The magnitude of the rest length influences both the surge amplitude and the heave displacement, 16% and 12% respectively, between the biggest and smallest length tested; the effect, as it was expected, is more evident on the surge mode since the increasing of the mooring lines allows large horizontal excursion of the floater, Fig. 6.2. In these tests, the stiffness was set always as 3000000 N/m and the damping coefficient as 1000. The rest length was 0.425 m, 0.43m and 0.442 m, respectively for the three different tests.The difference in the length tended to change also lightly the period of the movements, about the 8%.

Then tests to analyse the influence of the stiffness were carried out. The stiffness was equal to 5000000 N/m, 3500000 and N/m 3000000 N/m, while the rest length was 0.425
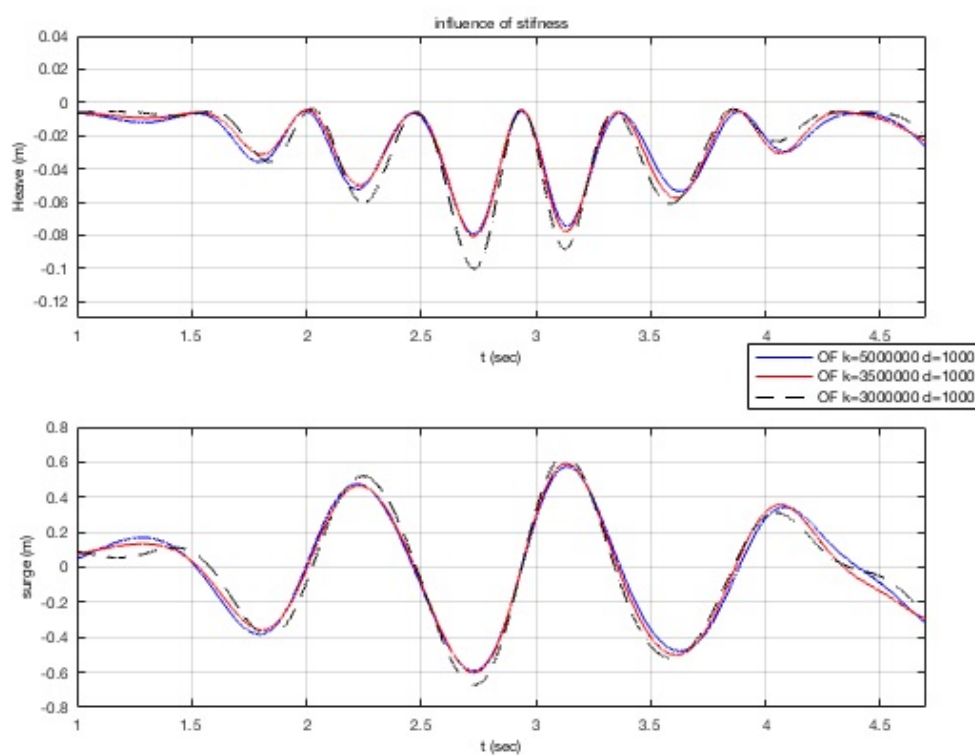
Figure 6.3: *Influence of spring parameters: stiffness. The blue line is for stiffness equal to 5000000, the red line is for stiffness equal to N/m 3500000 and the dot line is for stiffness equal to N/m 3000000 N/m.*
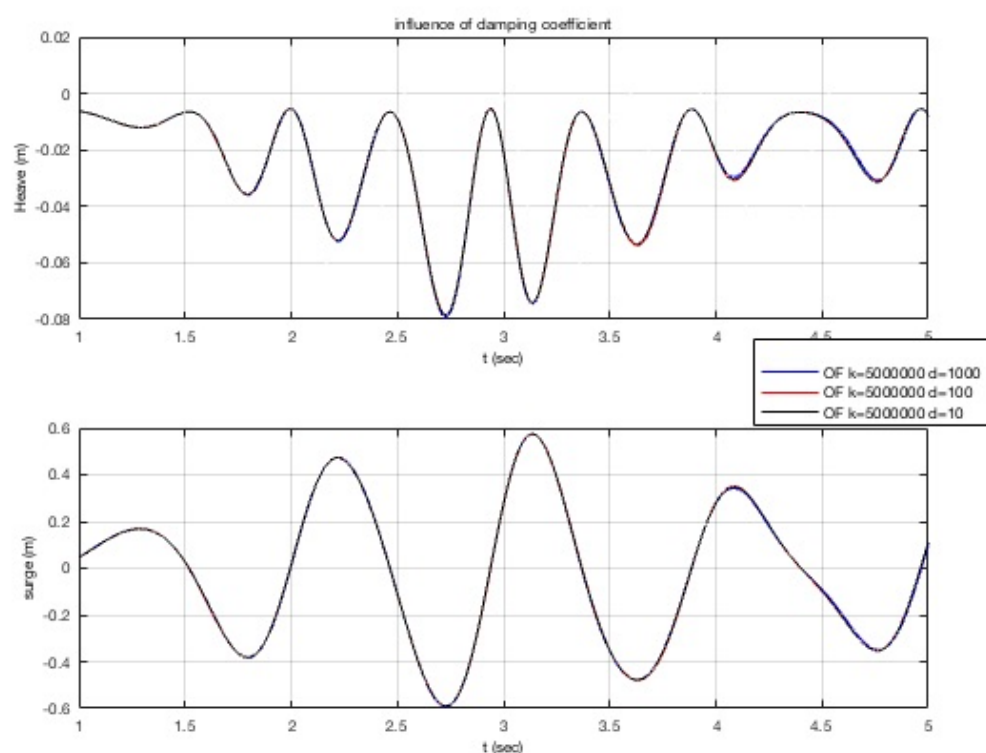
Figure 6.4: *Influence of spring parameters: damping coefficient.*

m and and the damping coefficient as 1000, in all the tests. The stiffness of the cable had a greater effect on the heave amplitude, 30%, than on the surge displacement, 10%. It did not influence the period of the oscillation. From Fig. 6.4 it can be argued that the damping coefficient effect is negligible, it is due to the fact that the damping effect caused by the lines becomes important for very long cables and large values of relative velocity between the cables and the fluid. The main conclusions of the sensitivity analysis are:

-the length of the line mostly affects the amplitude of surge mode, while its influence is reduced for the heave mode;

- the stiffness of the line has a great influence on the amplitude of the heave response;

-the damping coefficient has a really small influence on the dynamic response, but it is quite important to consider into the equation for numerical stability.

In order to validate the new implemented code, tests of a submerged caisson are carried out and compared with experimental data, as explained in the next session.

6.4 Validation of the New Code

The study presented by Rahman et al. (66) has been selected to validate the new cable model implementation in OpenFOAM. The tests focused on a rectangular floating caisson moored with four tension lines under the action of several regular waves. Two configurations were tested: the first one with vertical lines and the second one with inclined lines (see figures 6.5, 6.6 and 6.14).

6.4.1 Experimental Tests

The experiments were carried out in a wave flume at Nagoya University. The experimental setup is shown in the figure 6.5.

The wave tank was 30 m long, 0.7 m wide and 0.9 m deep. The floating caisson considered in this study was a pontoon type breakwater. It was 30.4 cm long, 68 cm wide and 13.7 cm high. The body was anchored to the bottom of the tank with four mooring chains. The relative inclinations between the mooring lines and the flat bottom of the wave tank were varied between $\theta = 90°$ (vertical) and $\theta = 60°$. Water depth (h) was equal to 65 cm and the top surface of the body was submerged by 3 cm (d). The mass of the floating body was 18700 g. Tension in the mooring lines was guaranteed by the buoyancy force acting on the structure. Regular waves were generated from the flap type wave generator (66). Comparison between numerical and experimental results
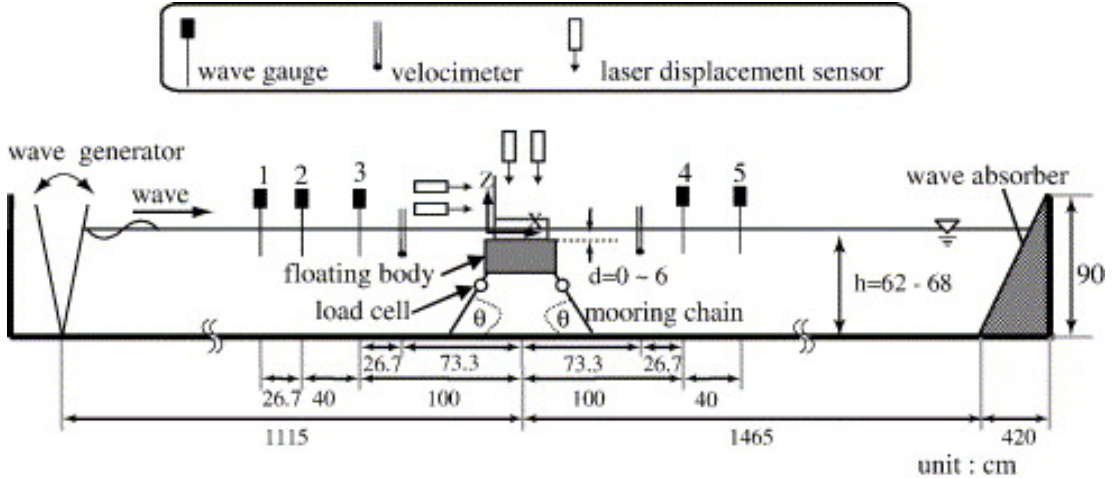
Figure 6.5: *Detail experiment setup, (66).*

are performed for two configurations listed in the table 6.3. Due to the necessity of experimental results in terms of time series, the adopted benchmark configurations are selected throughout Rahman's paper in order to have the widest number of parameters to use in the validation process. Even though, some information are missing in the paper, the the stiffness of the mooring lines, that hereby is estimated thank to the initial tension, the wave gauges signals during the simulations, so they cannot be compared, and the tensions on the lines for case A.

	H (cm)	T (sec)	h(cm)	Inclination of the mooring lines (deg)
A	7.3	1.3	65	90
B	3.1	1	65	60

Table 6.3: *Setting of the tests*

6.4.2 Numerical test

The numerical wave tank was 36106 cells. The refinement zone was done by Snappy-HexMesh tool available in OpenFOAM around the floating caisson. A right-handed Cartesian coordinate system is located at lowest-right angle of the domain, and the centre of mass is positioned in the middle of the caisson because of the mass is uniformly assigned. The numerical domain could be shorter than the physical one thank to the boundary conditions that can actively absorb, so the time of the simulations was largely reduced. The computational domain characteristics are listed in table 6.4, while
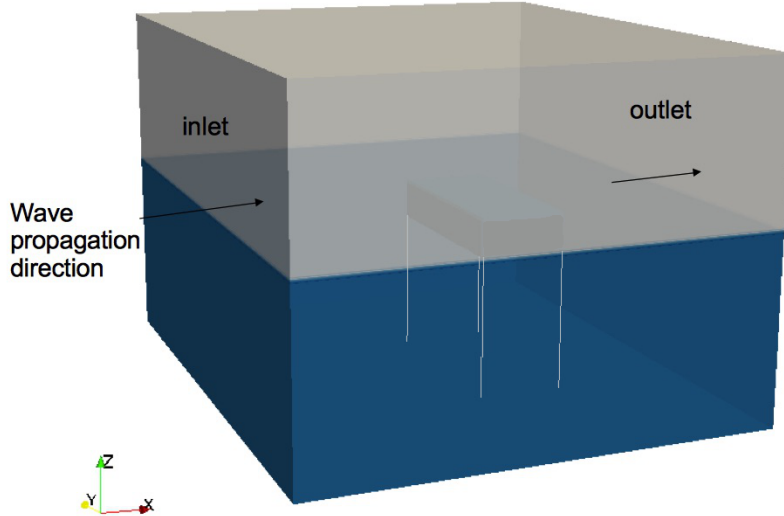
Figure 6.6: *Computational domain, case A.*

the floating caisson features are in table 6.5 and shown in fig. 6.6. The waves were forced from the first free surface gauge record of the laboratory test.

	Tot. Dimension (m)	Number of cells	Cell size (m)
X	1.6	160	0.01
Y	1.9	190	0.01
Z	1.2	120	0.01

Table 6.4: *Computational domain characteristics.*

Centre of mass (m)	(1, 0.45, 0.55)
Radius of gyraton (m)	(0.86, 0.75, 0.17)
Mass (kg)	18.7

Table 6.5: *Floating caisson characteristics.*

	Number of cells	Δx	Δy	Δz	N.points/ perimeter in the refin.zone	Number of processors	$F(N)$	C_d	CPU time(h)
mesh1	6152	0.1	0.1	0.1	36	8	1.4571	1.0232	1.5
mesh2	41528	0.05	0.05	0.05	70	8	1.7155	1.2046	4.5
mesh3	3619440	0.01	0.01	0.01	88	8	2.0238	1.4212	10
mesh4	7374000	0.02	0.02	0.02	174	8	2.0113	1.4124	15
mesh5	7438440	0.008	0.0076	0.008	112	8	1.9809	1.39	16

Table 6.6: *Mesh sensitivity.*

Three numerical free surface gauges were positioned along the channel, G1=0.3 m, G2=0.6 m, G3 = 1.55 m, as sketch in figure , G1 and G2 are before the caisson and G3 after.

6.4.2.1 Mesh Sensitivity Analysis

A mesh sensitivity analysis was carried out in order to be able to choose the best mesh discretization to run numerical simulations.

This analysis was done compared theoretical and numerical results of the drag coefficient of a rectangular shape in a linear current. The current induced by the mean horizontal velocity originated by the wave conditions simulated in case A (H=7.3 cm, t=1.3 sec) is calculated as u=0.175 m/s. The corresponding force generated on the caisson was calculated. For a rectangular shape as this case, in literature, the drag coefficient was found as 1.4 (87). With this value, the theoretical force resulted 1.98 N. Then, the forces and the drag coefficients were calculated for 5 different grid mesh discretizations, listed in the table 6.6, through the numerical code and compared with the theorical results. The tests were runned on a HPC machine (2.6 GHz), using 8 processors. At the end of this analysis, it was possible to see that from mesh3 the convergency was reached. So, mesh3 was chosen because it was enough detailed to capture the forces on the object and the flow around it, but not extremely fine to need too much expensive computational costs.

6.4.2.2 Case A

First validation test was run according to case A presented in table 3. Water depth, (h) was 0.65 m, mooring lines are vertical ($\theta = 90°$) and their length at rest position is 0.47 m. The wave height, H, is 7.3 cm and the wave period, T, was 1.3 s. The stiffness of the lines is set as 236000 N/m, as stated, this information missed in Rahman's paper, so it is found compared the initial tensions on the lines.

The free surface signals from the gauges are presented in figure 6.8.
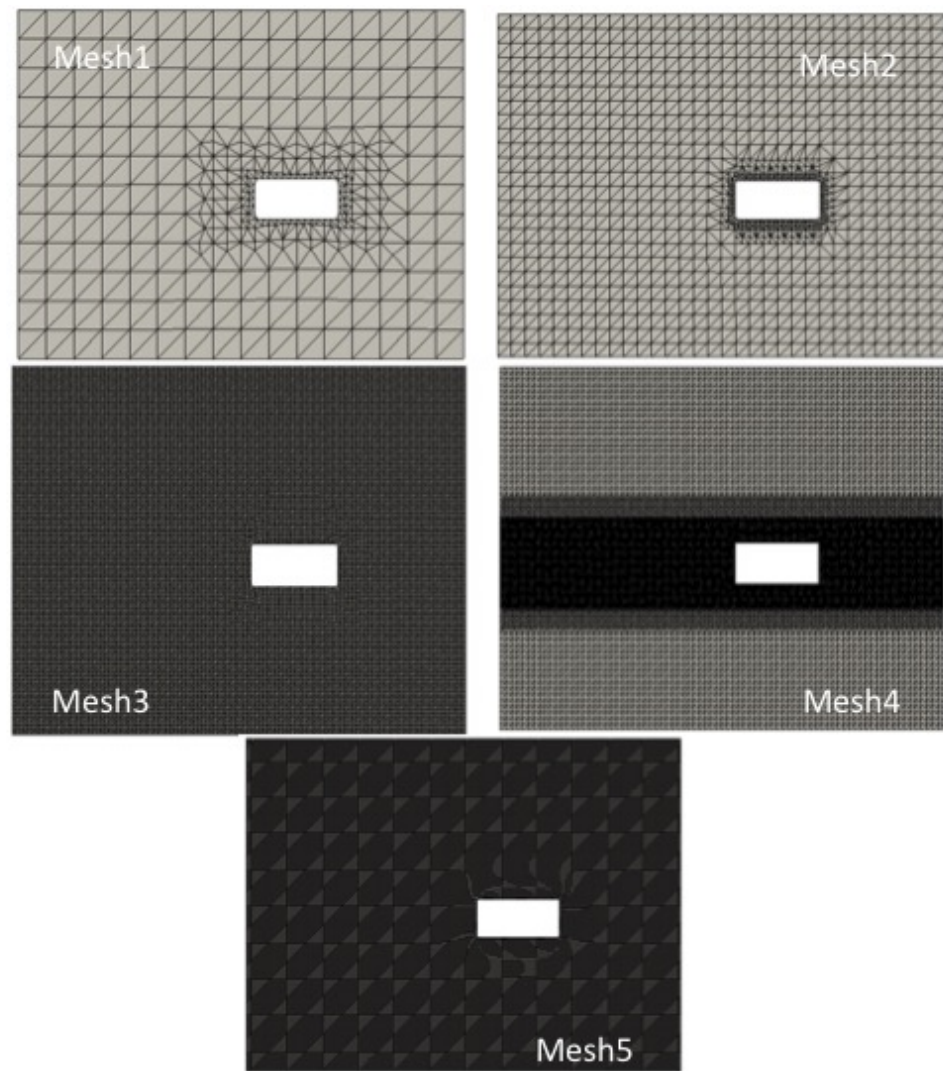
Figure 6.7: *Mesh sensitivity analysis.*

Figure 6.8: *Free surface gauges: gauge 1 = 0.3 m, gauge 2 = 0.6 m, gauge 3 = 1.55 m.*
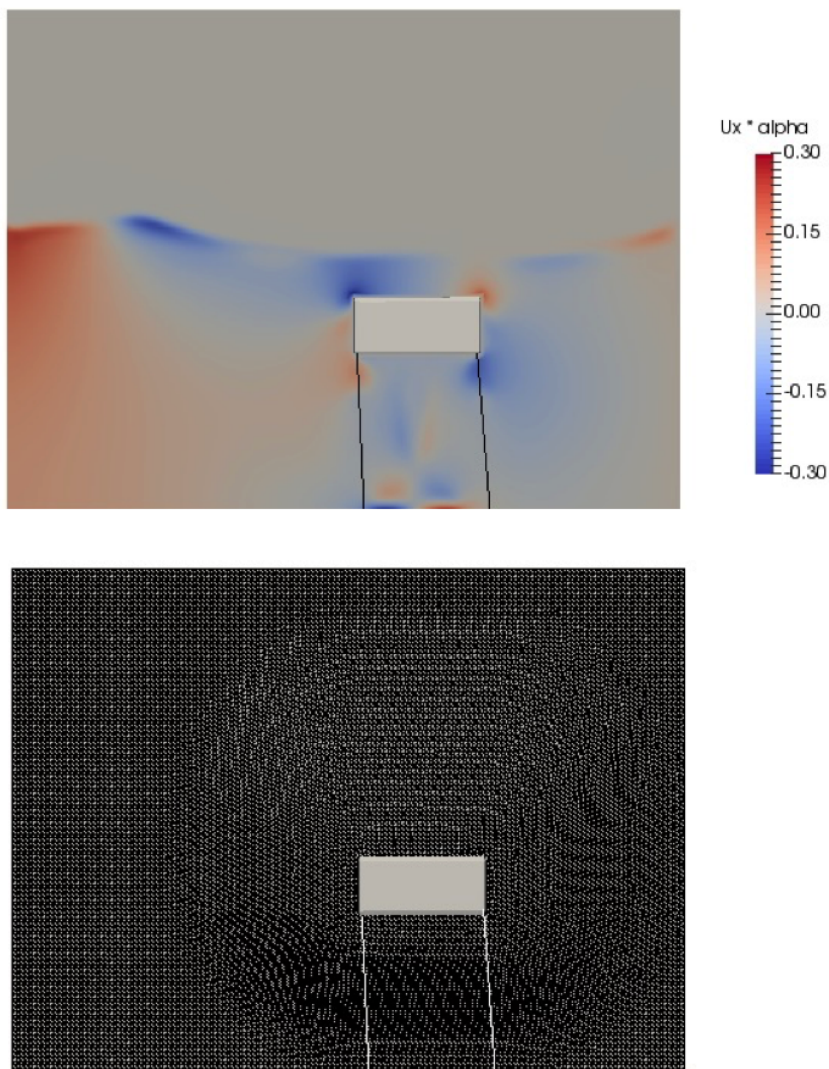
Figure 6.9: *Snapshot of the CFD simulation with velocity field and mesh deformation, t/T=0.*
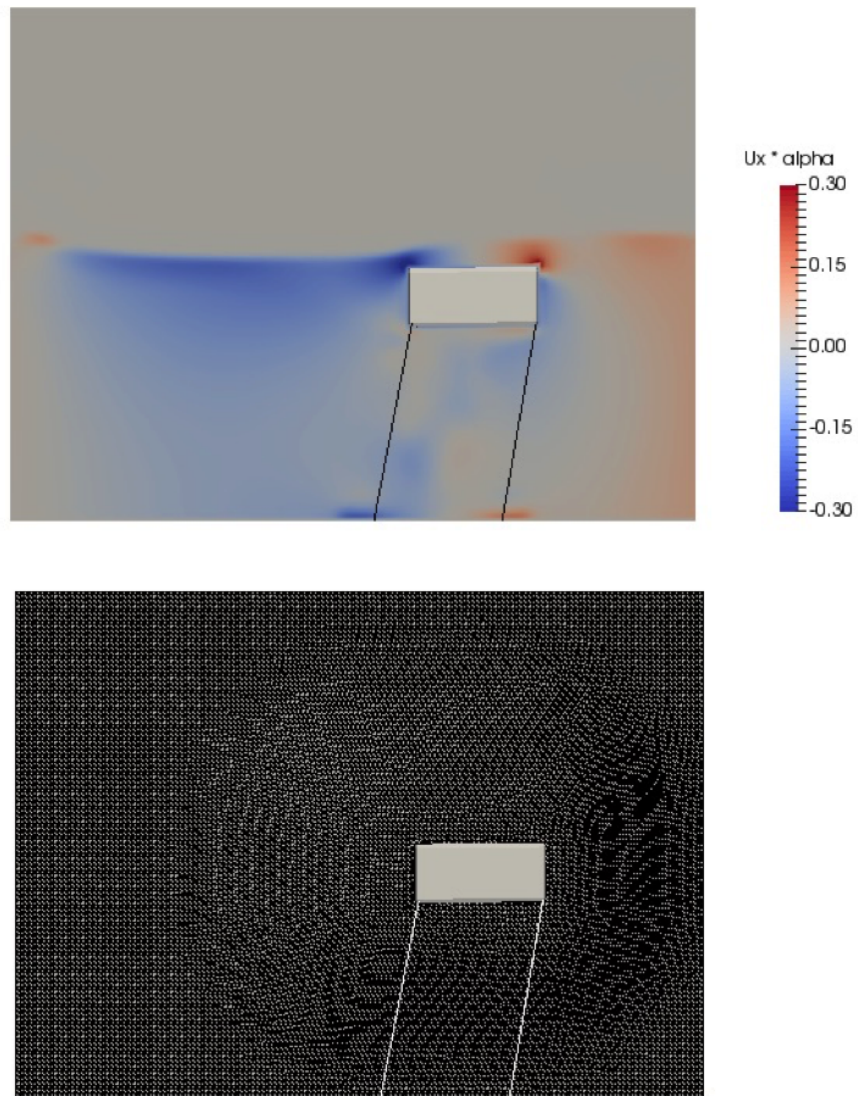
Figure 6.10: *Snapshot of the CFD simulation with velocity field and mesh deformation, t/T=1.*
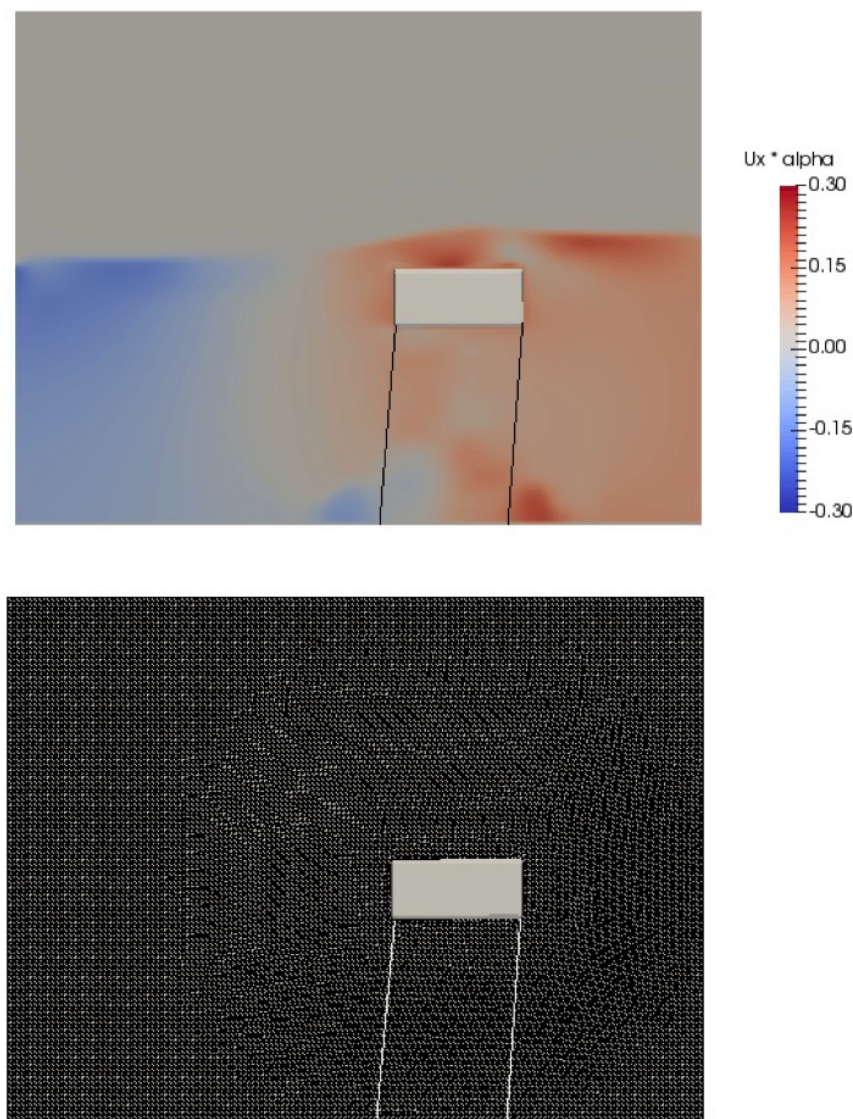
Figure 6.11: *Snapshot of the CFD simulation with velocity field and mesh deformation, t/T=2.*

Figure 6.12: *Snapshot of the CFD simulation with velocity field and mesh deformation, t/T=3.*
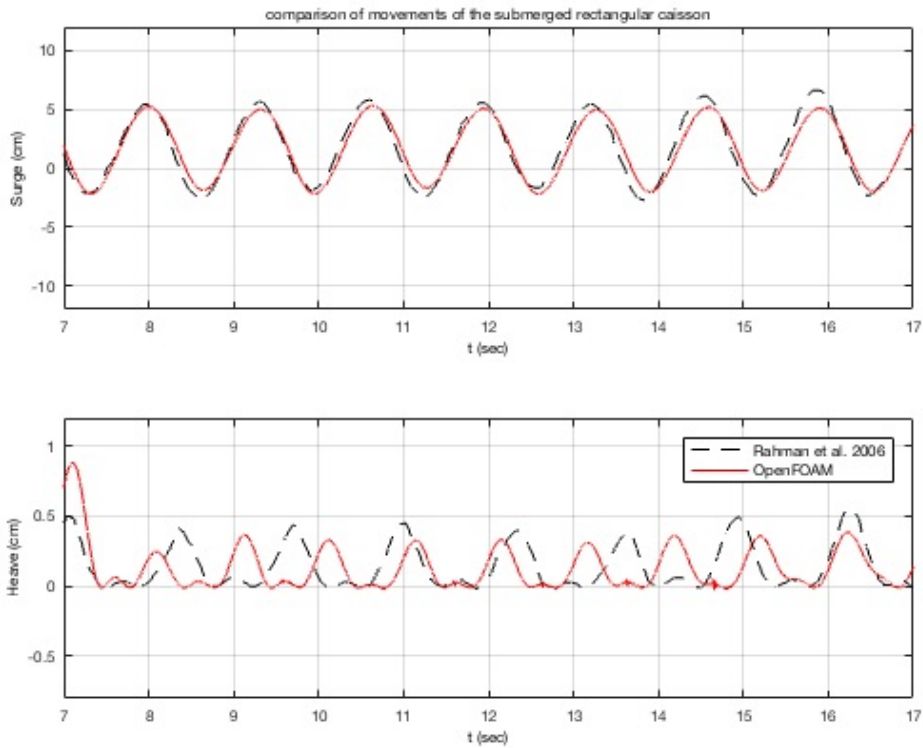
Figure 6.13: *Case A results in surge and heave.*

In the fig. 6.13, the results are reported in term of movement of the centre of mass of the submerged caisson in surge and heave. In the paper of Rahman (66) movements along the wave propagation direction were called sway, but it is not the correct term, so hereby this is surge.

The comparison for surge displacement is satisfying. It means that the developed mooring line was well designed and able to represent the real cable. Focusing on the movements in heave, in the physical tests, the damping effects and the weight of the chain can cause a delay in the heave response of the body compared to the numerical one. In numerical test, the mooring lines are represented as a line so these phenomena are neglected. Otherwise, many values of the damping coefficient were tested, but no one could change the results. So it is deducible that this coefficient is not able to solve the issue. It is possible to see that this problem happens just in vertical displacements with vertical lines, because of that phenomena are relevant and influent just in this configuration. For the case A is not possible to compare the forces because in Rahman's
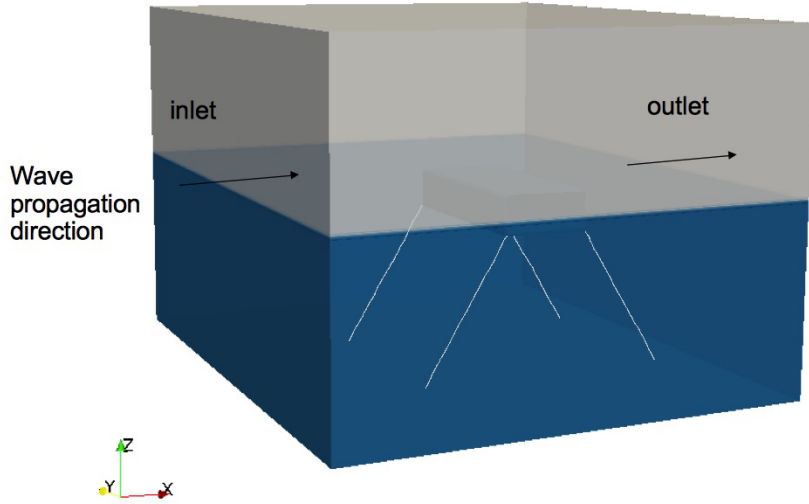
Figure 6.14: *Computational domain, caseB.*

paper they are not reported. It is possible to conclude, for this test, that the comparison between the data is good. The CFD code is able to predict fairly the behaviour of the floating caisson and the movements, there is just a shift (or delay) for the heave response, as discussed before.

6.4.2.3 Case B

Then, the second validation test is run according to case B presented in table 3. Water depth, (h) is 65 cm, mooring lines are inclined ($\theta = 60°$) and their length at rest position is 0.67 m. The wave height, H, is 3.1 cm and the wave period, T, was 1.0 s. The stiffness of the lines was set as 236000 N/m, as stated before, this information missed in Rahman's paper, so it is found compared the initial tensions on the lines. The computational domain and mesh characteristics were equal to case A.

The free surface signals from the gauges are presented in figure 6.15.

The comparison for all the movements, in the three degrees of freedom, results very
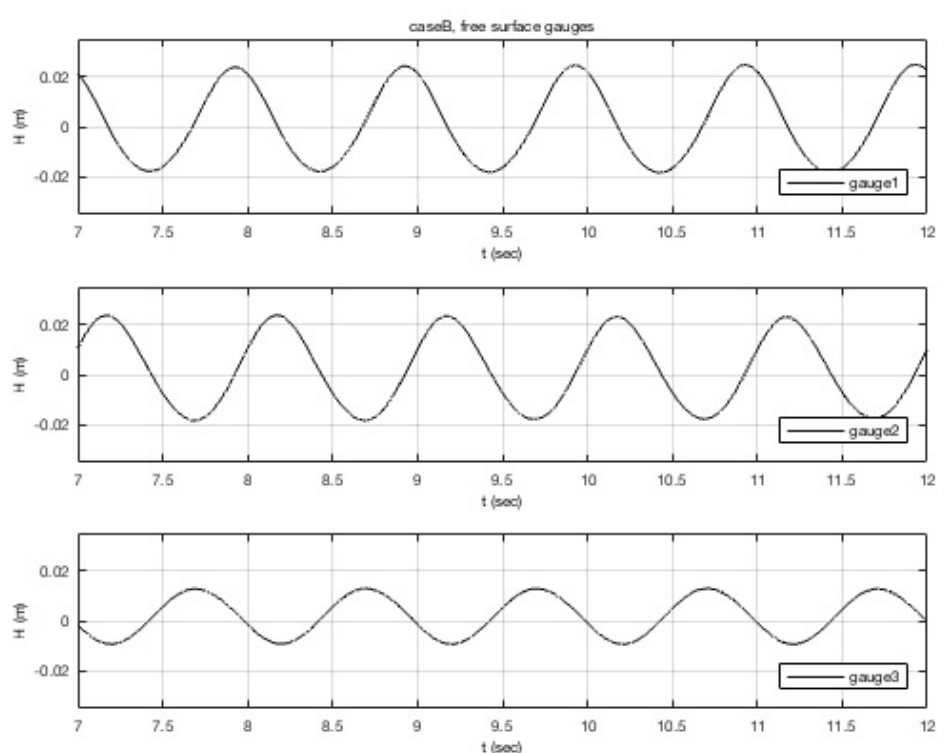
Figure 6.15: *Free surface gauges: gauge 1 = 0.3 m, gauge 2 = 0.6 m, gauge 3 = 1.55 m.*

Figure 6.16: *Snapshot of the CFD simulation with velocity field and mesh deformation, t/T=0.*
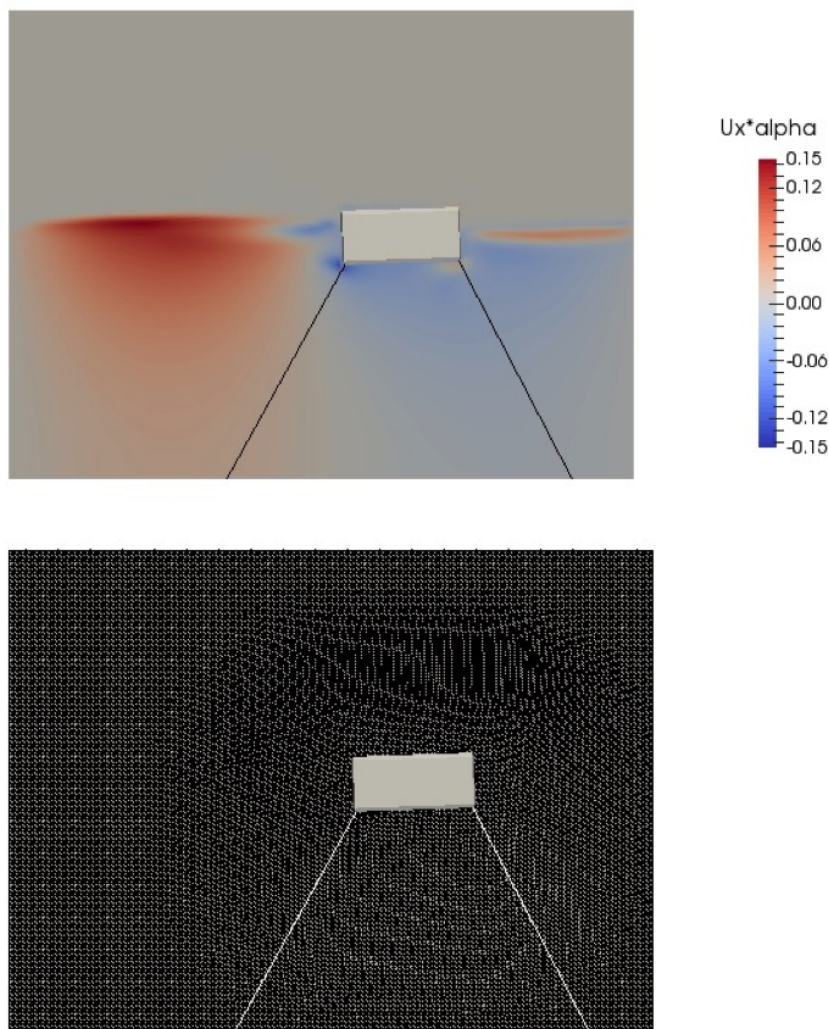
Figure 6.17: *Snapshot of the CFD simulation with velocity field and mesh deformation, t/T=1.*
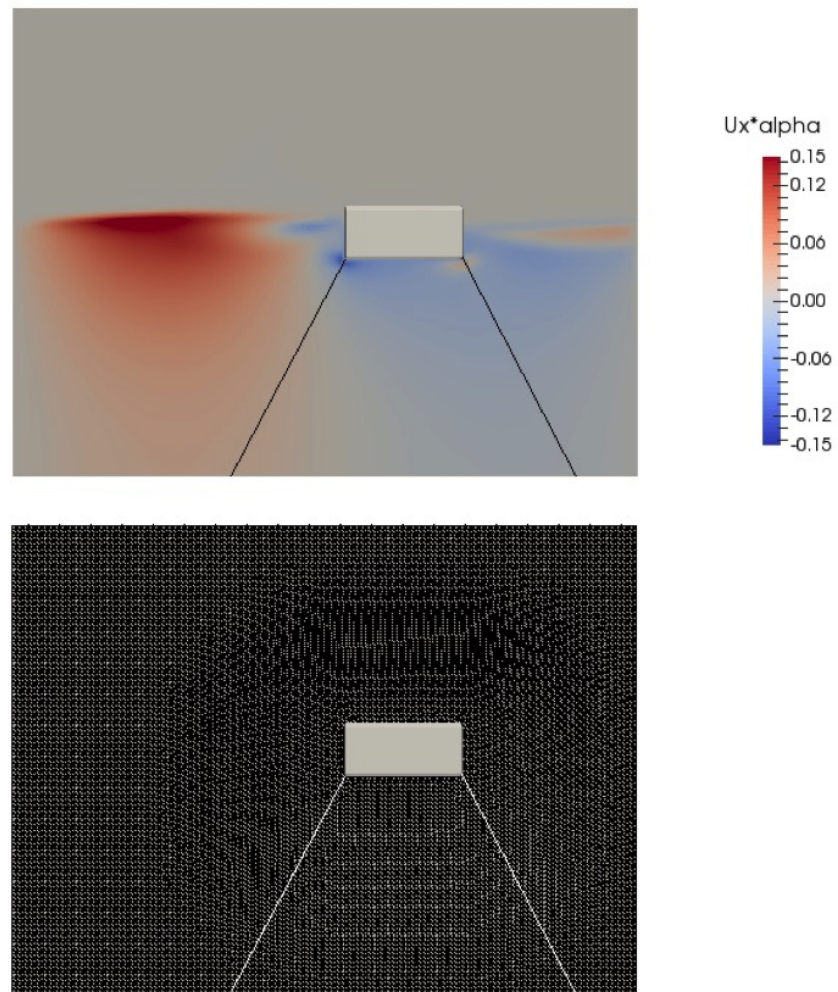
Figure 6.18: *Snapshot of the CFD simulation with velocity field and mesh deformation, t/T=2.*
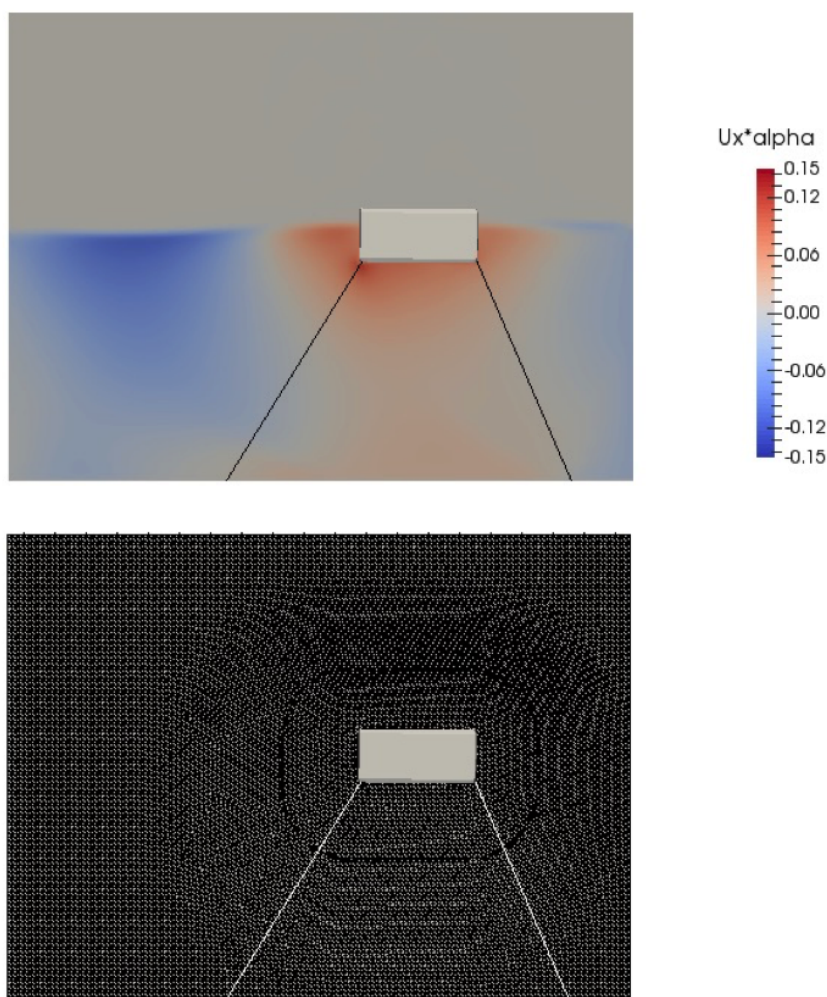
Figure 6.19: *Snapshot of the CFD simulation with velocity field and mesh deformation, t/T=3.*

Figure 6.20: *Snapshot of the CFD simulation with velocity field and mesh deformation, t/T=4.*

Figure 6.21: *Case B results in surge, heave and roll.*
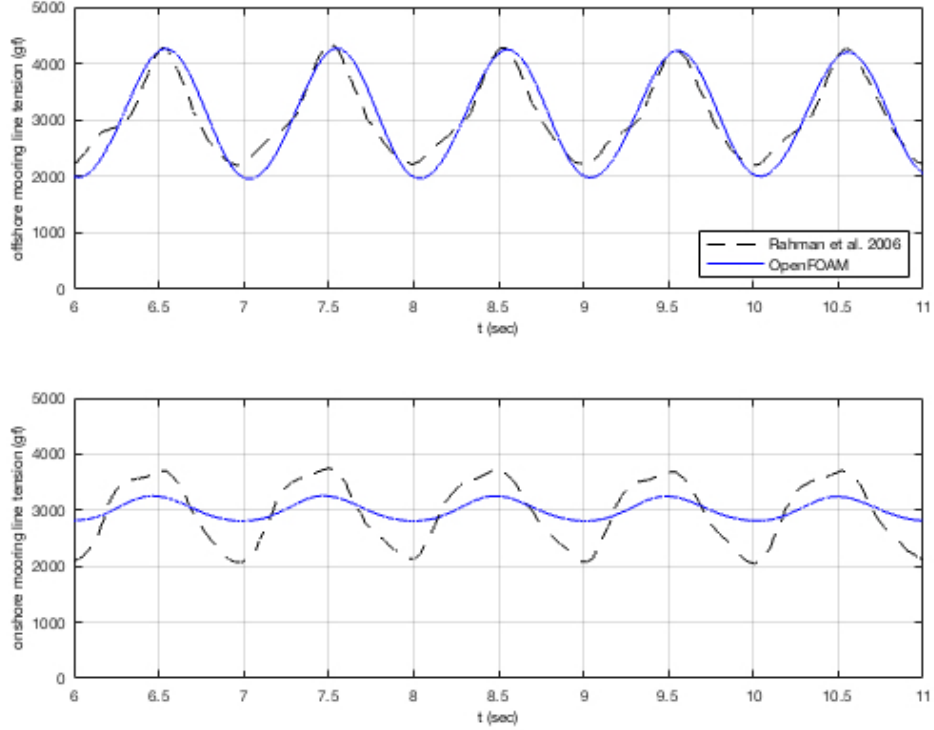
Figure 6.22: *Case B results, in terms of tension on the mooring lines.*

good for the case B. It can be highlighted that the numerical code is able to predict perfectly the period of the oscillations and also the magnitude for heave and surge. Only for the roll, the CFD model slightly underestimates the amplitude of the movement. For this case, it is possible to compare the forces on the mooring lines too.

From the figures 6.21 and 6.22, it is possible to check that the offshore lines are modelled very well, as the forces are the same as in the physical experiments. On the onshore moorings, the magnitude of the forces seems underestimated by the numerical code. It may occur because of the floating body do not stress the onshore cable, that remains perpendicular to the object, without recording variation of the tensions. Furthermore, the drag force usually induces an increase of the load on the offshore line and a decrease on the onshore one, as resulted in the numerical code. At the end of the comparison, it results that The new implemented mooring line code is well designed and it is able to reproduce the behaviour and response of a floating structure and its mooring systems.

6.5   Wave and Current Interaction

In order to show others applications of the code, the same floating caisson, in both the mooring systems configurations (case A and case B), hit by different waves conditions and various current flows and current plus waves, was analysed. Furthermore, another type of structure, a vertical cylinder, was tested under different currents conditions. In IHFOAM waves and currents can be generated together, as explained and illustrated in chap. 5.

6.5.1   Case A and Case B

The following tests are carried out: Vertical mooring lines (case A):
- caseA1: only current = 0.25 m/s
- caseA2: only current = 0.5 m/s
- caseA3: current (0.25 m/s) and wave (H=0.73 m, T=1.3 s, the same tested during the validation) in same direction (T_r=1.15 sec)
- caseA4: current (0.25 m/s) and wave (H=0.73 m, T=1.3 s, the same tested during the validation) in opposite direction (T_r=1.5 sec)
- caseA5: H=0.45m, T=1s
- caseA6: H=0.045m, T=1.315s
- caseA7: H=0.1m, T=1.315s
- caseA8: H=0.085m, T=1s
- caseA9: irregular wave: H=0.073 m, T=1.3 sec

   Inclined mooring lines (case B):
- caseB1: H=0.08m, T=1s
- caseB2: H=0.1m, T=1s
- caseB3: H=0.08m, T=1.315s
- caseB4: H=0.045m, T=1.315s
- caseB5: irregular wave: H=0.031m, T=1s
- caseB6: only current = 0.25 m/s
- caseB7: only current = 0.5 m/s
- caseB8: current (0.25 m/s) + wave (H=0.31 m, T=1 s, the same tested during the validation) in same direction (T_r = 0.86 sec)
- caseB9: current (0.25 m/s) + wave (H=0.31 m, T=1 s, the same tested during the validation) in opposite direction (T_r = 1.19 sec)
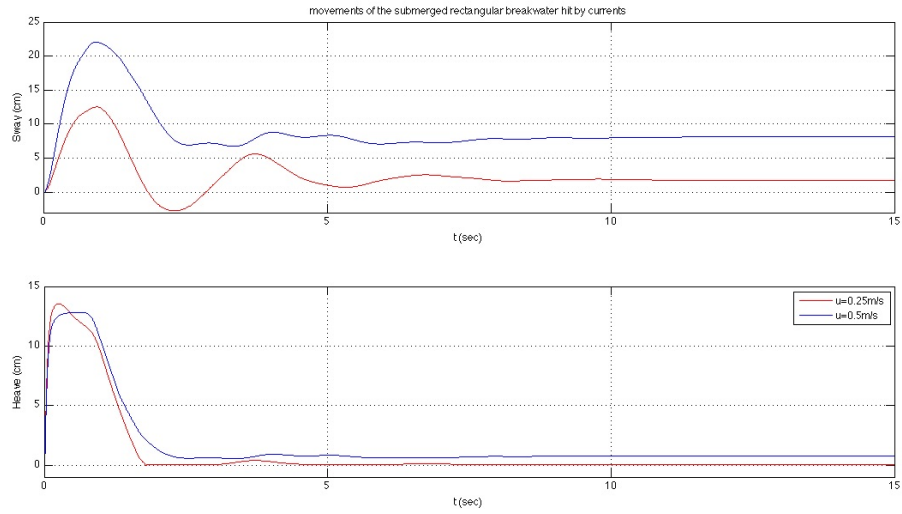
Figure 6.23: *Case A6 and Case A7, (u=0.25m/s and u=0.5 m/s).*

As written above, the wave conditions tested are the same used for the validation, respectively for case A and case B, instead the magnitude the currents were chosen in order to represent offshore (or at least not near shore) conditions, where never very strong currents happen. All the results are reported and discussed below.

6.5.1.1 Case A

In Case A, the water depth, h, was 65 cm and the mooring lines were inclined with an angle θ of 90° and long 0.47 m. The stiffness of the lines was set as 236000 N/m. The setting at rest position was previously presented in figure 6.6. The results of all the wave and current simulations are reported hereby.

Then, the different wave conditions, listed before, and irregular waves were tested on the same structure.

6.5.1.2 Case B

Then, case B was run. The water depth, h, was 0.65 m and the mooring lines were inclined with an angle θ of 60° and long 0.67 m. The stiffness of the lines was set as 236000 N/m. The setting at rest position was previously presented in figure 6.14. The
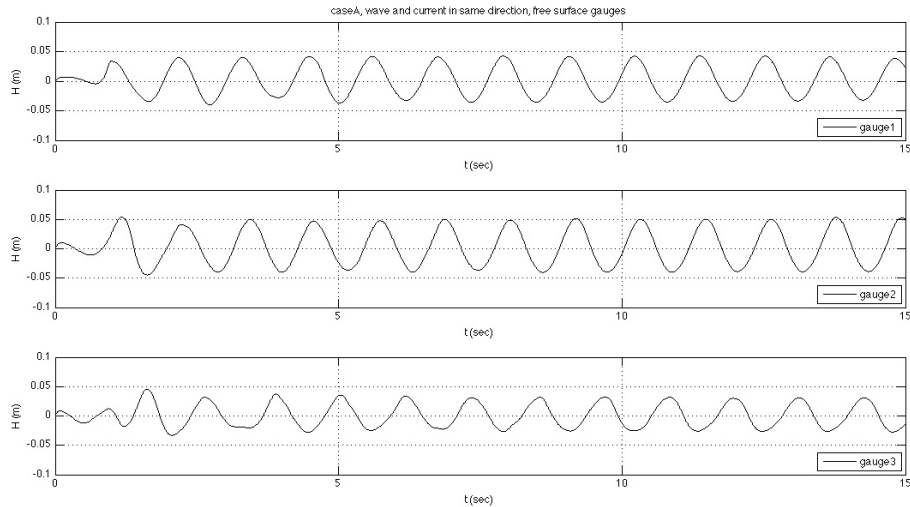
Figure 6.24: *Free surface Gauges in case A8.*
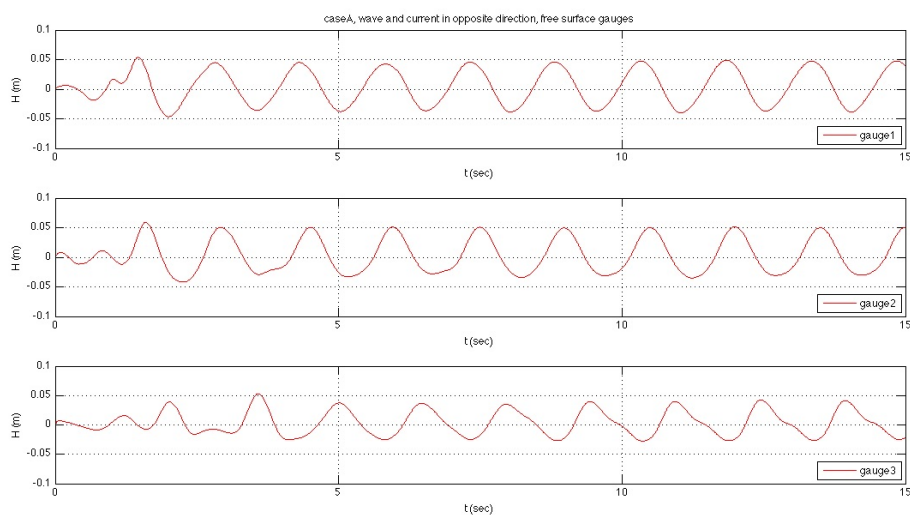
Figure 6.25: *Wave Gauges in case A9.*

95
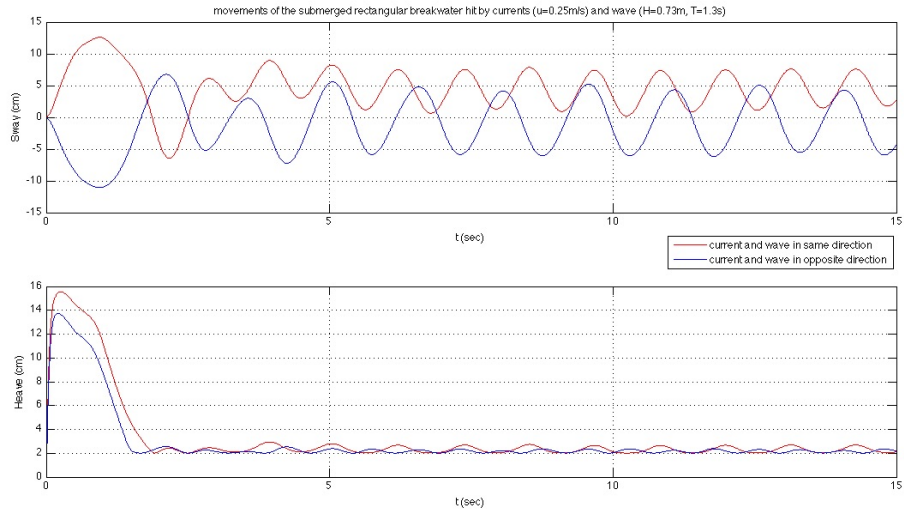
Figure 6.26: *Case A8 and Case A9.*
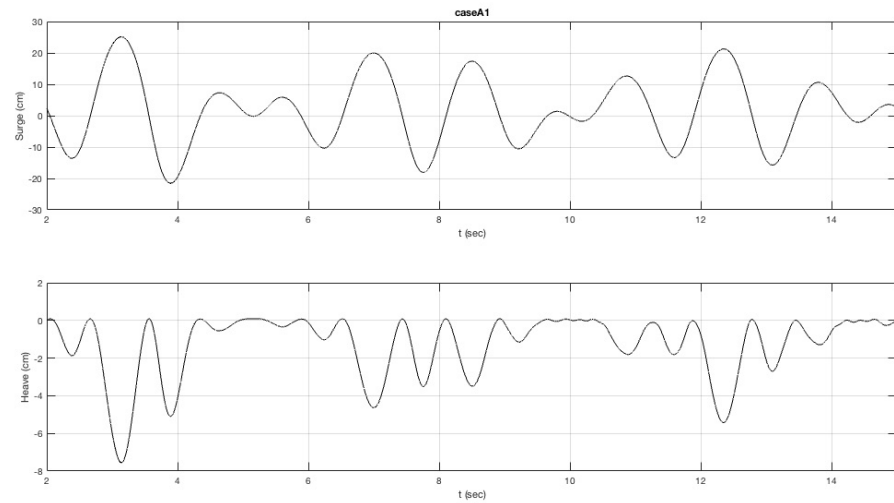
Figure 6.27: *Case A1 (H=0.1m, T=1.315s).*
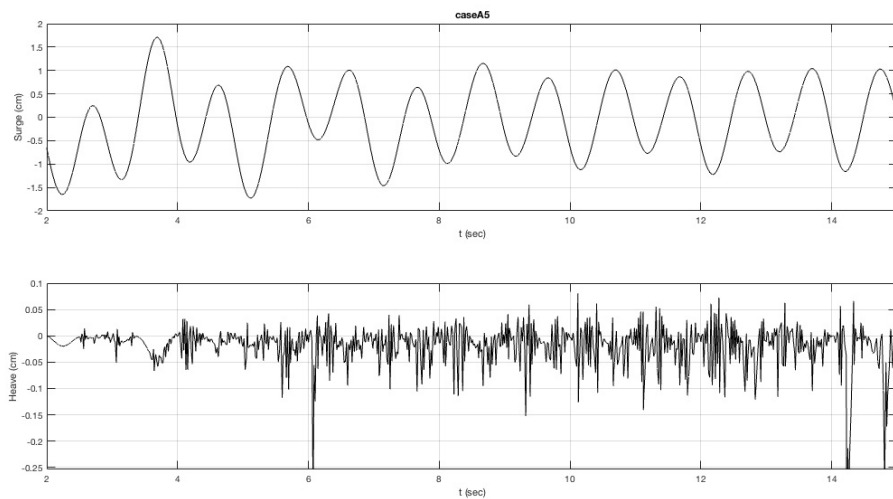
Figure 6.28: *Case A5 (H=0.45m, T=1s).*
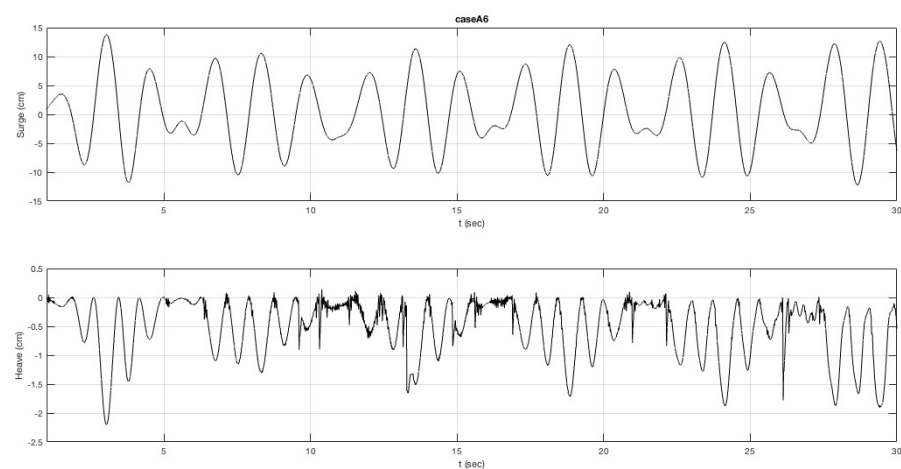
Figure 6.29: *Case A6 (H=0.045m, T=1.315s).*
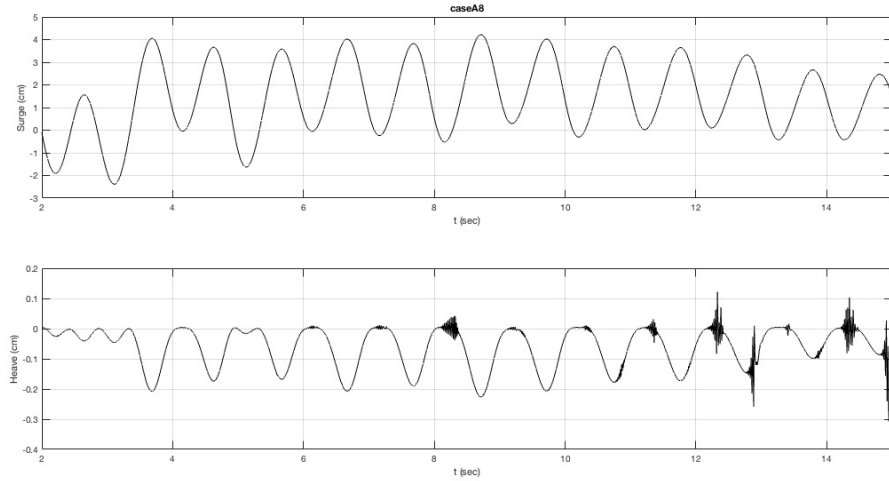
Figure 6.30: *Case A8 (H=0.085m, T=1s)*.
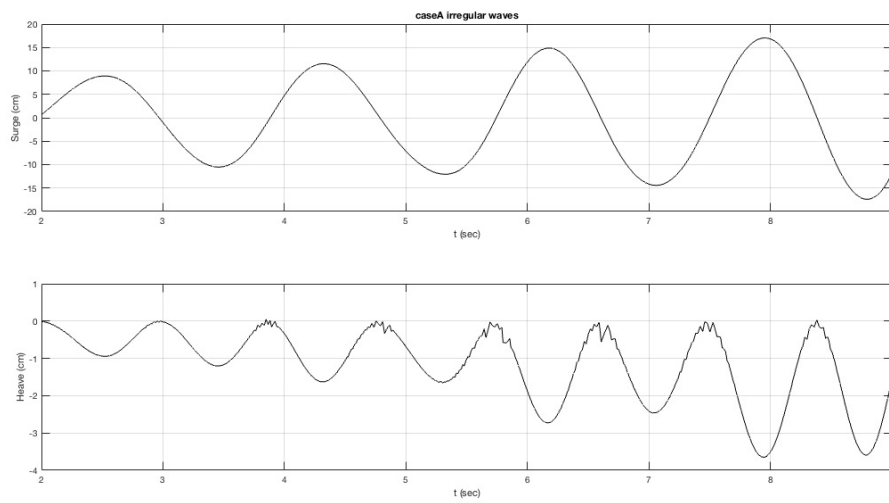
Figure 6.31: *Case A9*.
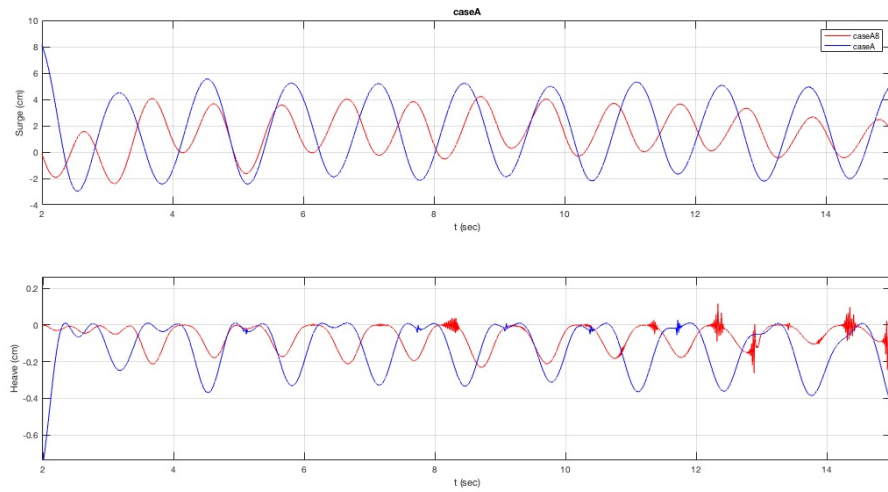
Figure 6.32: *Comparison cases A and A8.*
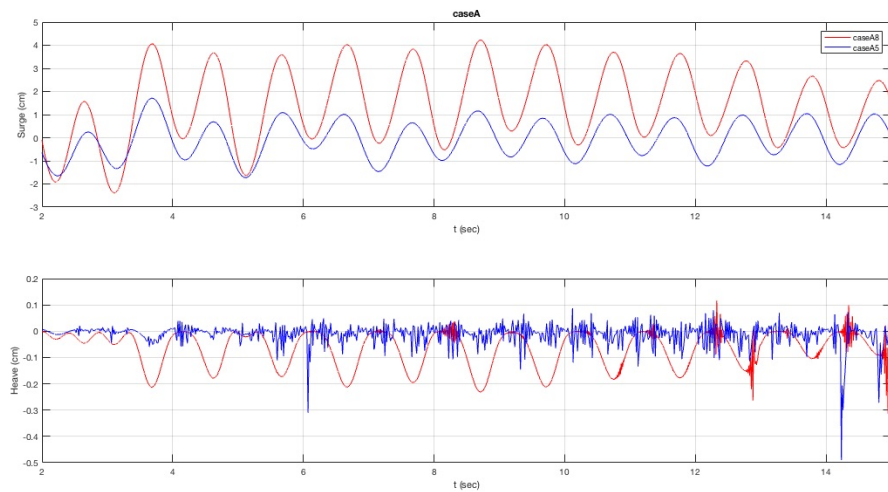
Figure 6.33: *Comparison cases A5 and A8.*
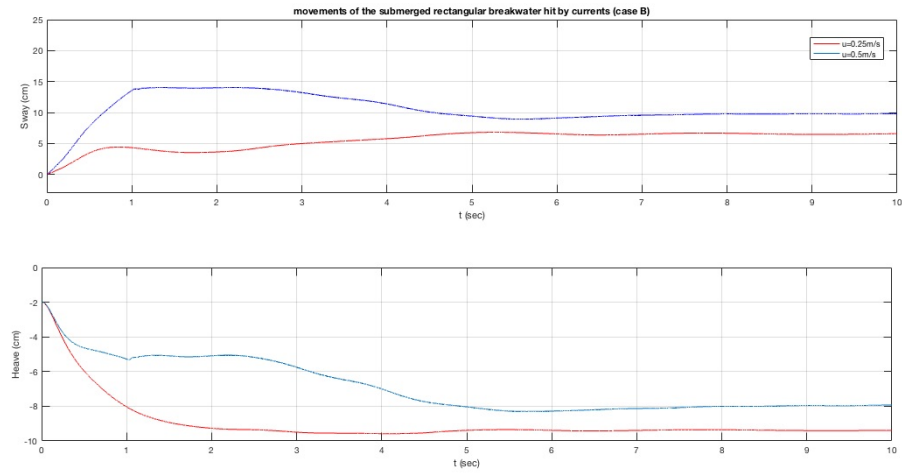
Figure 6.34: *Case B6 and B7 (u=0.25m/s and u=0.5 m/s).*

results of all the wave and current simulations are reported hereby.

Then, the different wave conditions, listed before, and irregular waves were tested on the same structure.

It is possible to see that wave period has a greater influence on the behaviour of the floating caisson, for both the two cases, with vertical and inclined lines. On the other hand, it is clear that inclined-mooring lines restrict the movements, especially the surge, more that the vertical ones.

In these kind of moored system, the worst situation is when the mooring lines become slack, it is not connected to an huge load, for this reason the pre-load of the mooring line is very important. For all the done cases, the tensions on both offshore and onshore mooring lines were recorded and analysed. The most relevant deductions are that with the inclined lines setting, the stress on the cables are largely reduced, for all the conditions. Another clear conclusion is that the onshore line is less stressed.

Furthermore, it is important to underline that when waves and currents act together, the maximum drag force is not the linear sum of the two components, but it is a quadratic resistance. Talking about the effects of simultaneous wave and current, when the current direction is opposite to wave propagation, the load on the mooring lines is lighter.
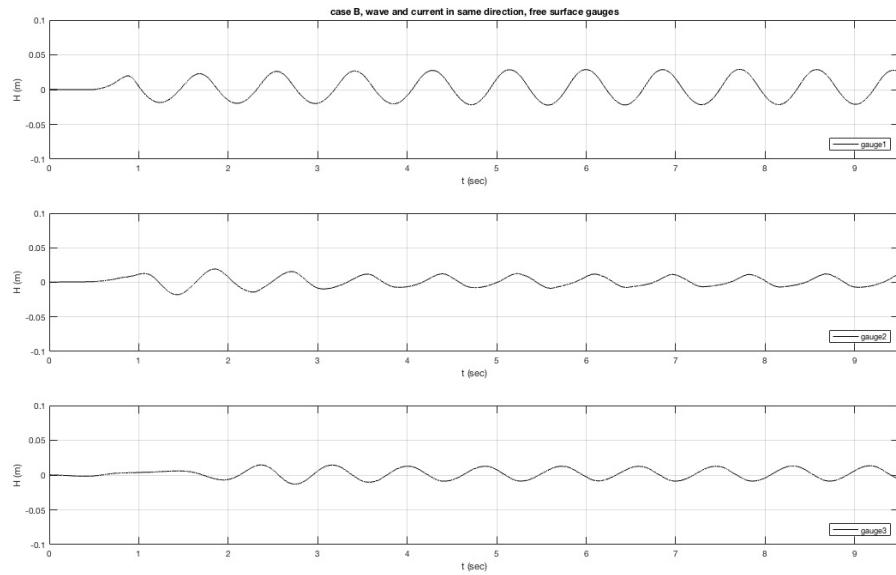
Figure 6.35: *Wave Gauges in case B8.*
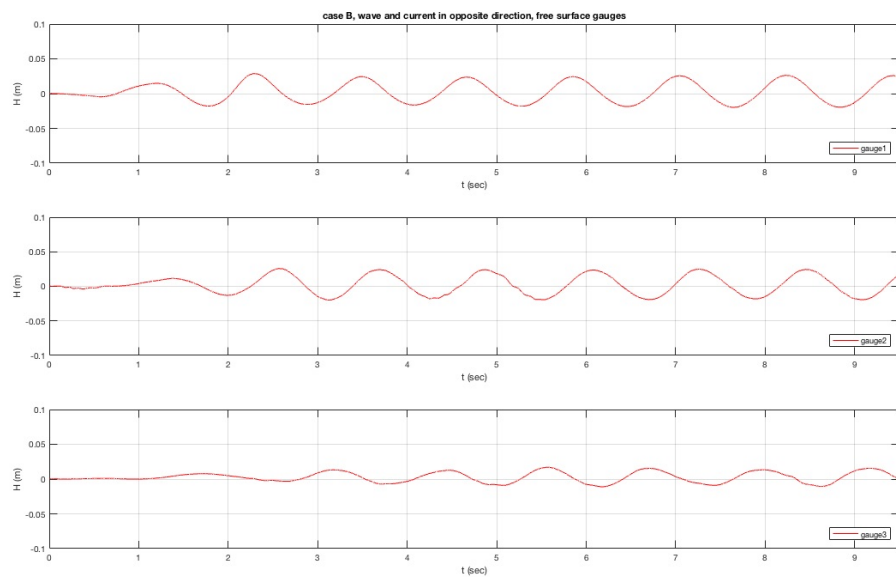
Figure 6.36: *Wave Gauges in case B9.*
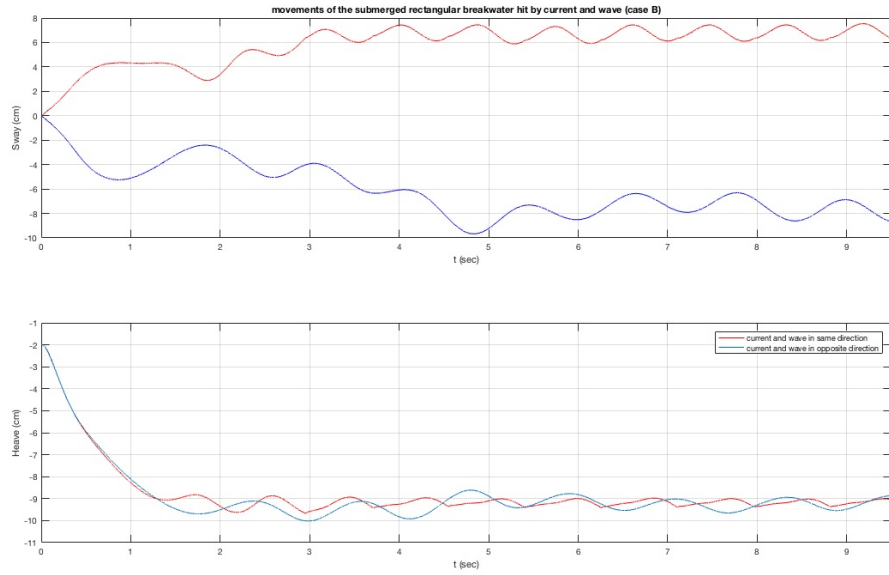
Figure 6.37: *Case B8 (red line) and B9 (blue line).*
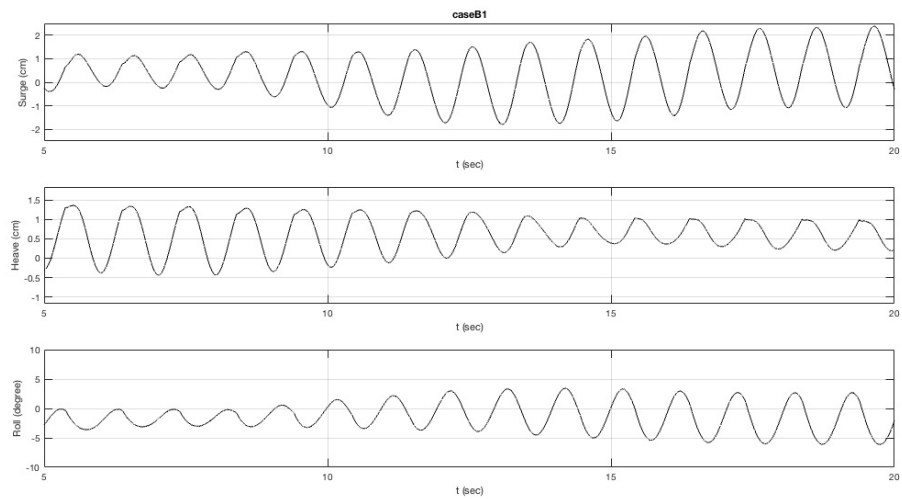
Figure 6.38: *Case B1 (H=0.08m, T=1s).*
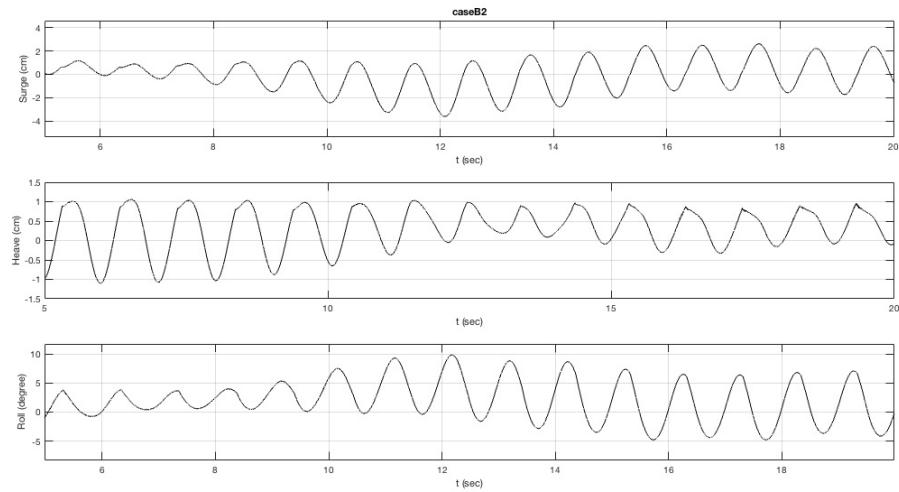
Figure 6.39: *Case B2 (H=0.1m, T=1s).*
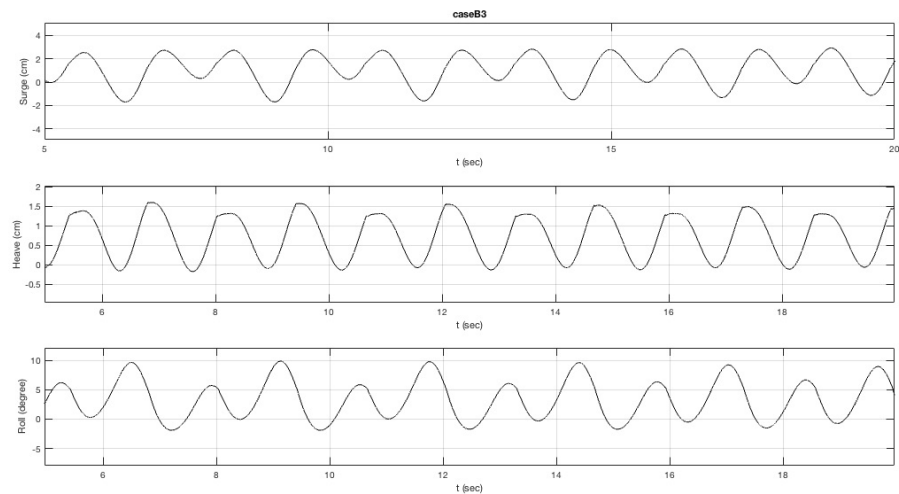
Figure 6.40: *Case B3 (H=0.08m, T=1.315s).*
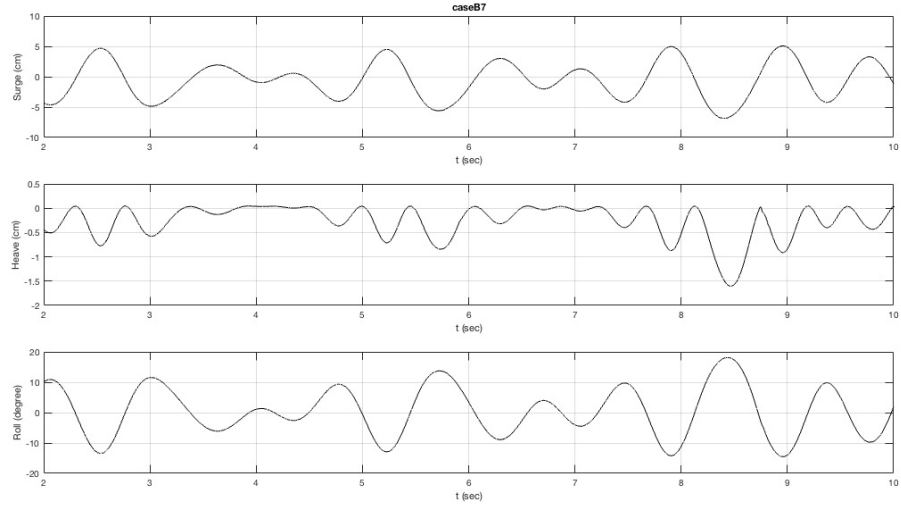
Figure 6.41: *Case B4 (H=0.045m, T=1.315s).*
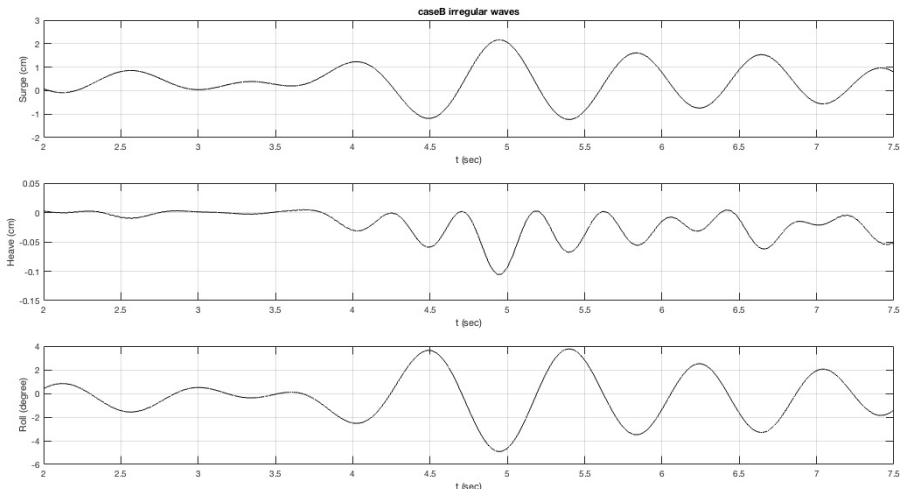
Figure 6.42: *Case B5.*
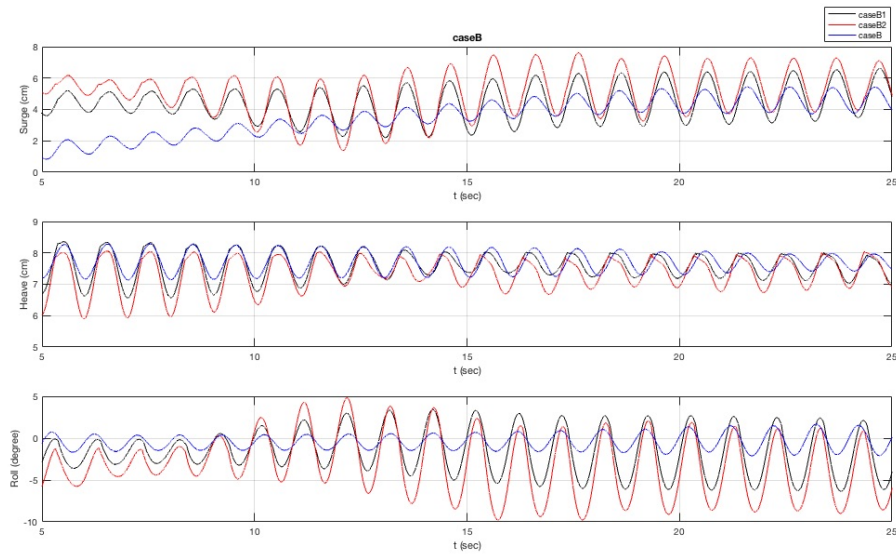
Figure 6.43: *Comparison between Case B, B1 and B2.*
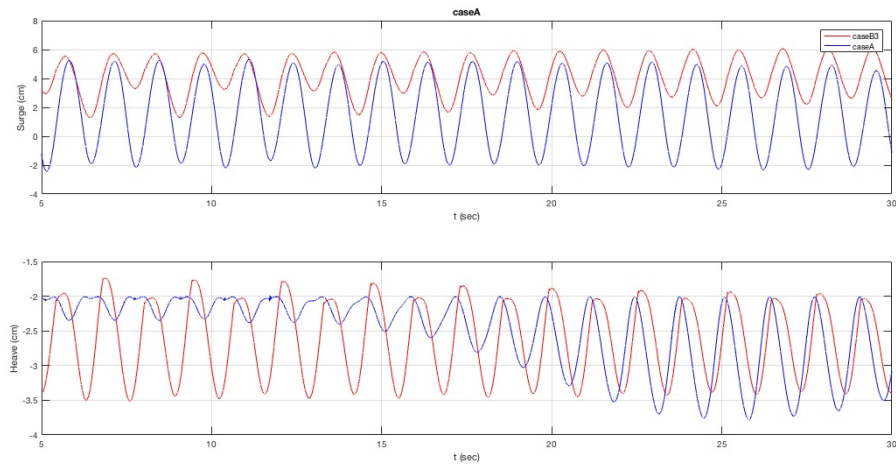
Figure 6.44: *Comparison between Case B3 and A.*

6.5.2   Vertical Cylinder Tests

Then, different kind of floating structures were analysed, in particular a vertical cylinder, in order to represent a sub-structure of a floating wind turbine. For this case, the responses of the moored body hit by currents were studied. Different mooring configurations, single and multiples lines and vertical and inclined settings, and various current intensities were evaluated.

The numerical wave tank was made of 3150000 cells. The domain discretization was more refined around the floating body. The refinement zone was done by Snappy-HexMesh tool available in OpenFOAM. The computational domain characteristics are listed in table 6.7, while the floating caisson features are in table 6.8. The main results are shown in term of heave and surge displacements from fig. 6.46 to fig. 6.49.

	Tot. Dimension (m)	Number of cells	Cell size (m)
X	7	280	0.025
Y	2.5	50	0.05
Z	4.5	225	0.02

Table 6.7: *Computational domain characteristics.*

Centre of mass (m)	$(1, 0, -0.5)$
Radius of gyraton (m)	(2.51, 2.51, 1.26)
Mass (kg)	62.8

Table 6.8: *Cylindrical structure characteristics.*

Thank to these tests it was possible to study the response of different floating structures and see specific features, for example, when the body reaches a steady state.All these different tests were reported as examples, to show the functionality and versatility of the code and the results and informations that can be achieved thanks to it. Moreover, the last simulations illustrated the capacity of the code to generate wave and currents coupled.
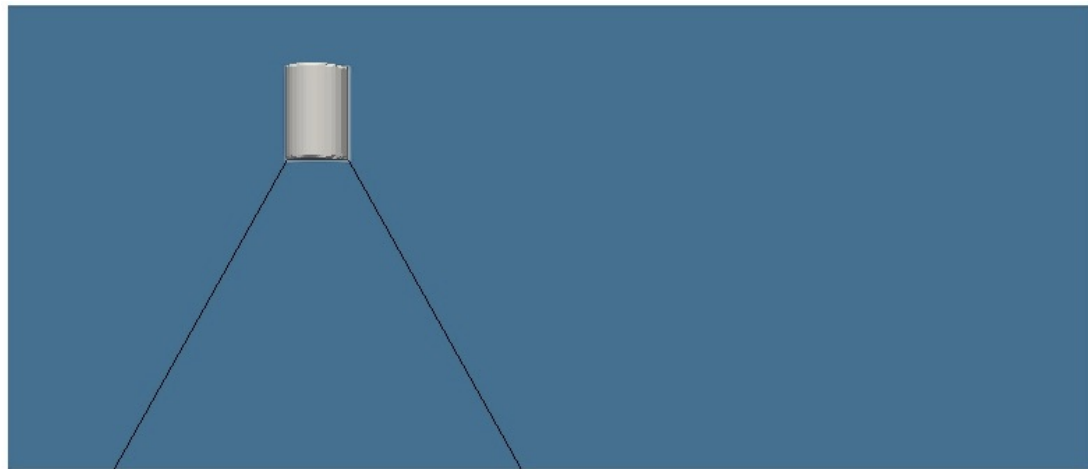
Figure 6.45: *Numerical wave-current flume setting for the vertical cylinder.*
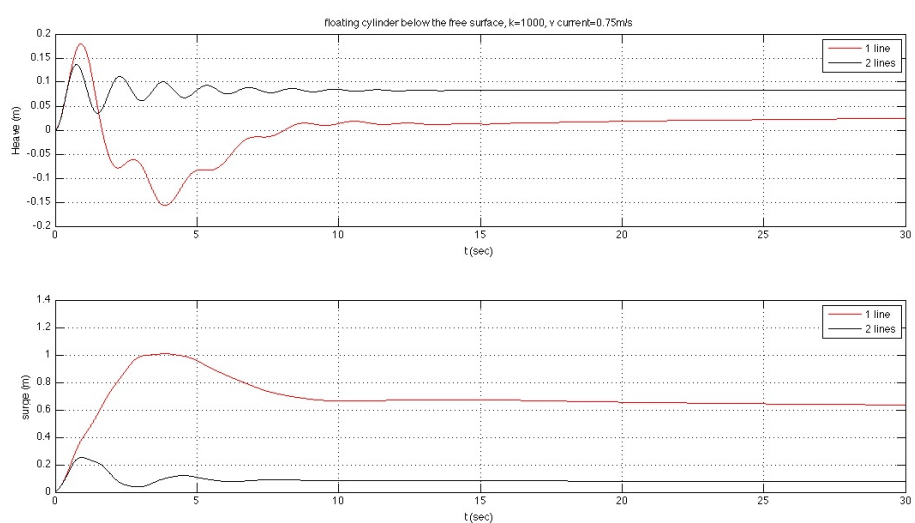
Figure 6.46: *Different responses of the moored cylinder with one (red) or two (black) lines hit by a current of 0.75 m/s.*
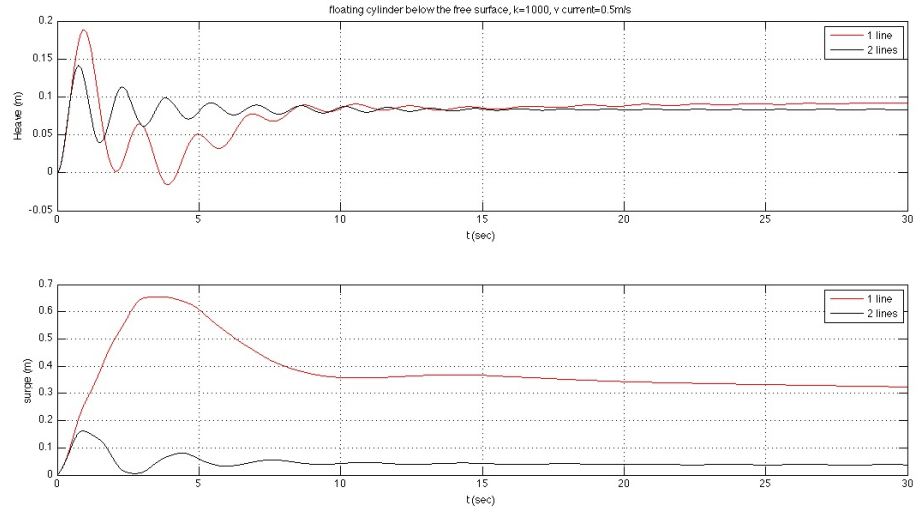
Figure 6.47: *Different responses of the moored cylinder with one (red) or two (black) lines hit by a current of 0.5 m/s.*
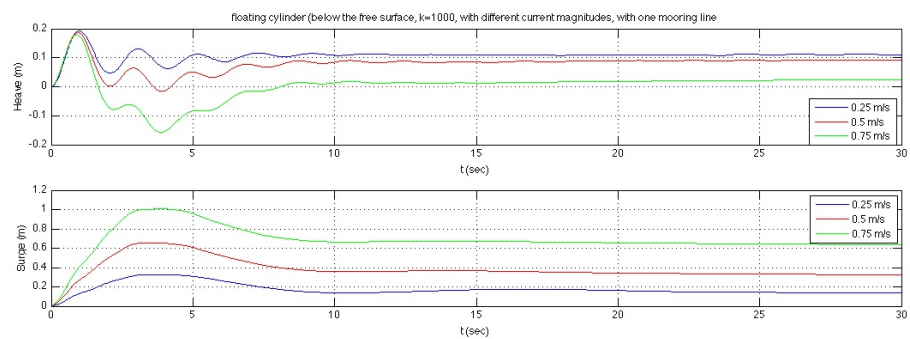
Figure 6.48: *Different responses of the moored cylinder with one mooring line hit by different current intensities.*
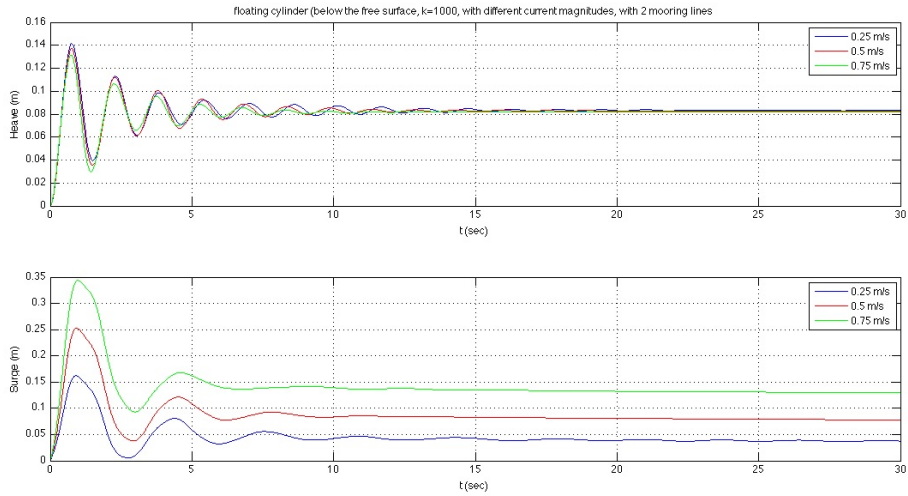
Figure 6.49: *Different responses of the moored cylinder with two mooring line hit by different current intensities.*

6.6 Conclusions

The new implemented code was calibrated for all the parameters and validated thank to the comparison with experimental data. Others tests were carried out in order to show different applications of the code.

For the case A, it was possible to conclude that the comparison between the data was good. The CFD code was able to predict fairly the behaviour of the floating caisson and predict the movements, there was just a shift or delay for the heave, because the damping effects and the weight of the chain, that happens in physical tests, can cause a delay in the heave response of the body compared to the numerical one. In numerical test, the mooring lines were represented as a line so this phenomena were neglected. Furthermore, it was possible to see that this problem happens just in vertical displacements with vertical lines, because of that phenomena was relevant and influent just in this particular configuration.

Supporting that assumption, all the results from the numerical simulations of case B corresponded to the experimental ones. That confirmed that the new implemented mooring line code was well designed and it was able to reproduce the behaviour and response of a floating structure and its mooring systems.

Running these cases and comparing OpenFOAM results with the Rahman's experimental data, we were able to say that the new CFD tool can predict well the movement of

the floating structure. There were some differences between the CFD and experimental results, maybe due to the fact that the Rahman's paper did not report the mooring lines parameters so they were estimated by comparing the initial forces. Finally, it was possible to say that the numerical code, OpenFOAM + IHFOAM + new mooring system, was validated. On the other hand, this is just the first step to develop a more general CFD mooring tool able to represent every kind of anchoring lines that are used in offshore and coastal engineering. in this thesis, just tension legs were considered, but also catenary one will be implemented.

Furthermore, we can conclude that is a valid instrument to investigate floating and submerged structures for all the coastal and offshore engineering applications. The capacity of the code to generate and absorb wave and wave and currents coupled was demonstrated.

It can be a very useful and, last but not least aspect, totally open-source tool that engineers can use during all the design phases, as and with experimental tests.

7

Case of Study: Floating Wind Turbine in the Mediterranean Sea

7.1   Introduction

As the aim of the thesis was to implement a valid numerical instrument to simulate and analyse floating offshore structures, hit by waves and currents, and thank to all the tests done during the Ph.D. research, the new code was calibrated and validated, finally it can be applied to a real study case. In this way, I was able to analyse the response of a real floating wind turbine in the Meditteranean Sea, in order to perform a preliminary design of an offshore floating wind farm in Italy. As the most windy zones of the country are around Sardinia and Sicily, a deep water area offshore of Mazara del Vallo (Sicily) was chosen for this application. In the following sections, technical characteristics of the area are illustrated, then the selected type of wind turbine is described and the results of numerical simulations are presented.

7.2   Site Description

The criteria for selecting suitable locations for the deployment of the offshore park should not only include technical-engineering terms but also ecological-environmental considerations and socio-economic aspects (75). The area of study is located in the Southern Mediterranean Sea, off the coast of Mazara del Vallo (Italy) as depicted in Fig. 7.1.

Wind and wave climate in the Meditteranean Sea (4) are shown in the figures 7.2 and 7.3. It is possible to see that the mean wind velocity is very promising, as it is

7. CASE OF STUDY: FLOATING WIND TURBINE IN THE MEDITERRANEAN SEA

Figure 7.1: *Design area for the floating wind turbine in the Mediterranean Sea.*

around 7 m/s (4), the best range of wind in which commercial turbines are designed to produce. At the same time, the mean wave height of the site is less than 1.2 m (4), as it can be feasible to build a floating wind park. In order to get more detail design values, wave conditions of Mazara del Vallo were checked in the Italian Wave Atlas (22). The significant wave height, H_s, and the peak wave period, T_p, with a return period of 50 years (usual design life of a wind turbine) resulted:

H_s= 7 m, T_p=11.2 sec.

Then, for a return period of 2 years (more frequent conditions):

H_s=5 m, T_p= 10.4 sec.

The area for the offshore wind park was settled sufficiently off the coast, about 40 km offshore, in order to avoid the visual impact from the land (43) and to prevent any disagreement due to tourism activities.

A detail bathymetry of the offshore area is reported in Figures 7.4 and 7.5. It outcomes that the area where could possible to install wind turbines is about 100 m depth.
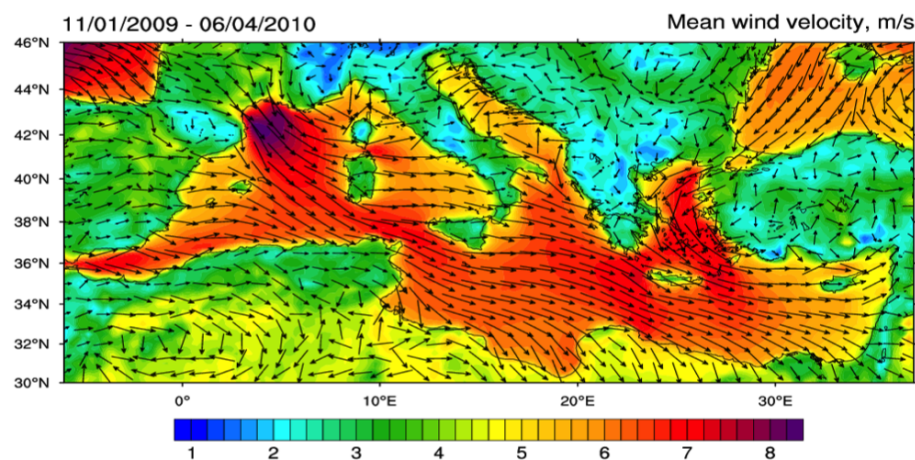
Figure 7.2: *Wind data of the Mediterranean Sea (4).*
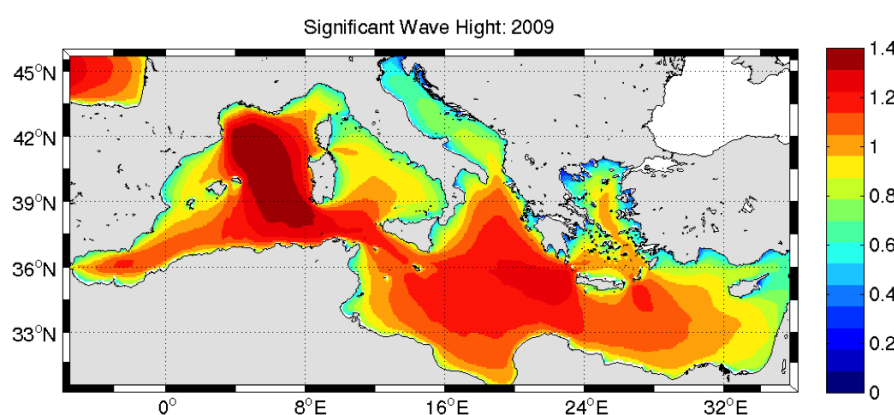
Figure 7.3: *Wave data of the Mediterranean Sea (4).*
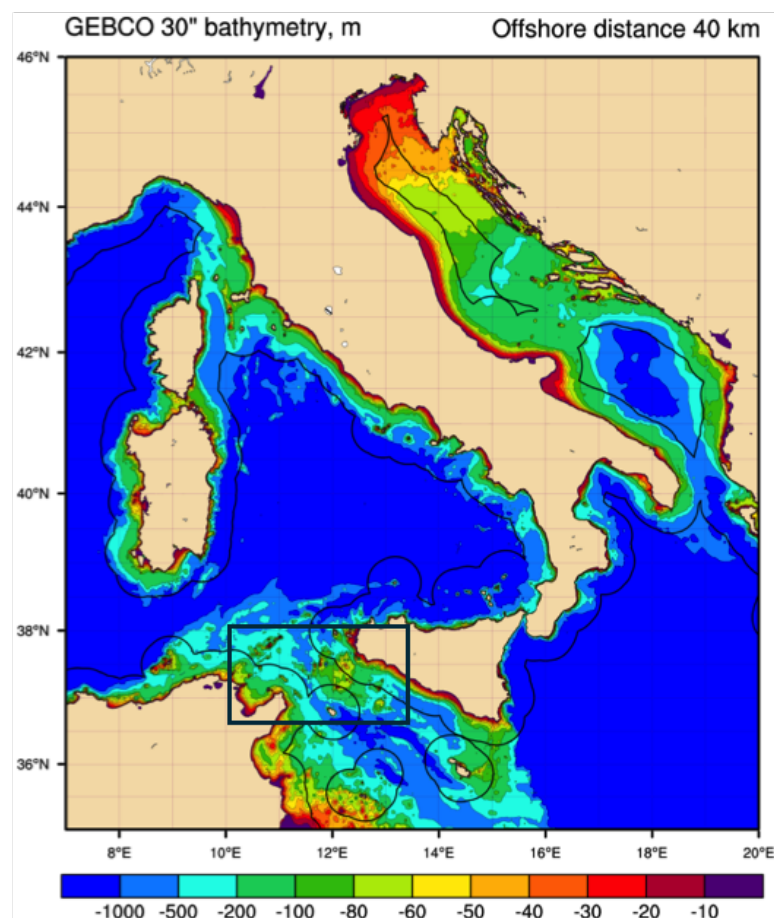
Figure 7.4: *Bathymetry data of Italian Sea (4).*

Figure 7.5: *Detail of bathymetry data of the chosen area for the floating wind farm in the Mediterranean Sea (4).*

7.3 Floating Wind Turbine Details

The Hywind turbine (55), developed and licensed in 2007 by the Norwegian company Statoil, was considered in this study. The structure is a spar floater foundation type and it features a hub height of 100 m above the sea level and the draught is 80 m and the diameter of the substructure is 15 m. The mass of the system is about 11500 tons. The Hywind turbine was chosen because of the charateristics of the chosen site offshore Mazara del Vallo are similar in term of water depth and wind and wave climate, to those in Aberdeen, UK, North Sea, where the Scotland Pilot Park have been installed by Statoil, with this floating turbine (Fig. 7.6). The rated power is 3.6 MW and the power curve, that provides an indicator of the power as a function of the average wind speed at the level of the rotor hub, is given in Fig. 7.7. As it can be observed, the cut-in wind speed is between 3 and 5 m/s, the rated power at 12-13 m/s and the cut-out wind speed at 25 m/s. The capacity factor of the turbine at the study area has been calculated from such power curve and resulting equal to 25% and an average power of 0.9 MW. A comparatively higher capacity factor was the main reason for choosing this model of turbine, selected among all those currently suitable for the European market.

In order to estimate the investment costs and revenues of an offshore wind farm
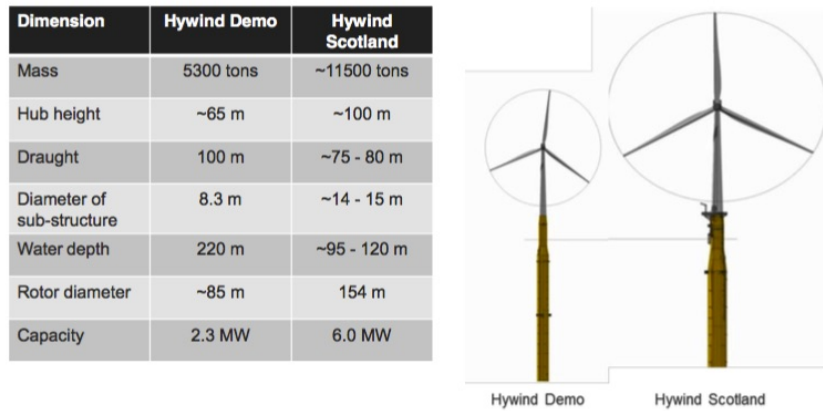
Figure 7.6: *Hywind turbine characteristics.*
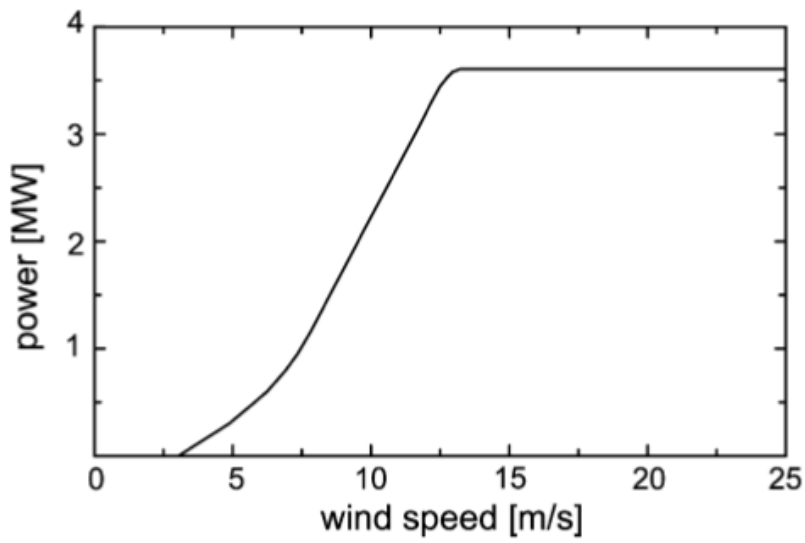
Figure 7.7: *Power curve for the wind turbine selected for this study.*
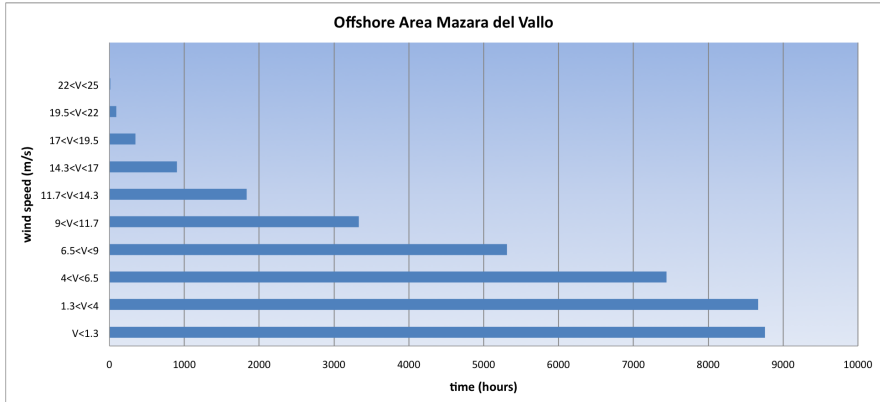
Figure 7.8: *Energy production capacity of the turbine in Mazara del Vallo.*

to be installed at the area of study, an arrangement featuring 60 turbines for a total installed capacity of 216 MW. In order to maintain the shear losses, due to the interaction between turbines, below 9.75% in the favourable case and 11% in the unfavourable case (75), the distance between the structures has been maintained equal to 850 m, resulting a total area covered by the park as a square long 8.5 km and wide 5 km.

Analysing the wind data of the site, the production of the wind turbine was estimated (Fig 7.8). The capacity factor of each turbine in this site is around 20%, and the product energy could be 10800 MWh/year, that is the requirements of 4 thousand families.

7.4 Numerical Modelling of the Structure

In the present work, the numerical code was applied to analyse the response of the selected spar floater structure to sea states of the site. So, for the wave conditions listed in section 7.2, numerical simulations were carried out with the new code.

The water depth was set at 100 m, based on the bathymetry data, as explained before. The numerical wave tank was 292 m long and 150 m wide, as explained in detail in Tab.7.1, in z-direction, a refinement zone around the free surface level was applied, in order to reduce the computational cost and time, but preserving the accuracy of the simulation. Dimension of the cells were calculated considering the main rules related to wave numerical modelling, as in x (wave propagation direction) Δx is equal to $\lambda/120$, where λ is the wave length, and in z direction, in the refined area, Δz is equal to $H/120$, where H is wave height. This domain dimensions were the same for all the tests.
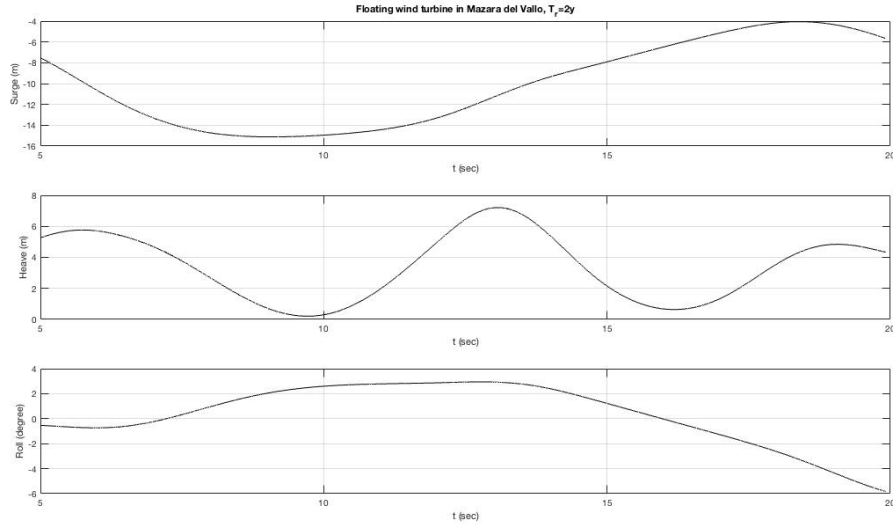
Figure 7.9: *Results of the numerical simulation for wave conditions of t_r=2 years, in terms of heave, surge and roll.*

The structure features were considered as the ones of the real turbine. Floating Wind turbine characteristics:

-mass of the structure=11500000 kg

-centre of mass of the structure= (146.25, 75, 21)

-mooring lines: 3 lines

-restlength of the mooring lines=72 m

-stiffness of the mooring lines= 17200200 N/m

-damping of the mooring lines=0

	Tot. Dimension (m)	Number of cells	Cell size (m)
X	292.5	180	1.625
Y	150	75	2
Z	125	41	min=0.8, max=3

Table 7.1: *Computational domain characteristics.*

With these results, the response of the selected floating turbine was analysed in terms of movements of the hull related to wave impacts (see Figures 7.9, 7.10 ad 7.11). Snapshots of the simulations are reported in Figures 7.12 to 7.16.
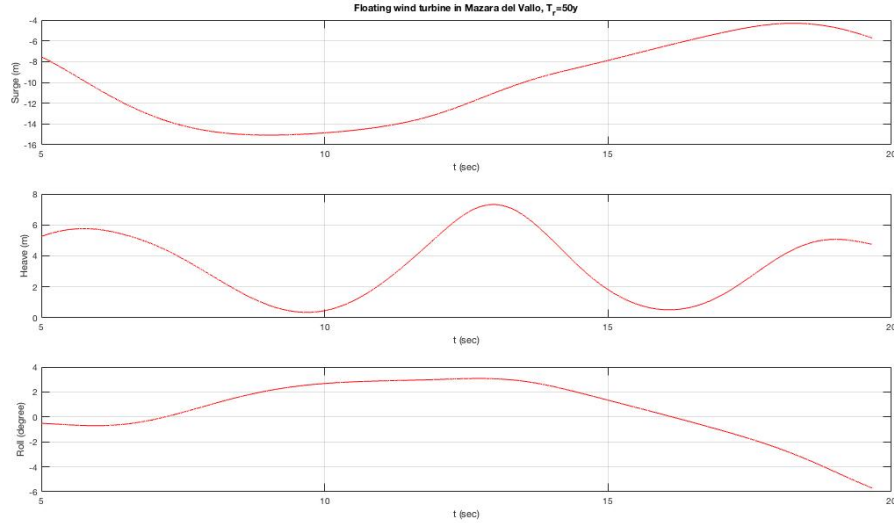
Figure 7.10: *Results of the numerical simulations for wave conditions of t_r=50 years, in terms of heave, surge and roll.*
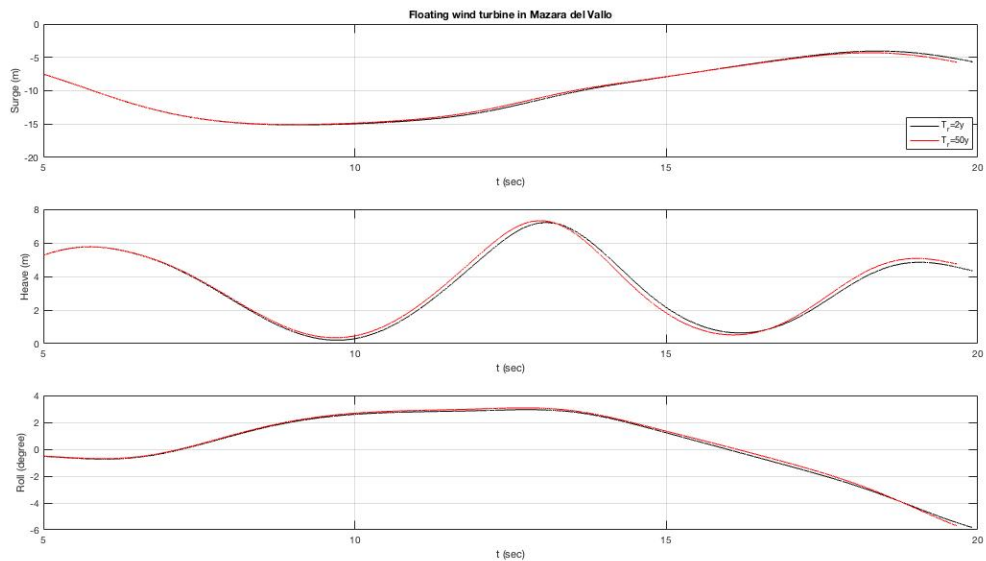
Figure 7.11: *Comparison of numerical results, in terms of heave, surge and roll.*
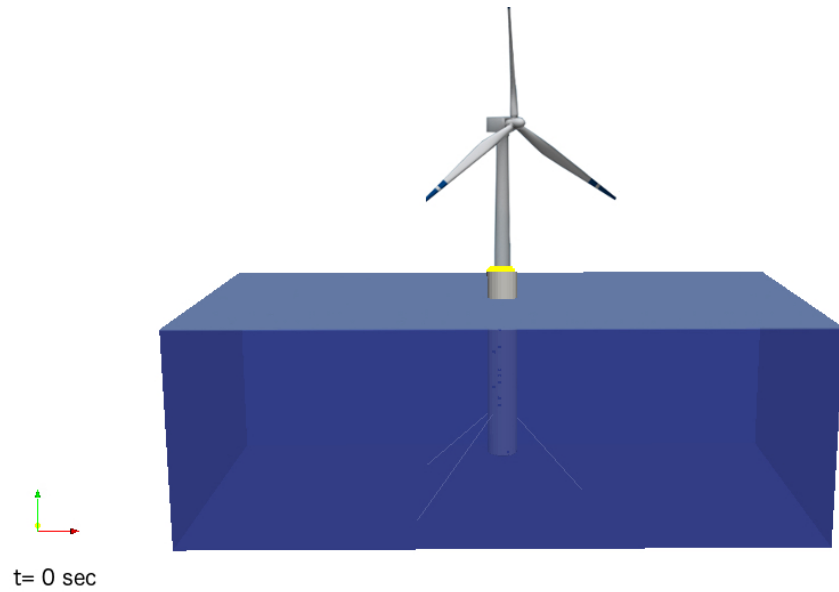
Figure 7.12: *Snapshot of the CFD simulation, t/T=0 sec.*
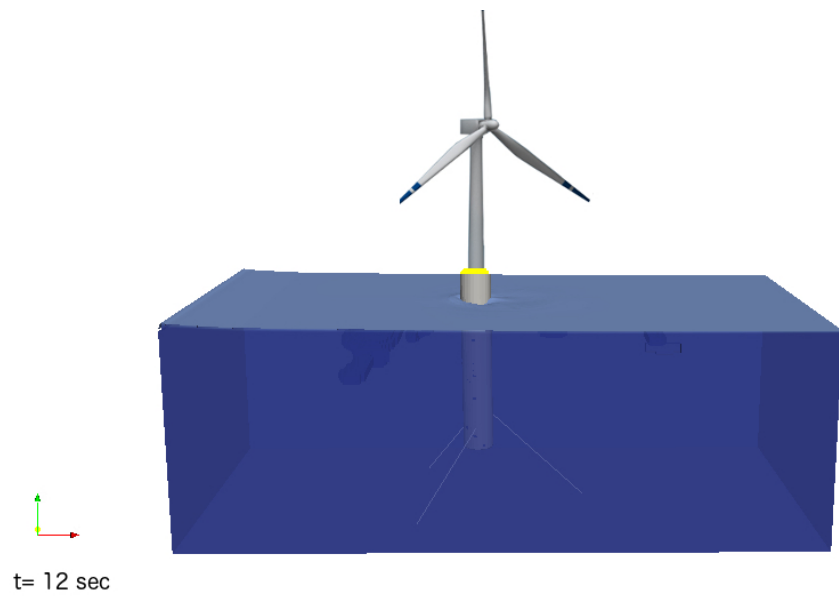
Figure 7.13: *Snapshot of the CFD simulation, t/T=1 sec.*

t= 20 sec
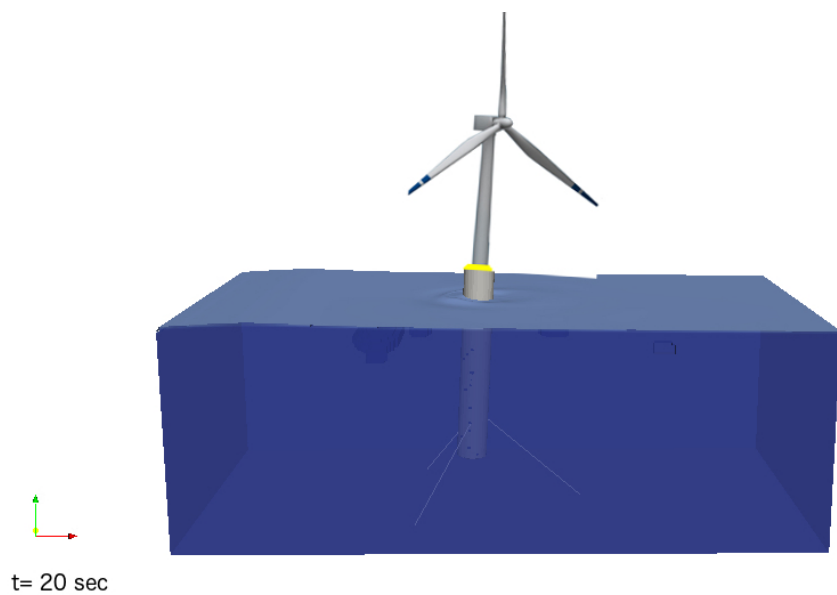
Figure 7.14: *Snapshot of the CFD simulation, t/T=2 sec.*

t= 24 sec
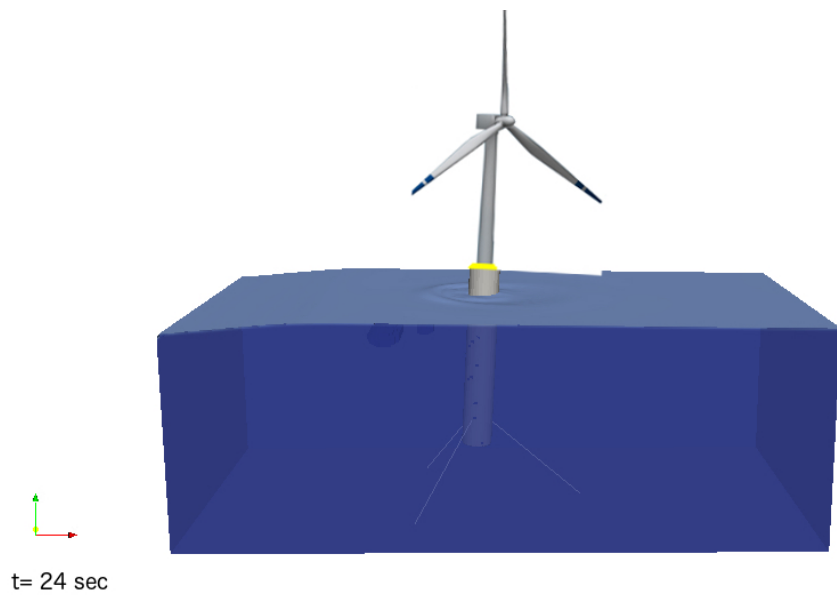
Figure 7.15: *Snapshot of the CFD simulation, t/T=2.5 sec.*
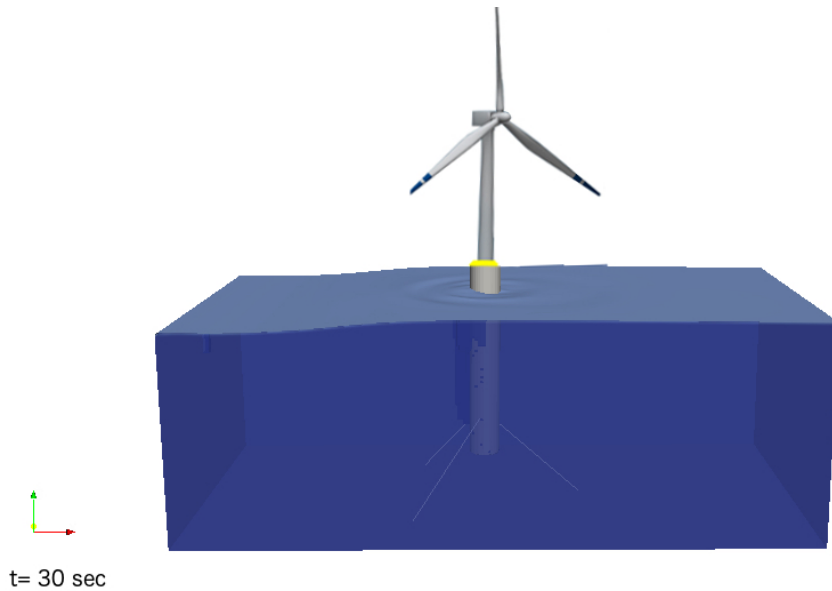
Figure 7.16: *Snapshot of the CFD simulation, t/T=3 sec.*

7.5   Results and Conclusions

Thank to the tests carried out in the new numerical wave tank, it is possible to deduce
that the designed floating turbine can head the sea conditions of the area offshore
Mazara del Vallo.

The movements of the hull induced by the 50 years return period wave are lim-
ited to a small range, the heave displacement is around 5% of the dimension of the
structure, that would not compromise operation of the system; the roll is limited to
an acceptable range; instead, the surge is quite relevant. Otherwise, it is possible to
study an alternative setting of the mooring lines in order to reduce the amplitude of
the movements. Further analysis will be carried on with this aim. The mooring lines,
as designed, resulted able to effort these loads. The others wave conditions tested, as
foreseeable, induced smaller amplitude in heave, surge and roll. It has been shown that
the code can also reproduce regular and irregular waves, currents and waves and cur-
rents coupled, so many others tests can be done on the structure in order to investigate
all its technical features and responses.

In conclusion, even though, of course more investigation are need in order to design
the better floating structure and mooring system and cost assessment need to be done,
but based on this preliminary analysis, it is possible to state that the considered spar

buoy type floating wind turbine can be a suitable structure to be installed in Mazara del Vallo, Sicily, Italy. Furthermore, the feasibility of a floating wind park in the south area of Italy could become a solution for the energy demand in the next future.

From the snapshots of the simulations, it is clear that the new code is perfectly able to model the complete floating wind turbine system.
We can conclude that the numerical developed tool can be applied to real cases, not just to research applications. One more time, thank to that simulations, it is possible to say that it is a valid instrument to investigate floating and submerged structures for all coastal and offshore engineering designs.

Nowadays floating structures are more and more adopted, so it can become a very useful, rapid and helpful instrument.

8

Conclusions

The aim of my Ph.D. research was to implement and validate a tool able to simulate the entire floating system and to assist offshore and harbour engineers during the design phase. In other words, the objectives of this work was to fill the gaps that have been found in previous studies and to enhance features that currently the code, i.e. Open-FOAM, has in order to make it a fully validated and ready tool to be applied in the design process of floating structures.

Initially, the new numerical wave basin was set up for every wave conditions, filling the gap IHFOAM had for deep water regimes. To achieve this goal, new boundary conditions were implemented and a new turbulence model was studied and added to the code to avoid wave damping along the domain and the simulation time. These new numerical features were validated with analytical and experimental tests and their efficiency was demonstrated.

It is, nevertheless, useful to remind that, when simulating in deep-water conditions, the ramping time has to be larger and the choice of turbulence model has a great influence on both period and height of waves. It was possible to point out that for deep water conditions, the new turbulent model is very important and can influence the wave shape and it is able to reduce the wave damping along the numerical channel. Finally, thank to new boundary conditions and new turbulent model, IHFOAM is totally able to generate and absorb every kind of waves and it can be used for all coastal and offshore applications. Furthermore, a new active absorption boundary condition was implemented to deal simultaneously with waves and current. It can be applied at both the inflow and the outflow boundaries to allow waves leaving the domain. The method introduced a modification of the inflow boundary condition according to the adjustment of the inflow mass flux. It is a dynamic method which allows to cancel out reflected

wave-current flow along the simulation. Consequently, it can be applied for both regular and random wave conditions without restrictions to wave theory.

With the new improvements done on the model regarding the active absorption, it is possible to reduce the domain covered by the 3D model and to simulate the detailed interaction between sea states and the structure in competitive times and computational costs. By achieving this objective the engineers can benefit from an advanced tool to assist in taking decisions and to obtain more optimal designs.

Then, in this new numerical wave basin, floating structure modelling was set up because the coupling between floating bodies and wave generation had not yet been done when I started this work.

The new numerical mooring system takes into account the real response of a tension line; the restraint equation has been changed to reproduce the effect of a mooring line. In this way, the results of the simulations improved and the approach can be adopted to predict dynamics of a floating structure and tensions on mooring systems, by the mean of OpenFOAM, without other specialised and licensed codes. This thesis focused on the taut mooring systems, in future works, also the catenary lines will be implemented. Furthermore, the interaction between many linked floating bodies will be studied and added to the code.

The new code was validated thanks to the comparison with experimental tests. The comparison showed very good agreements, so I can conclude that the new code can represent real floating anchored structures, in both shallow and deep water.

Finally, in order to demonstrate the forcefulness and potentiality of the new numerical tool, the code was applied for the preliminary design of a floating wind turbine at prototype scale in an offshore site in Mazara del Vallo, Sicily, Italy. For this case, many other studies can be carried out with the aim of the new tool, for example, different configurations of the mooring lines can be analysed, as the interaction between all the turbines of the farm.

The real case application demonstrated that the model can be helpful in the design phase and it can be used for a wide range of applications, from harbour to coastal and offshore structures.

Numerical model cannot substitute physical experiments, in fact, the combined use of both techniques can help to identify the pros and cons of each method, as there are processes than can only be replicated experimentally or numerically because of their time or space requirements. This field is called composite modelling: it integrates and balances the use of physical and numerical models. Furthermore, numerical modelling

can be applied to extend the database obtained with physical tests, simulating different wave conditions and structural alternatives at the same time and at a fraction of the cost of performing them in the laboratory. Moreover, designed structures can be run at prototype scale, avoiding scale effects.

At the end of my research activity, I can conclude this new tool based on OpenFOAM and IHFOAM is very promising and can be helpful for every kind of coastal and ocean studies and designs.

Bibliography

[1] ANTONINI, A., GAETA, M.G. & LAMBERTI, A. (2012). Wave-induced devices for the oxygenation of deep layer: a physical investigation. *Coastal Engineering Proceedings*, **1**, 56.

[2] ANTONINI, A., LAMBERTI, A. & ARCHETTI, R. (2015). Oxyflux, an innovative wave-driven device for the oxygenation of deep layers in coastal areas: A physical investigation. *Coastal Engineering*, **104**, 54–68.

[3] ANTONINI, A., LAMBERTI, A., ARCHETTI, R. & MIQUEL, A.M. (2016). Dynamic overset rans simulation of a wave-driven device for the oxygenation of deep layers. *Ocean Engineering*, **127**, 335–348.

[4] ARCHETTI, R., PINARDI, N., LAMBERTI, A., CESARI, F., PASSONI, G., PETTENUZZO, D. *et al.* (2010). Quale e quanta energia disponibile nei nostri mari? In *Secondo Convegno Nazionale di Oceanografia Operativa*, Oceanografia Operativa.

[5] AUBAULT, A., CERMELLI, C. & RODDIER, D. (2009). Windfloat: A floating foundation for offshore wind turbines. part iii: Structural analysis. In *Proceedings of 28th International Conference on Ocean, Offshore and Arctic Engineering, Honolulu, HI, Paper No. OMAE2009-79232*.

[6] BACHYNSKI, E.E. & MOAN, T. (2012). Design considerations for tension leg platform wind turbines. *Marine Structures*, **29**, 89–114.

[7] BORGEN, E. (2010). Floating wind power in deep water-competitive with shallow-water wind farms? *Modern Energy Review*, **2**, 49–53.

[8] BOUSCASSE, B., COLAGROSSI, A., MARRONE, S. & ANTUONO, M. (2013). Nonlinear water wave interaction with floating bodies in sph. *Journal of Fluids and Structures*, **42**, 112–129.

[9] BROWN, S.A., MAGAR, V., GREAVES, D.M. & CONLEY, D.C. (2014). An evaluation of rans turbulence closure models for spilling breakers. *Coastal Engineering Proceedings*, **1**, 5.

[10] CAO, H., WAN, D. *et al.* (2012). Numerical investigation of extreme wave effects on cylindrical offshore structures. In *The Twenty-second International Offshore and Polar Engineering Conference*, International Society of Offshore and Polar Engineers.

[11] CERMELLI, C., RODDIER, D. & AUBAULT, A. (2009). Windfloat: a floating foundation for offshore wind turbines. part ii: hydrodynamics analysis. In *Proceedings of 28th International Conference on Ocean, Offshore and Arctic Engineering, Honolulu, HI, Paper No. OMAE2009-79231*.

[12] CHAKRABARTI, S. (2005). *Handbook of Offshore Engineering (2-volume set)*. Elsevier.

[13] CHEN, L., ZANG, J., HILLIS, A., MORGAN, G. & PLUMMER, A. (2014). Numerical investigation of wave–structure interaction using openfoam. *Ocean Engineering*, **88**, 91–109.

[14] CHRISTENSEN, M. & FRIGAARD, P. (1994). Design of absorbing wave maker based on digital filters. Tech. rep., Hydraulics & Coastal Engineering Laboratory, Department of Civil Engineering, Aalborg University.

[15] COURANT, R., FRIEDRICHS, K. & LEWY, H. (1959). On the partial difference equations of mathematical physics. Tech. rep., CALIFORNIA UNIV LOS ANGELES.

[16] DEVOLDER, B., RAUWOENS, P. & TROCH, P. (2017). Application of a buoyancy-modified k-ω sst turbulence model to simulate wave run-up around a monopile subjected to regular waves using openfoam®. *Coastal Engineering*, **125**, 81–94.

[17] DODARAN, A.A. & PARK, S.K. (2012). Development of design static property analysis of mooring system caisson for offshore floating wind turbine. *International Journal of Ocean System Engineering*, **2**, 97–105.

[18] EL SAFTI, H., BONAKDAR, L. & OUMERACI, H. (2014). A hybrid 2d-3d cfd model system for offshore pile groups subject to wave loading. In *ASME 2014 33rd International Conference on Ocean, Offshore and Arctic Engineering*, V002T08A040–V002T08A040, American Society of Mechanical Engineers.

[19] ELHANAFI, A., FLEMING, A., LEONG, Z. & MACFARLANE, G. (2017). Effect of rans-based turbulence models on nonlinear wave generation in a two-phase numerical wave tank. *Progress in Computational Fluid Dynamics, an International Journal*, **17**, 141–158.

[20] FALTINSEN, O. (1990). Sea loads on ships and ocean structures. *Cambridge University, Cambridge, UK*.

[21] FERRI, F. & PALM, J. (2015). Implementation of a dynamic mooring solver (moody) into a wave to wire model of a simple wec. Tech. rep., Technical Report.

[22] FRANCO, L., PISCOPIA, R., CORSINI, S. & INGHILESI, R. (2004). L'atlante delle onde nei mari italiani-italian wave atlas.

[23] GOUPEE, A.J., KOO, B., LAMBRAKOS, K., KIMBALL, R. *et al.* (2012). Model tests for three floating wind turbine concepts. In *Offshore technology conference*, Offshore Technology Conference.

[24] HALES, L.Z. (1981). Floating breakwaters: State-of-the-art literature review. Tech. rep., COASTAL ENGINEERING RESEARCH CENTER FORT BELVOIR VA.

[25] HANSEN, A.D. & HANSEN, L.H. (2007). Wind turbine concept market penetration over 10 years (1995–2004). *Wind energy*, **10**, 81–97.

[26] HIGUERA, P. (2015). *Application of computational fluid dynamics to wave action on structures*. Ph.D. thesis, Ph. D. thesis, Univ. de Cantabria, Santander, Spain.

[27] HIGUERA, P., LARA, J.L. & LOSADA, I.J. (2013). Realistic wave generation and active wave absorption for navier–stokes models: Application to openfoam®. *Coastal Engineering*, **71**, 102–118.

BIBLIOGRAPHY

[28] Higuera, P., Lara, J.L. & Losada, I.J. (2013). Simulating coastal engineering processes with openfoam®. *Coastal Engineering*, **71**, 119–134.

[29] Hirt, C.W. & Nichols, B.D. (1981). Volume of fluid (vof) method for the dynamics of free boundaries. *Journal of computational physics*, **39**, 201–225.

[30] Jacobsen, N.G., Fuhrman, D.R. & Fredsøe, J. (2012). A wave generation toolbox for the open - source cfd library: Openfoam®. *International Journal for Numerical Methods in Fluids*, **70**, 1073–1088.

[31] Jasak, H. (1996). Error analysis and estimation for finite volume method with applications to fluid flow.

[32] Jasak, H. & Tuković, Ž. (2010). Dynamic mesh handling in openfoam applied to fluid-structure interaction simulations. In *Proceedings of the V European Conference on Computational Fluid Dynamics ECCOMAS CFD 2010*.

[33] Jasak, H., Jemcov, A., Tukovic, Z. *et al.* (2007). Openfoam: A c++ library for complex physics simulations. In *International workshop on coupled methods in numerical dynamics*, vol. 1000, 1–20, IUC Dubrovnik, Croatia.

[34] Jeon, S., Cho, Y., Seo, M., Cho, J. & Jeong, W. (2013). Dynamic response of floating substructure of spar-type offshore wind turbine with catenary mooring cables. *Ocean Engineering*, **72**, 356–364.

[35] Ji, C.Y., Yu-Chan, G., Cui, J., Yuan, Z.M. & Ma, X.J. (2016). 3d experimental study on a cylindrical floating breakwater system. *Ocean Engineering*, **125**, 38–50.

[36] Jonkman, J. & Musial, W. (2010). Offshore code comparison collaboration (oc3) for iea task 23 offshore wind technology and deployment. *Contract*, **303**, 275–3000.

[37] Jonkman, J.M. (2009). Dynamics of offshore floating wind turbines - model development and verification. *Wind energy*, **12**, 459–492.

[38] Kamath, A., Alagan Chella, M., Bihs, H. & Arntsen, Ø.A. (2015). Evaluating wave forces on groups of three and nine cylinders using a 3d numerical wave tank. *Engineering Applications of Computational Fluid Mechanics*, **9**, 343–354.

[39] Karimirad, M. (2010). Dynamic response of floating wind turbine. *Scientia Iranica. Transaction B, Mechanical Engineering*, **17**, 146.

[40] Karimirad, M. & Moan, T. (2012). A simplified method for coupled analysis of floating offshore wind turbines. *Marine Structures*, **27**, 45–63.

[41] Karimirad, M., Meissonnier, Q., Gao, Z. & Moan, T. (2011). Hydroelastic code-to-code comparison for a tension leg spar-type floating wind turbine. *Marine Structures*, **24**, 412–435.

[42] Kim, B.W., Sung, H.G., Kim, J.H. & Hong, S.Y. (2013). Comparison of linear spring and nonlinear fem methods in dynamic coupled analysis of floating structure and mooring system. *Journal of Fluids and Structures*, **42**, 205–227.

[43] Ladenburg, J. (2009). Visual impact assessment of offshore wind farms and prior experience. *Applied Energy*, **86**, 380 – 387.

[44] Lara, J.L., Higuera, P., Guanche, R. & Losada, I.J. (2013). Wave interaction with piled structures: Application with ih-foam. In *Proceedings of the 32nd International Conference on Ocean, Offshore and Arctic Engineering*, ASME Nantes, France.

[45] Lee, K.H. (2005). *Responses of floating wind turbines to wind and wave excitation*. Ph.D. thesis, Massachusetts Institute of Technology.

[46] Lee, S. *et al.* (2008). Dynamic response analysis of spar buoy floating wind turbine systems.

[47] Lind, S., Stansby, P. & Rogers, B. (2016). Fixed and moored bodies in steep and breaking waves using sph with the froude–krylov approximation. *Journal of Ocean Engineering and Marine Energy*, **2**, 331–354.

[48] Madsen, P.A. & Fuhrman, D.R. (2010). High-order boussinesq-type modelling of nonlinear wave phenomena in deep and shallow water. In *Advances in numerical simulation of nonlinear water waves*, 245–285, World Scientific.

[49] Masciola, M., Robertson, A., Jonkman, J. & Driscoll, F. (2011). Investigation of a fast-orcaflex coupling module for integrating turbine and mooring dynamics of offshore floating wind turbines: Preprint. Tech. rep., National Renewable Energy Laboratory (NREL), Golden, CO.

[50] Mayer, S. & Madsen, P.A. (2001). Simulation of breaking waves in the surf zone using a navier-stokes solver. In *Coastal Engineering 2000*, 928–941.

[51] McCartney, B.L. (1985). Floating breakwater design. *Journal of Waterway, Port, Coastal, and Ocean Engineering*, **111**, 304–318.

[52] McCormick, M.E. (2009). *Ocean engineering mechanics: with applications*. Cambridge University Press.

[53] Menter, F., Kuntz, M. & Bender, R. (2003). A scale-adaptive simulation model for turbulent flow predictions. In *41st aerospace sciences meeting and exhibit*, 767.

[54] Morgan, G. & Zang, J. (2011). Application of openfoam to coastal and offshore modelling. *The 26th IWWWFB. Athens, Greece*.

[55] Nielsen, F. (2010). The hywind idea. *Presentation, Statoil ASA, Oslo*.

[56] Nielsen, F.G., Hanson, T.D., Skaare, B. *et al.* (2006). Integrated dynamic analysis of floating offshore wind turbines. In *Proceedings of 25th International Conference on Offshore Mechanics and Arctic Engineering, Hamburg, Germany, OMAE2006-92291*.

[57] Oggiano, L., Arens, E., Myhr, A., Nygaard, T.A., Evans, S. *et al.* (2015). Cfd simulations on a tension leg buoy platform for offshore wind turbines and comparison with experiments. In *The Twenty-fifth International Ocean and Polar Engineering Conference*, International Society of Offshore and Polar Engineers.

[58] Omidvar, P., Stansby, P.K. & Rogers, B.D. (2012). Wave body interaction in 2d using smoothed particle hydrodynamics (sph) with variable particle mass. *International Journal for Numerical Methods in Fluids*, **68**, 686–705.

[59] Open, C. (2011). Openfoam uprogrammer's guide. *OpenFOAM Foundation*, **2**.

[60] Osher, S. & Sethian, J.A. (1988). Fronts propagating with curvature-dependent speed: algorithms based on hamilton-jacobi formulations. *Journal of computational physics*, **79**, 12–49.

[61] Paci, A., Gaeta, M.G., Antonini, A., Archetti, R. et al. (2016). 3d-numerical analysis of wave-floating structure interaction with openfoam. In *The 26th International Ocean and Polar Engineering Conference*, International Society of Offshore and Polar Engineers.

[62] Palemón-Arcos, L., Torres-Freyermuth, A., Chang, K.A., Pastrana-Maldonado, D., Salles, P. et al. (2014). Modeling wave-structure interaction and its implications in offshore structure stability. In *The Twenty-fourth International Ocean and Polar Engineering Conference*, International Society of Offshore and Polar Engineers.

[63] Palm, J., Eskilsson, C., Paredes, G.M. & Bergdahl, L. (2016). Coupled mooring analysis for floating wave energy converters using cfd: Formulation and validation. *International Journal of Marine Energy*, **16**, 83–99.

[64] Paulsen, B.T., Bredmose, H. & Bingham, H.B. (2014). An efficient domain decomposition strategy for wave loads on surface piercing circular cylinders. *Coastal Engineering*, **86**, 57–76.

[65] Peng, W., Lee, K.H., Shin, S.H. & Mizutani, N. (2013). Numerical simulation of interactions between water waves and inclined-moored submerged floating breakwaters. *Coastal engineering*, **82**, 76–87.

[66] Rahman, M.A., Mizutani, N. & Kawasaki, K. (2006). Numerical modeling of dynamic responses and mooring forces of submerged floating breakwater. *Coastal Engineering*, **53**, 799–815.

[67] Ransley, E., Hann, M., Greaves, D., Raby, A. & Simmonds, D. (2013). Numerical and physical modelling of extreme wave impacts on a fixed truncated circular cylinder. In *Proceedings of the 10th European wave and tidal energy conference (EWTEC)*.

[68] Roddier, D., Cermelli, C., Aubault, A. & Weinstein, A. (2010). Windfloat: A floating foundation for offshore wind turbines. *Journal of renewable and sustainable energy*, **2**, 033104.

[69] Rogers, B.D., Dalrymple, R.A. & Stansby, P.K. (2010). Simulation of caisson breakwater movement using 2-d sph. *Journal of Hydraulic Research*, **48**, 135–141.

[70] Rudstrøm, L. (2012). Hywind-a proven floating offshore wind technology.

[71] Ruiz-Minguela, J., Marón, A., Prieto, M., Rodríguez, R., Ricci, P., Fernández, D. & Taboada, M. (2008). Design and testing of the mooring system for a new offshore wave energy converter. In *Proceedings of the 2nd International Conference on Ocean Energy (ICOE)*, 1–9.

[72] Rusche, H. (2002). Computational fluid dynamics of dispersed two-phase flows at high phase fractions. 2003. *Imperial College London (University of London)*.

[73] Salter, S.H. (1981). Absorbing wave makers and wide tanks. Proceedings of the Conference on Directional Wave Applications.

[74] Schäffer, H.A. & Klopman, G. (2000). Review of multidirectional active wave absorption methods. *Journal of waterway, port, coastal, and ocean engineering*, **126**, 88–97.

[75] Schweizer, J., Antonini, A., Govoni, L., Gottardi, G., Archetti, R., Supino, E., Berretta, C., Casadei, C. & Ozzi, C. (2016). Investigating the potential and feasibility of an offshore wind farm in the northern adriatic sea. *Applied Energy*, **177**, 449 – 463.

[76] Stewart, G.M. & Lackner, M.A. (2012). Determining optimal tuned mass damper parameters for offshore wind turbines using a genetic algorithm. In *50th AIAA Aerospace Sciences Meeting including the New Horizons Forum and Aerospace Exposition, AIAA paper*, vol. 376.

[77] Tong, K. (1998). Technical and economic aspects of a floating offshore wind farm. *Journal of Wind Engineering and Industrial Aerodynamics*, **74**, 399–410.

[78] Torres-Freyermuth, A., Lara, J.L. & Losada, I.J. (2010). Numerical modelling of short-and long-wave transformation on a barred beach. *Coastal Engineering*, **57**, 317–330.

[79] Tracy, C.C.H. (2007). *Parametric design of floating wind turbines*. Ph.D. thesis, Massachusetts Institute of Technology.

[80] Utsunomiya, T. & Nishida, E. (2010). On sea experiment of a hybrid spar for floating offshore wind turbine 1/10 scale model. *Proc. of 29th OMAE, OMAE2010-20730*.

[81] Van Maele, K. & Merci, B. (2006). Application of two buoyancy-modified k–ε turbulence models to different types of buoyant plumes. *Fire Safety Journal*, **41**, 122–138.

[82] Vanneste, D. & Troch, P. (2015). 2d numerical simulation of large-scale physical model tests of wave interaction with a rubble-mound breakwater. *Coastal Engineering*, **103**, 22–41.

[83] Versteeg, H.K. & Malalasekera, W. (2007). *An introduction to computational fluid dynamics: the finite volume method*. Pearson Education.

[84] Wang, C. & Tay, Z. (2011). Very large floating structures: applications, research and development. *Procedia Engineering*, **14**, 62–72.

[85] Wellens, P.R. (2012). Wave simulation in truncated domains for offshore applications.

[86] Yang, M., Teng, B., Ning, D. & Shi, Z. (2012). Coupled dynamic analysis for wave interaction with a truss spar and its mooring line/riser system in time domain. *Ocean Engineering*, **39**, 72–87.

[87] Yu, D. & Kareem, A. (1998). Parametric study of flow around rectangular prisms using les. *Journal of Wind Engineering and Industrial Aerodynamics*, **77**, 653–662.

[88] Zambrano, T., MacCready, T., Kiceniuk, T., Roddier, D.G. & Cermelli, C.A. (2006). Dynamic modeling of deepwater offshore wind turbine structures in gulf of mexico storm conditions. In *25th International Conference on Offshore Mechanics and Arctic Engineering*, 1–6, Hamburg.